SAND2019-14120C

# Biological and Chemical Sensors and Modeling Methods for Acoustic Devices

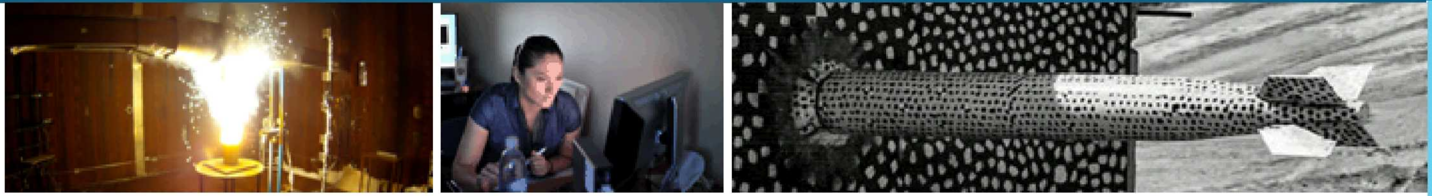

Darren W. Branch, Distinguished Member of Technical Staff

Biological and Chemical Sensors Department, 08634

Sandia National Laboratories, Albuquerque, NM 87122

Presentation: Oregon Health Science University (OHSU)

*dwbranc@sandia.gov*

Sandia National Laboratories is a multimission laboratory managed and operated by National Technology & Engineering Solutions of Sandia, LLC, a wholly owned subsidiary of Honeywell International Inc., for the U.S. Department of Energy's National Nuclear Security Administration under contract DE-NA0003525.

# Biological and Chemical Sensors

# Volatile Organic Compounds (VOCs): Human Health Monitoring

**Breath**

**Blood**

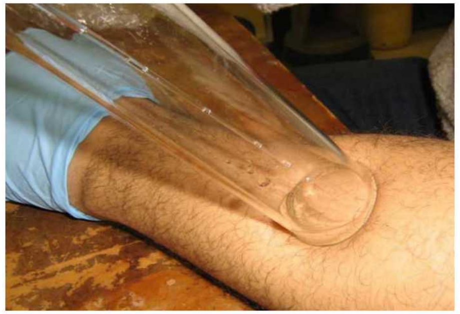

**Skin**

**Saliva**

## Gas Phase Sensing

Volatile organic compound (VOC) biomarkers for:

- Stress
- Infection- flu, TB, smallpox
- Performance degradation (fatigue)
- Disease- cancer, IBS, asthma
- Drug use
- Ketosis
- Hypoglycemia
- Hypoxia- *J. Breath Res.* **9** (2015) 047103
- Human identification

Variety of sample substrates available for analysis.

**Sweat**

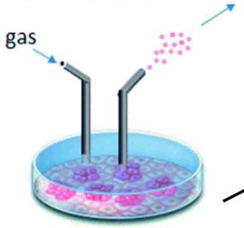

**Cell culture**

**Urine**

**Feces**

# Bacterial VOCs for pathogen ID

Bacterial VOCs specific to the species, strain, and serovar levels

- ~10-30 VOC specific markers and patterns from volatilome
- E.g. distinguish Shiga Toxin Producing E. coli (STEC) from non-STEC by ppm-sensitive e-nose with 16 hours of culturing

Large database of VOCs diagnostic for diseases, pathogens

- Bos et al, 2013; Lemfack et al, 2014
- Shnayderman *et al,* 2005; Zhu *et al,* 2010; Thorn *et al,* 2011

J. Zhu, *J. Clin. Microbio., (2010) 4426.*

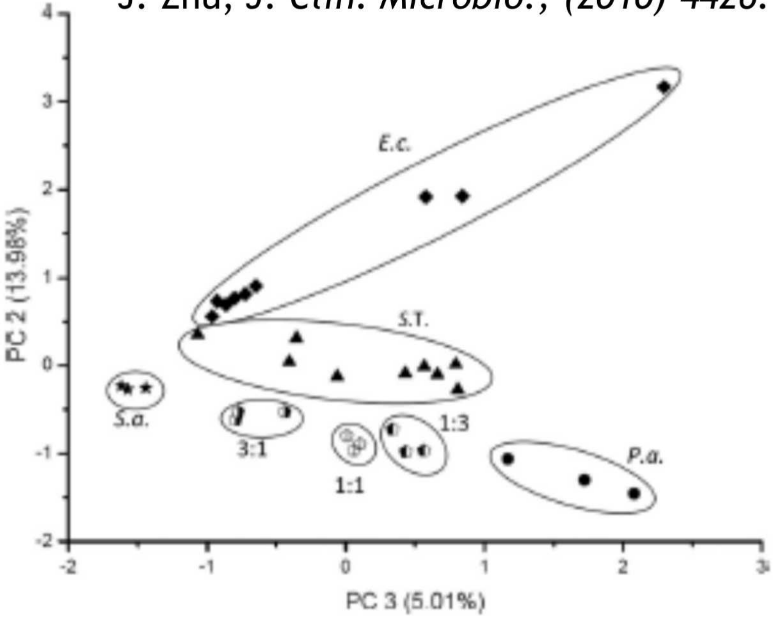

- GC-MS and statistics to identify bacteria – markers and patterns

Pathway to diagnostics that are complementary to, but orthogonal from, traditional liquid-based assays.

# *In vivo* detection of *M. bovis* in breath or blood/serum headspace

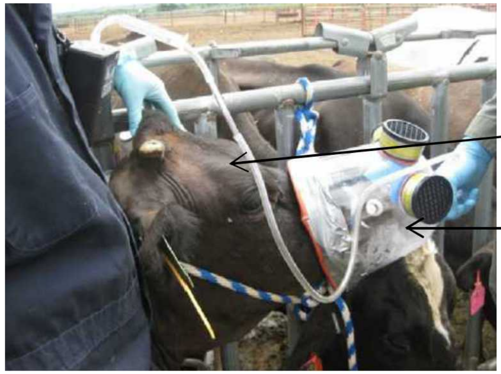

Cow

VOC collection mask

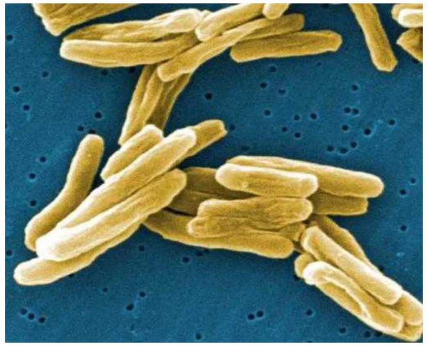

- C.K. Ellis *et al,* PLoS ONE, 9: e892280, 2014:

Exhaled cattle breath by GC-MS, PCA, LDA to distinguish healthy calves from calves with *M. bovis* infection with sensitivity and selectivity of 97% and 99%

- R. Fend *et al,* J. Clin. Microbiol., 43: 1745-1751, 2005:

Badgers, Cattle blood/serum headspace VOCs by e-Nose and PCA DFA identified all infected animals correctly

Our team has demonstrated detection of four characteristic VOC biomarkers of TB* at a 0.02 ppb LOD.

*J. Breath Res. 7 (2013) 037107.

Allows rapid assessment of potential infections and disease states.

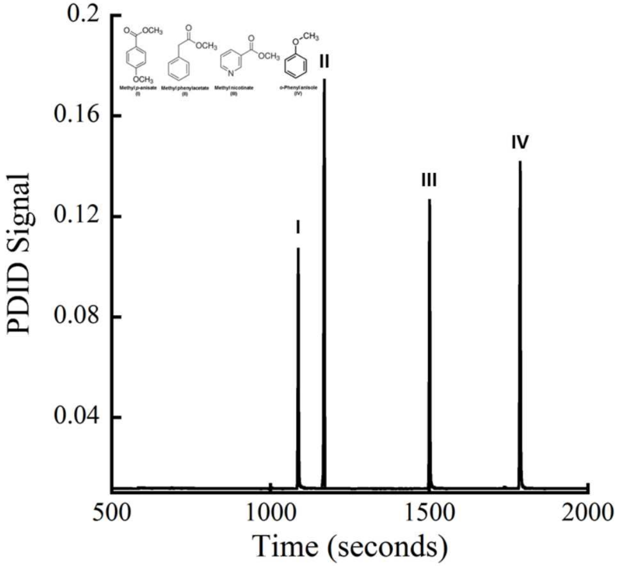

# VOC Sampling of Water-Stressed Adult Plants

VOC sampling

Soil VOC sampling

- Water stress experiments showed, VOC markers arising at different times: blue- < 24 hrs., green- 24 – 48 hrs., and red- > 48 hrs.

VOC markers diagnostic of health conditions exist for plants, animals, and humans.

| Analyte |
|---|
| 3-methyl-2-Heptanone |
| 2,4,4-trimethyl-Cyclopentanone |
| 2,3-Butanedione |
| 2-Pentanone |
| Levulinic acid |
| 2,6,6-trimethyl-1-Cyclohexene-1-carboxaldehyde |
| 2-Octanol |
| 3-Octen-2-ol |
| 4-Oxohex-2-enal |
| 2-methyl-butanoic acid |
| Isophorone |
| 3-Pentanone |
| 3-methyl-Butanoic acid |
| 3-Octanone |
| 2-methyl-Butanal |
| 3-methyl-Butanal |
| 2,2,6-trimethyl-Cyclohexanone |
| 2-ethyl-Furan |
| Pentanal |
| Acetic acid |
| Azulene |
| 1-methyl-4-(1-methylethenyl)-, trans-Cyclohexene |

# MicroChemlab Gas Phase Detection Technologies

Sandia's proven MicroChemlab sensor system:

- Field-tested/rugged
- Hand-portable
- Inexpensive
- Push button automation
- 1-2 minute analysis time
- New detector now allows for medical applications

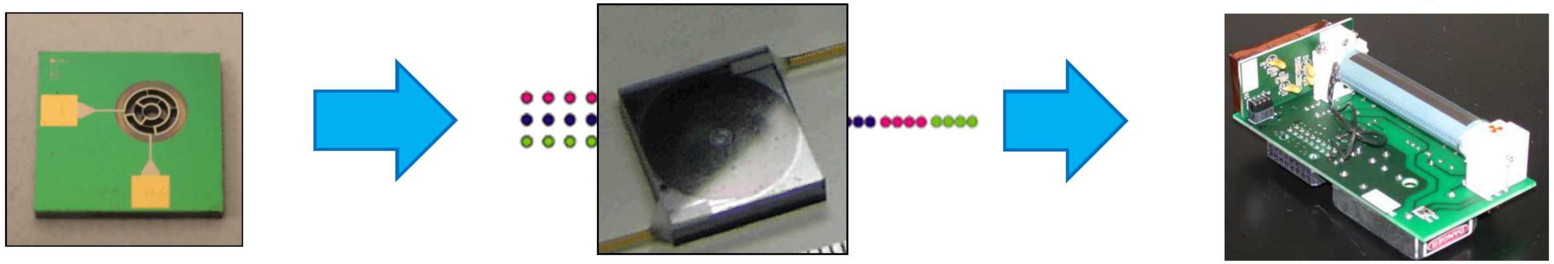

**Preconcentration Stage**

- Collects analyte
- Reduces false alarms

**Chromatography Stage**

- Separates complex chemical mixtures
- Increases analysis confidence

**IMS Detection Stage**

- Sub ppb sensitivity
- Wide applicability to VOC detection

This technology enables portable, VOC-based diagnostics.

# Sandia’s Chemical Sensing Methodology: Preconcentration

**Microfabricated Preconcentrators**

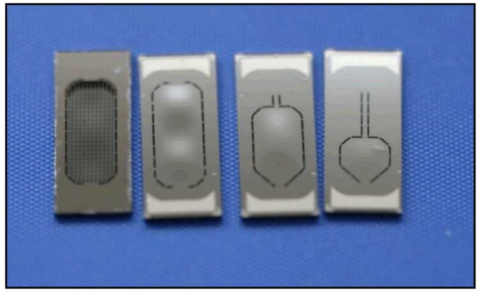

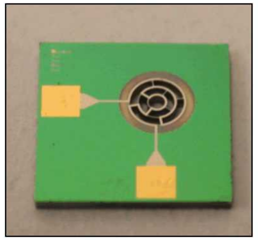

**The Preconcentrator accumulates species of interest in a chemical film and rejects interferents.**

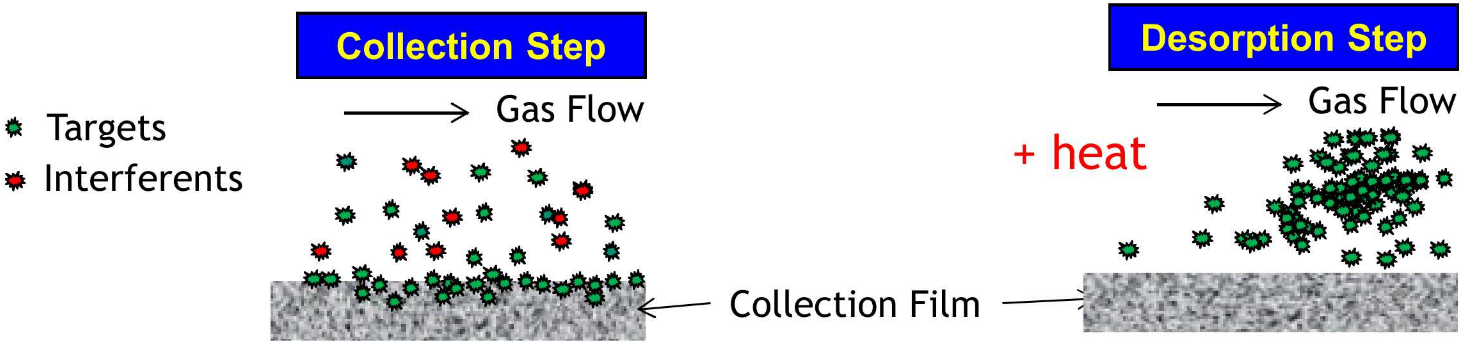

**Collection Step**

**Desorption Step**

● Targets
● Interferents

Gas Flow

+ heat

Collection Film

A high-surface area collection film is exposed to air flow. Targets preferentially absorb into the film due to their chemical affinity. Chemically-incompatible interferents are not captured.

- Tailoring the proper collection film for the target compounds is a critical system design detail.

The component is rapidly heated, causing the absorbed target chemicals to leave the collection film in a narrow, highly-concentrated pulse.

# Sandia's Chemical Sensing Methodology: Separation

**Example Chromatogram**

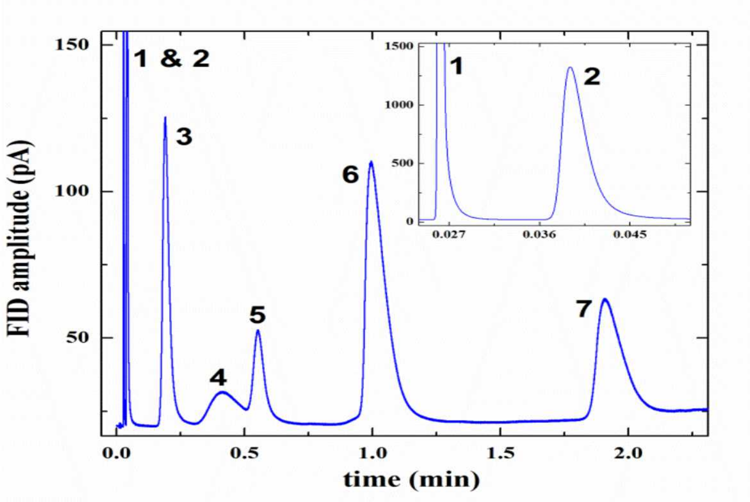

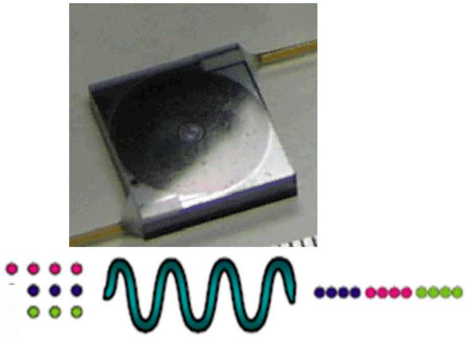

**Gas Chromatography:**
- **Separates chemical species passing through a channel based upon their affinity for a chemical coating.**

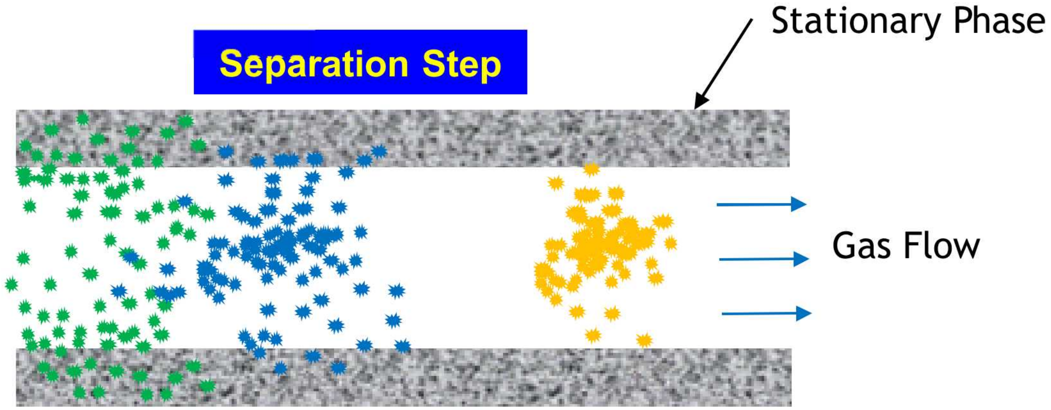

Analytes passing thru the channel have differing affinities for a chemical coating on the channel wall called a stationary phase. Chemicals with greater affinity for the stationary phase (✱) are more readily retained than those with a lesser affinity for the stationary phase (✱).

- The time it takes analytes to transit the channel helps identify the compound.
- In this way a complex mixture can be separated into simpler mixtures or single components which simplifies the detector's task.

# Sandia's Chemical Sensing Methodology: Detection

Sandia has recently developed an ion-mobility spectrometer (IMS) capable of detecting positive ions.

- Allows us to detect VOC targets.
- Sensitivity in the hundreds of picograms.

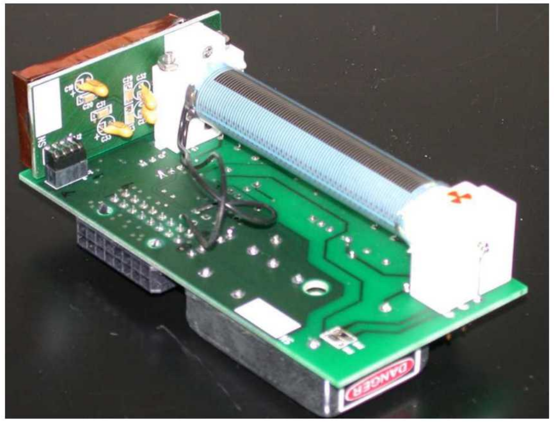

Sandia's Miniature IMS

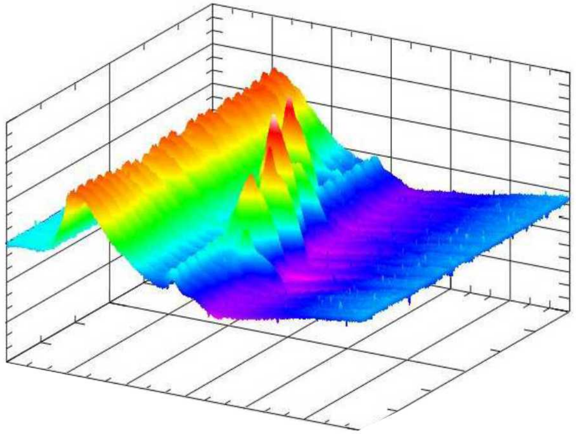

Detection of a VOC compound mix

Allows us to detect many VOCs that would otherwise have been undetectable before.

# Other Technology Applications: Synthetic Opioid Detection

Synthetic opioids, fentanyl being the most common, are an acutely toxic class of compounds.

- Thousands of suspected structural variants, or analogs, of this molecule class and < 200 have been synthesized and even fewer characterized.
- Carfentanil, an analog of fentanyl, is more toxic than VX gas nerve agent.

Current detection technology has limitations.

- No DEA-approved technology to detect synthetic opioids in the field at trace levels.
- Current technologies cannot detect unknown analogs and have high false alarm rates.
- Better detection technology is being requested by DHS, CTTSO, JPEO, and DoJ.

2-3 mg lethal dose of fentanyl

1 kg "brick" of fentanyl

# Other Technology Applications: Sandia's Unique Approach

Sandia is developing a novel solution that will be amenable to portable detection by leveraging our current portfolio of microsystem technologies.

- Amenable to swipe or particulate sampling.
- Low false alarm rates.
- Portable instrumentation being designed.

Results:

- Able to identify all fentanyl analogs tested thus far (12/12).
- Detected 3 µg of furanyl fentanyl even when mixed with 3 µg of five different cutting agents (lactose, baby formula, baking soda, acetaminophen, and procaine- total of 15 µg of interferents).


**Swipe Sampling**

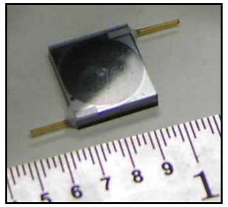
**Micro Gas Chromatograph (µGC)**

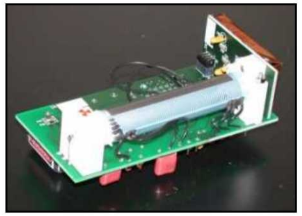
**Sandia's Miniature Ion Mobility Spectrometer (IMS)**


**Deployable Synthetic Opioid Detector**

No equivalent technical solutions on the horizon from industry or other government agencies.

# Microneedles

# Microneedles

Initially developed for drug delivery to overcome stratum corneum barrier

General requirements, one feature less than 500um

MN’s are associated with significantly less pain than 26 gauge hypodermic needles

Considered minimally invasive relative to hypodermic syringe

Can be self-administered

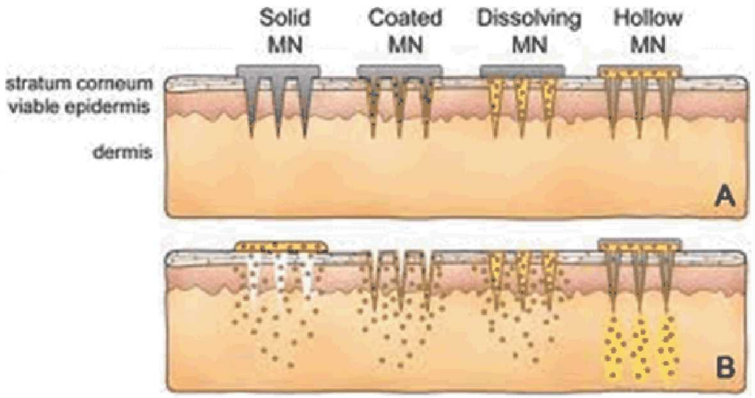

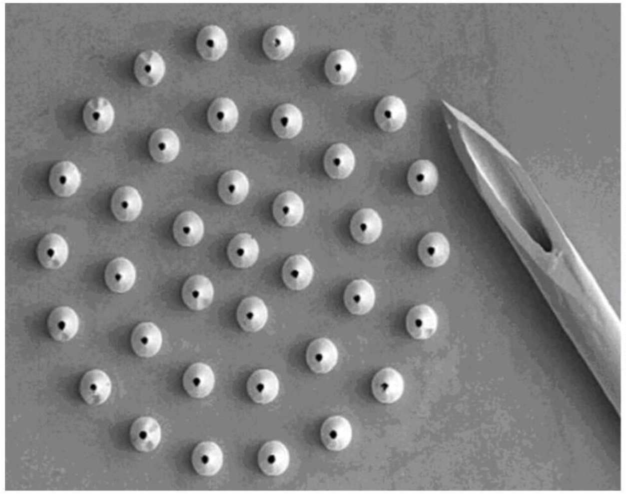

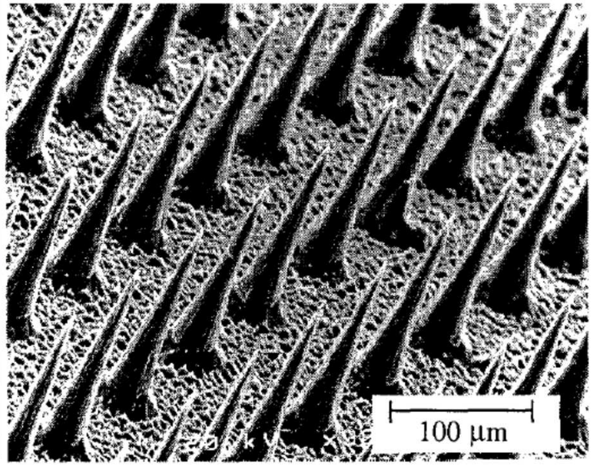

Henry et al., IEEE 1994(494-98)

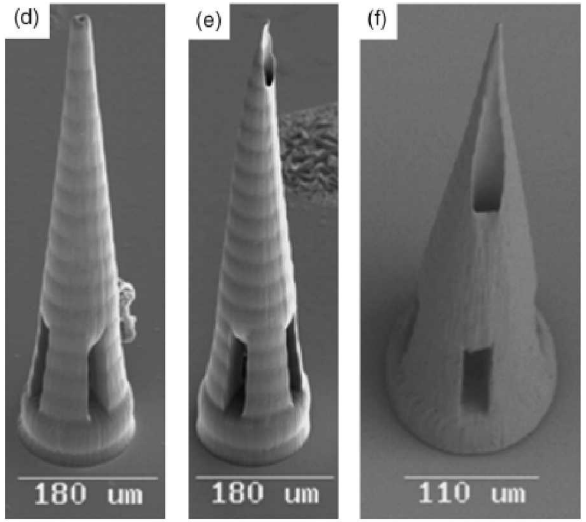

Doraiswamy et al., Acta Biomat 2006(2).

# Early Work on Microneedle: Small Molecule Detection

**Microneedle**

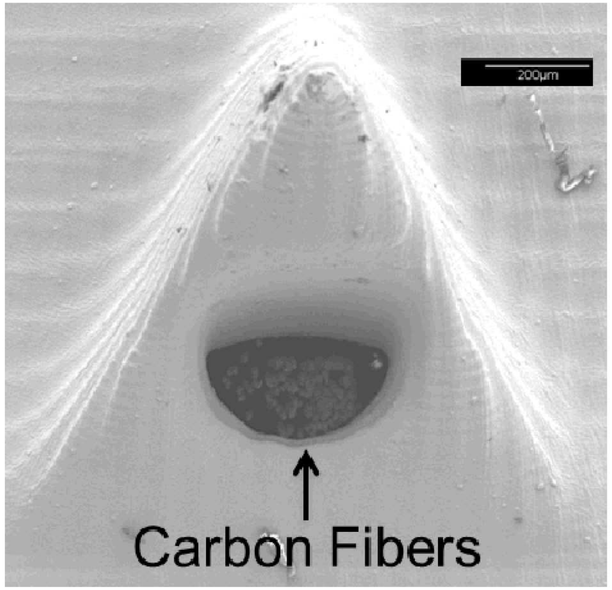

**Fabricated with Microstereolithography**

**Enzymatic Sensors**

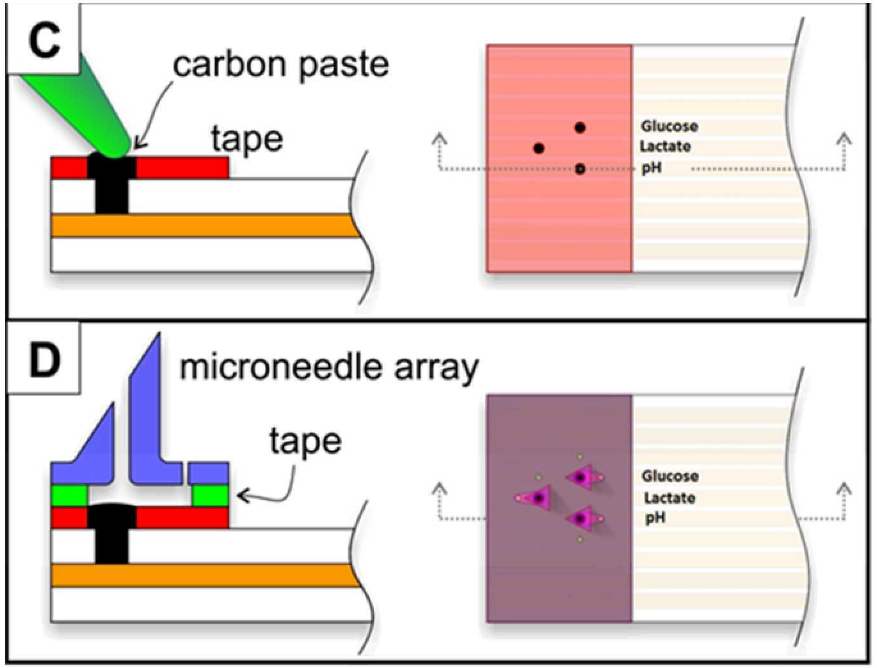

**Schematic of device**

**Protein Detection Chip**

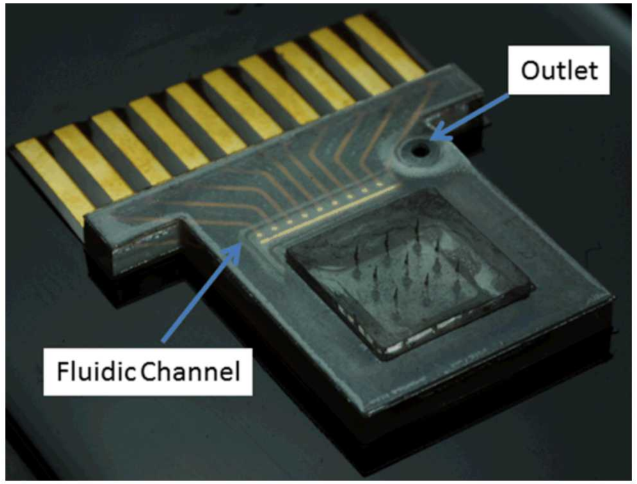

# Early Work on Microneedle: Small Molecule Detection

**Detecting reactive oxygen species ($H_2O_2$)**

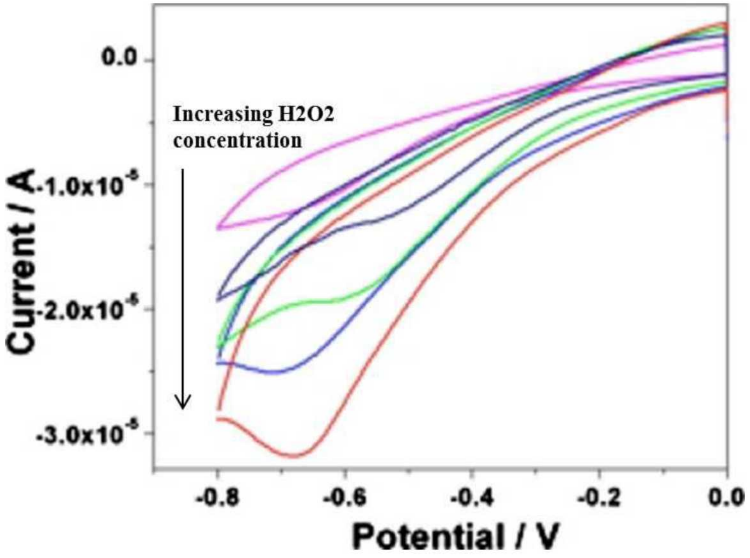

**Multiplexed detection of lactate, pH, and glucose**

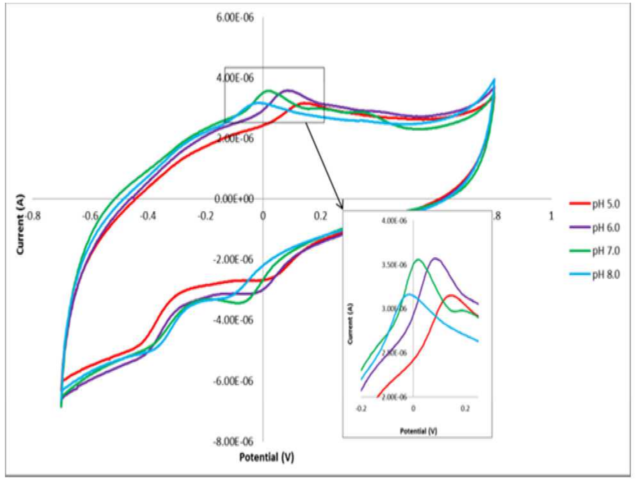

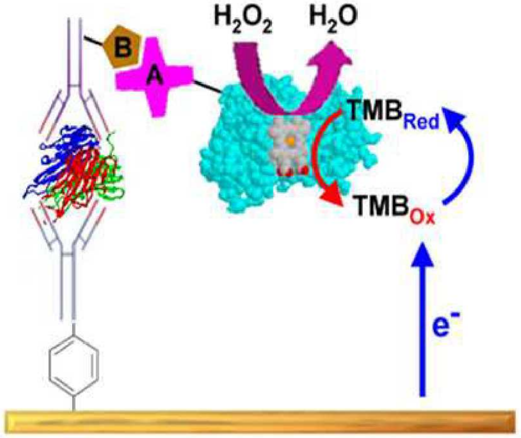

PR Miller, Biomicrofluidics 5.013415 (2011)

**Electrochemical detection of cardiac biomarkers**

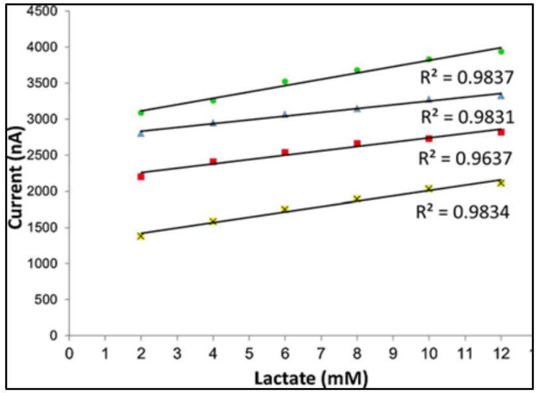

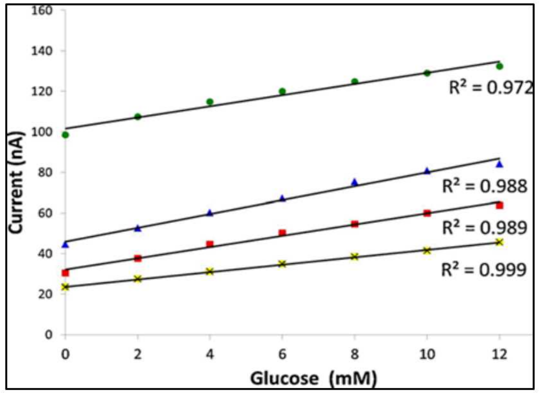

P.R. Miller et al.,Talanta 88 (2012)

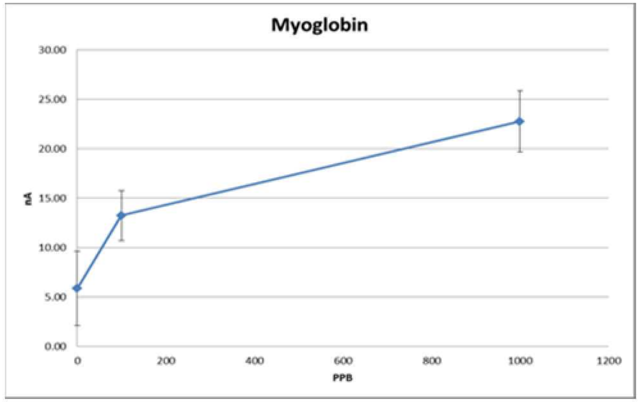

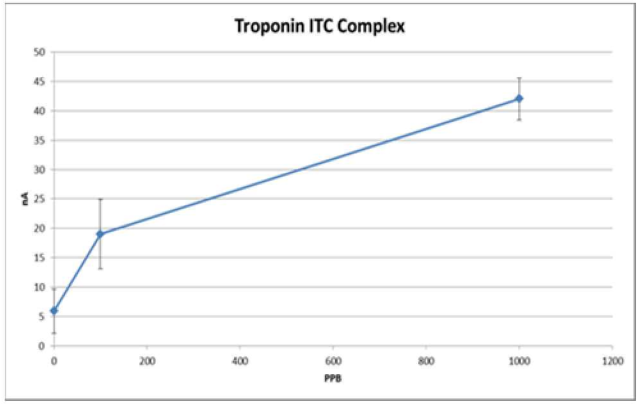

PR Miller, Electroanalysis, 28,6 (2016)

# Microneedle Fabrication

## Fabrication Process

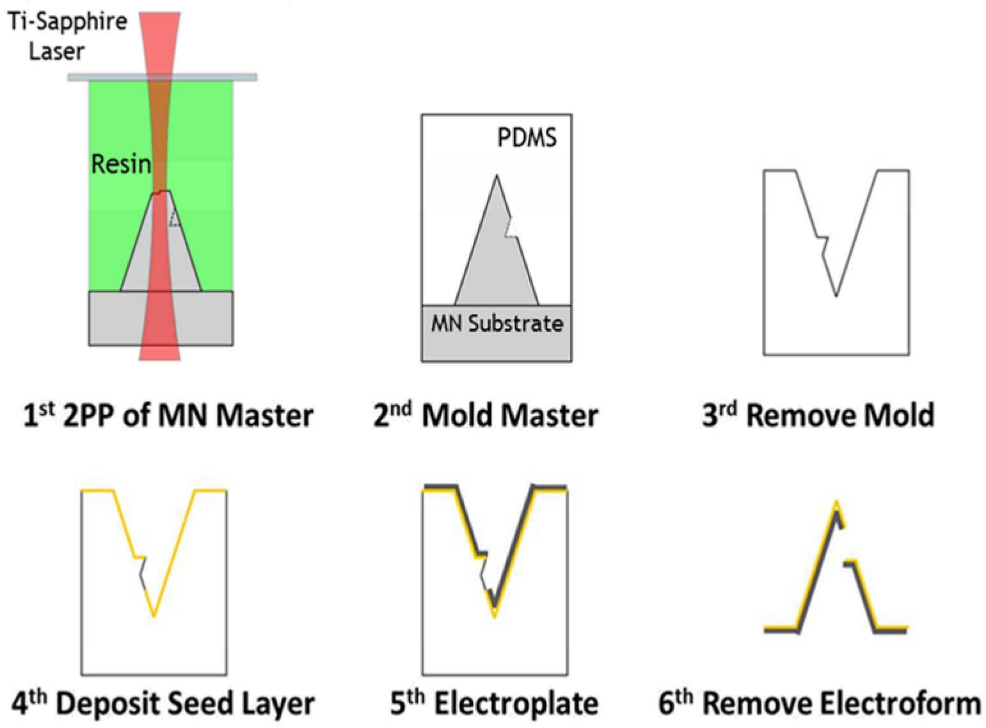

- Larger scalability, one master can make dozens of molds
- Molds may be reusable
- Can electroplate numerous arrays at once with dimensions produced from 2PP

## Cross-section of Microneedle Master

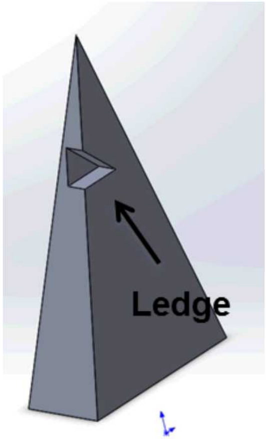

## Hollow Metal Microneedle Array

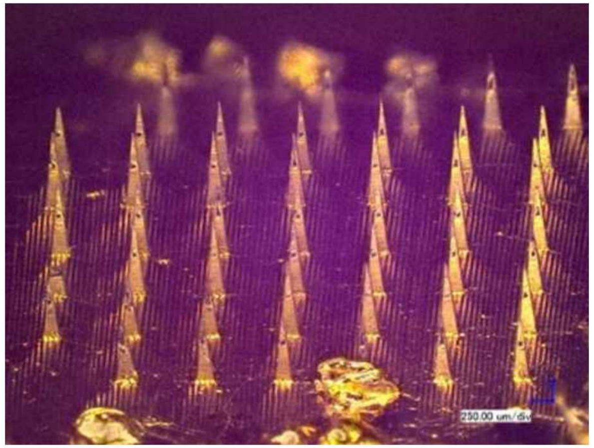

## Flexibility of Metal Microneedle Array Substrate

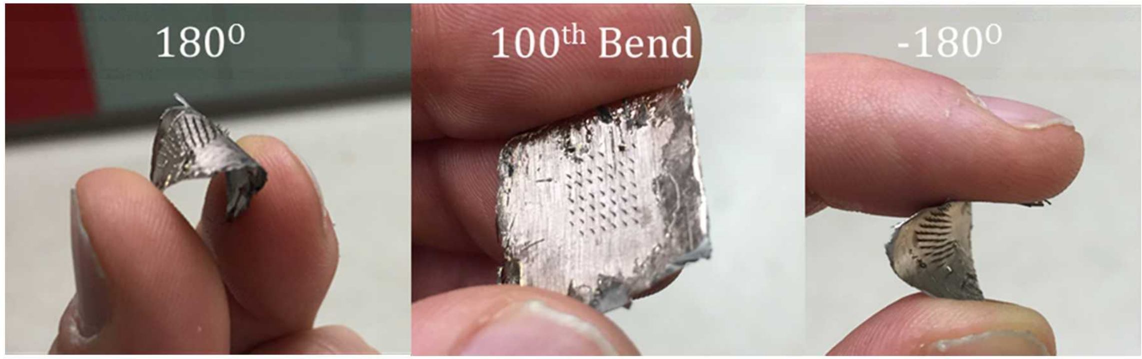

PR Miller, MRS Advances 2019

# Clinical Studies

- Optimized needle geometries for interstitial fluid extraction in humans and rats
- Needles and holders were designed to extract enough fluid for analysis in <20min
- Biochemical analysis of glucose, lactate, total protein, pH, proteomic and genomic profiles, and exosome

### Protein Expression in ISF

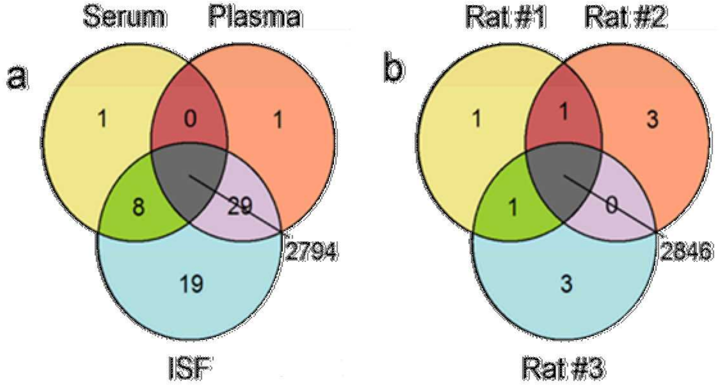

### RNA Profiles in ISF, Serum, and Plasma

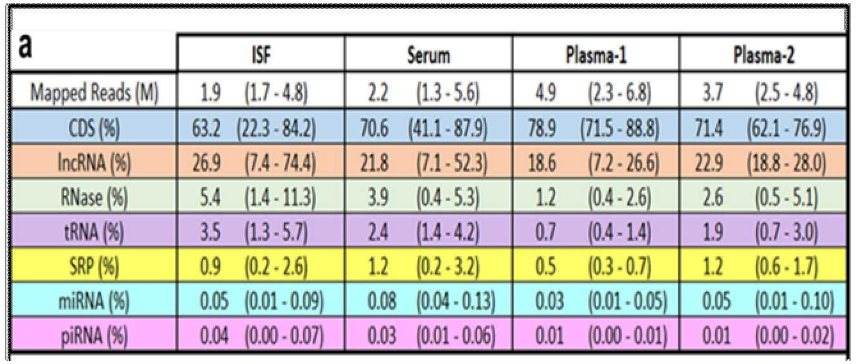

| a | ISF | Serum | Plasma-1 | Plasma-2 |
|---|---|---|---|---|
| Mapped Reads (M) | 1.9 (1.7 - 4.8) | 2.2 (1.3 - 5.6) | 4.9 (2.3 - 6.8) | 3.7 (2.5 - 4.8) |
| CDS (%) | 63.2 (22.3 - 84.2) | 70.6 (41.1 - 87.9) | 78.9 (71.5 - 88.8) | 71.4 (62.1 - 76.9) |
| lncRNA (%) | 26.9 (7.4 - 74.4) | 21.8 (7.1 - 52.3) | 18.6 (7.2 - 26.6) | 22.9 (18.8 - 28.0) |
| RNase (%) | 5.4 (1.4 - 11.3) | 3.9 (0.4 - 5.3) | 1.2 (0.4 - 2.6) | 2.6 (0.5 - 5.1) |
| tRNA (%) | 3.5 (1.3 - 5.7) | 2.4 (1.4 - 4.2) | 0.7 (0.4 - 1.4) | 1.9 (0.7 - 3.0) |
| SRP (%) | 0.9 (0.2 - 2.6) | 1.2 (0.2 - 3.2) | 0.5 (0.3 - 0.7) | 1.2 (0.6 - 1.7) |
| miRNA (%) | 0.05 (0.01 - 0.09) | 0.08 (0.04 - 0.13) | 0.03 (0.01 - 0.05) | 0.05 (0.01 - 0.10) |
| piRNA (%) | 0.04 (0.00 - 0.07) | 0.03 (0.01 - 0.06) | 0.01 (0.00 - 0.01) | 0.01 (0.00 - 0.02) |

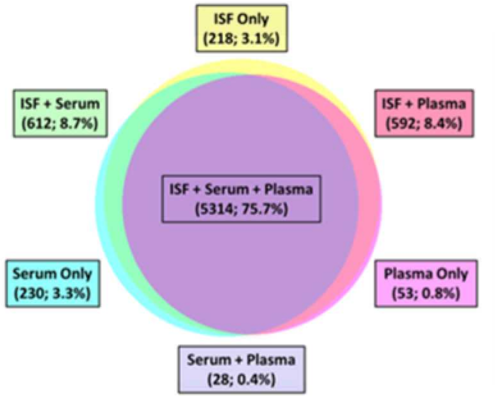

- Protein expression and comparison with serum and plasma with fluid collected from rats.
- Some ISF specific proteins were found however fluid composition mimics blood composition.
- RNA profiles in interstitial fluid extracted from rats compared with serum and plasma with Venn diagram distribution.
- Protein coding transcripts (CDS) were detected in all examples and proportion of transcripts detected in each sample is reflected in the size of the circle.

Miller et at, Comm Bio, 2018

# Exosome Extraction

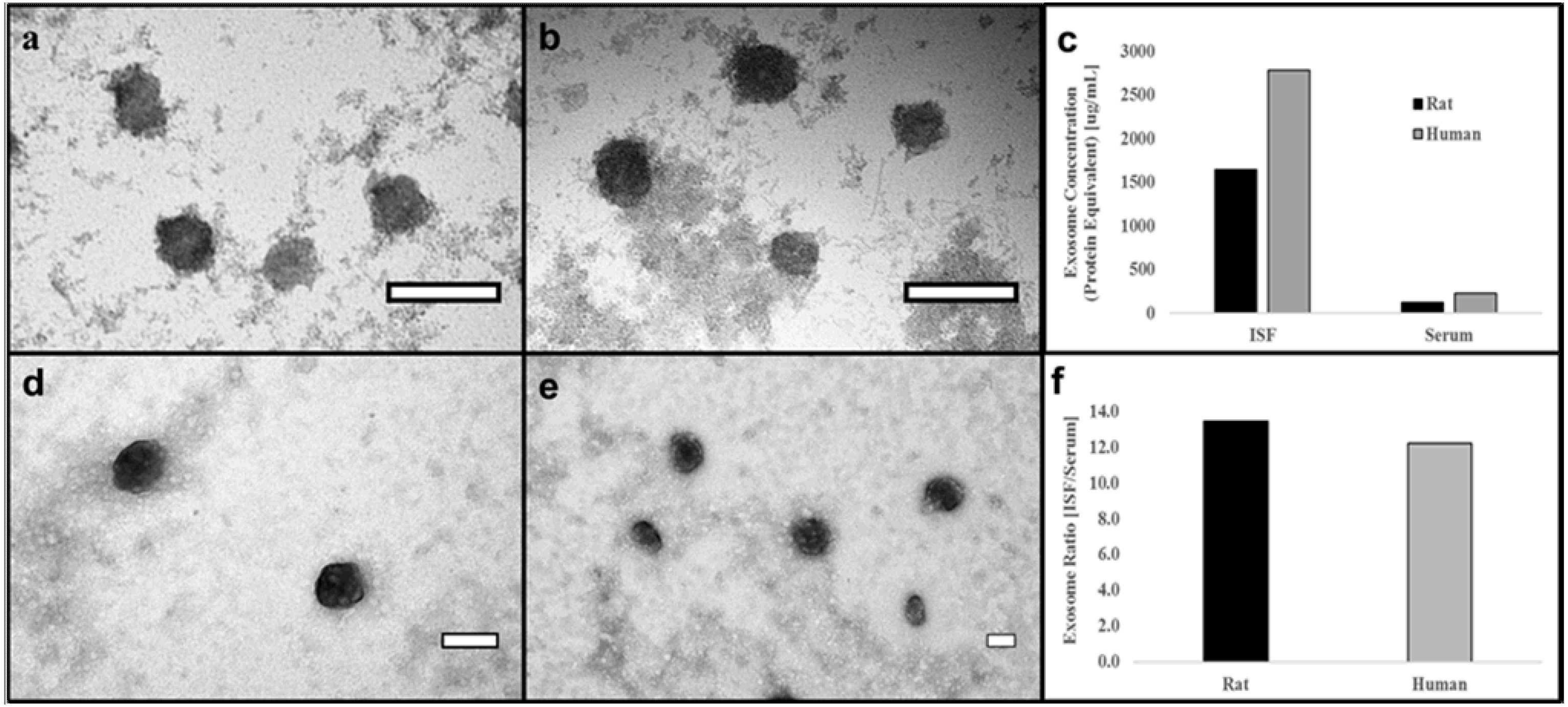

Exosome concentrations were higher in both rats and humans compared to serum. TEM images of rat (a and b) and human (d and e) exosomes purified from ISF (a and d) and serum (b and e). Concentrations (protein equivalent) were measured using a nanoDrop spectrophotometer (c). The exosome ratio of ISF vs. serum in rat and human samples is shown in f. Scale bars; a, b, d, and e: 100 nm.

Miller et at, Comm Bio, 2018

# Modeling Acoustic Wave Devices

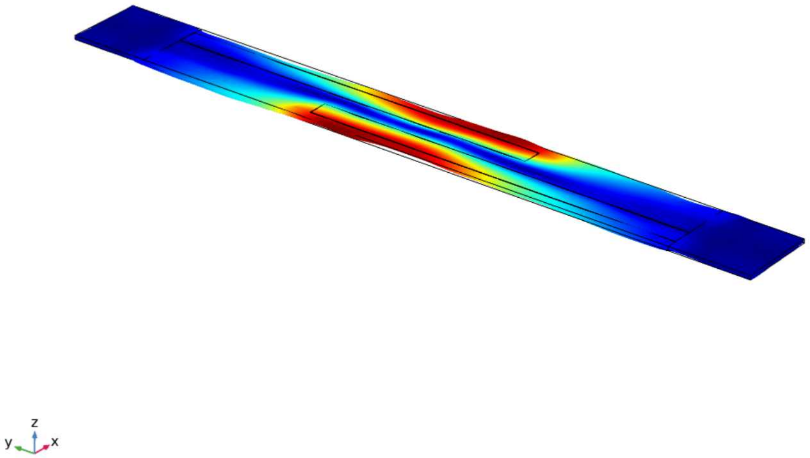

# Simulating Acoustic Wave Behavior from the Material Properties

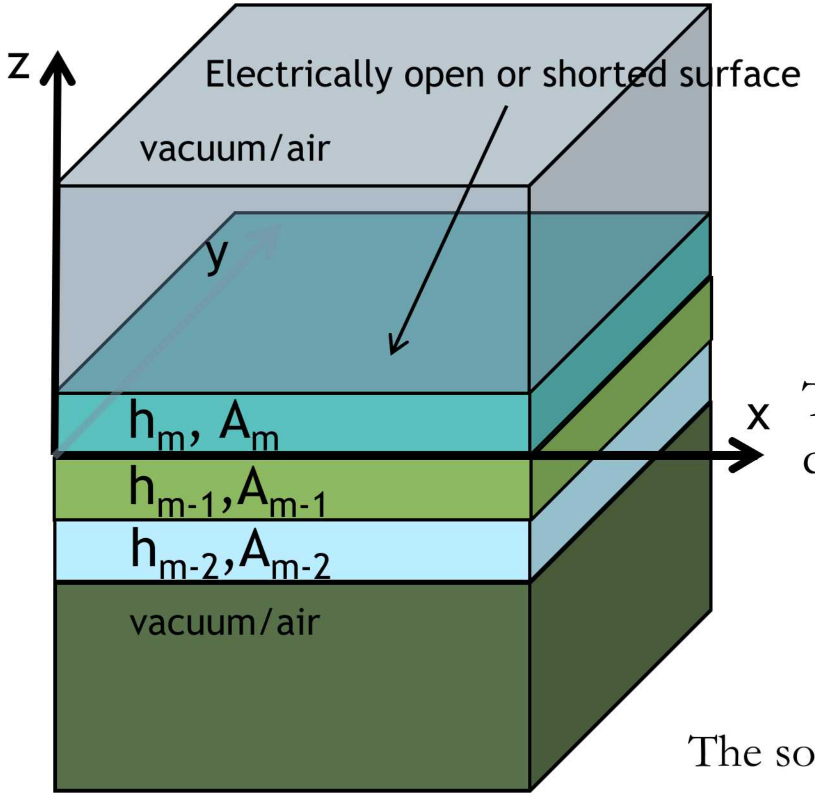

Classic Approach:

$$\frac{d}{dz}\begin{bmatrix}\boldsymbol{U}(z)\\ \boldsymbol{T}(z)\end{bmatrix} = i\boldsymbol{A}\begin{bmatrix}\boldsymbol{U}(z)\\ \boldsymbol{T}(z)\end{bmatrix}$$ Eigenvalue Problem

$\boldsymbol{U} = [u, \phi]^T$ $\quad \boldsymbol{u} = [u_1, u_2, u_3]$ displacement

$\boldsymbol{T} = [\sigma, D_3]^T$ $\quad \boldsymbol{\sigma} = [\sigma_{13}, \sigma_{23}, \sigma_{33}]$ stress

The general anisotropic electro-elastic media acoustic Stroh tensor (A) describes all wave behavior in each layer, (8x8):

$$\boldsymbol{A} = \begin{bmatrix} k_x \boldsymbol{X}\Gamma_{31} & -i\boldsymbol{X} \\ -i\left(\Gamma_{11} - \Gamma_{13}\boldsymbol{X}\Gamma_{31}\right)k_x^2 + i\rho\omega^2 \boldsymbol{I}' & k_x \Gamma_{13}\boldsymbol{X} \end{bmatrix} \qquad \Gamma_{ik} = \begin{bmatrix} c_{1i1k} & c_{1i2k} & c_{1i3k} & e_{k1i} \\ c_{2i1k} & c_{2i2k} & c_{2i3k} & e_{k2i} \\ c_{3i1k} & c_{3i2k} & c_{3i3k} & e_{k3i} \\ e_{i1k} & e_{i2k} & e_{i3k} & -\varepsilon_{ik} \end{bmatrix}$$

The solution above can be expressed by a transfer matrix B:

$$\xi(z+h) = B\xi(z)$$

$$B = e^{iAh}$$

The total transition matrix is product of individual layers:

$$B_J = B_j \prod_{i=1}^{J-1} B_i$$

# Simulating Acoustic Wave Behavior from the Material Properties, cont'd

**To avoid numerical instabilities, we convert the Transfer matrix (B) to a Stiffness matrix (K) then add up the thin layers recursively:**

$$B_J = B_j \prod_{i=1}^{J-1} B_i = \left[ B_{II}(h) \right]^N \Big|_{h/\lambda << 1} = \boldsymbol{B}_{II} = \left( I - i\frac{h}{2}\boldsymbol{A} \right)^{-1} \left( I + i\frac{h}{2}\boldsymbol{A} \right)$$

**Transforms the Asymptotic Transfer Matrix (B) to an Asymptotic Stiffness Matrix (K):**

$$\boldsymbol{K} = \begin{bmatrix} \boldsymbol{B}_{22}(\boldsymbol{B}_{12})^{-1} & \boldsymbol{B}_{21} - \boldsymbol{B}_{22}(\boldsymbol{B}_{12})^{-1}\boldsymbol{B}_{11} \\ (\boldsymbol{B}_{12})^{-1} & -(\boldsymbol{B}_{12})^{-1}\boldsymbol{B}_{11} \end{bmatrix} = K_{II} = \begin{bmatrix} \frac{\Gamma_{33}}{h} - (\Gamma_{31} - \Gamma_{13})\frac{ik_x}{2} + \frac{\Gamma_{11}hk_x^2}{4} - \frac{\rho h\omega^2}{4}I' & -\frac{\Gamma_{33}}{h} - (\Gamma_{31} + \Gamma_{13})\frac{ik_x}{2} + \frac{\Gamma_{11}hk_x^2}{4} - \frac{\rho h\omega^2}{4}I' \\ \frac{\Gamma_{33}}{h} - (\Gamma_{31} + \Gamma_{13})\frac{ik_x}{2} - \frac{\Gamma_{11}hk_x^2}{4} + \frac{\rho h\omega^2}{4}I' & -\frac{\Gamma_{33}}{h} - (\Gamma_{31} - \Gamma_{13})\frac{ik_x}{2} - \frac{\Gamma_{11}hk_x^2}{4} + \frac{\rho h\omega^2}{4}I' \end{bmatrix}$$

**K relates the displacement at layer m-1 to layer m:**

$$\begin{bmatrix} T(z+h) \\ T(z) \end{bmatrix} = K \begin{bmatrix} U(z+h) \\ U(z) \end{bmatrix} \qquad \begin{bmatrix} \boldsymbol{u} \\ \varphi \end{bmatrix} = \boldsymbol{G_S} \begin{bmatrix} \sigma \\ \gamma \end{bmatrix}, \boldsymbol{G_S} = \begin{bmatrix} S_S^f + \alpha\eta S_S^{fe} S_S^{ef} & -\alpha S_S^{fe} \\ \alpha S_S^{ef} & -\alpha S_S^e \end{bmatrix}$$

**This is convenient since it allows easy calculation of the "Green's Function" and "Effective Permittvity" which tells us where piezoelectric or non-piezoelectric modes exist:**

$$\varepsilon_{eff}(k_x,\omega) = \frac{D_3^{top}(k) - D_3^{bot}(k)}{|k_x| \cdot \phi(k_x,\omega)} = \frac{\bar{\sigma}(k_x,\omega)}{|k_x| \cdot \bar{\phi}(k_x,\omega)} = \varepsilon_o - \frac{1}{|k_x| G_s(4,4)}$$

# Simulating Acoustic Wave Behavior from the Material Properties, cont’d

Example: 128° Y-rotated X-propagating Lithium Niobate (0,38,0), <z,x,z>

Rayleigh SAW:

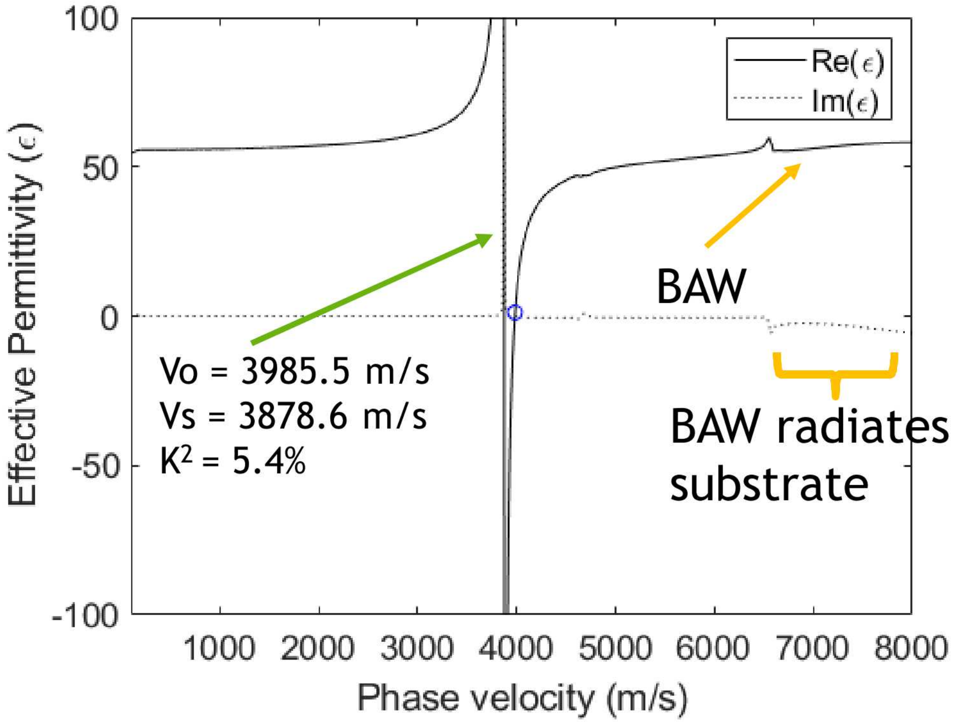

BAW

Vo = 3985.5 m/s
Vs = 3878.6 m/s
$K^2$ = 5.4%

BAW radiates into substrate

Example: 64° Y-rotated X-propagating Lithium Niobate (0,-26,0), <z,x,z>

Rayleigh SAW, Leaky SAW, and BAW

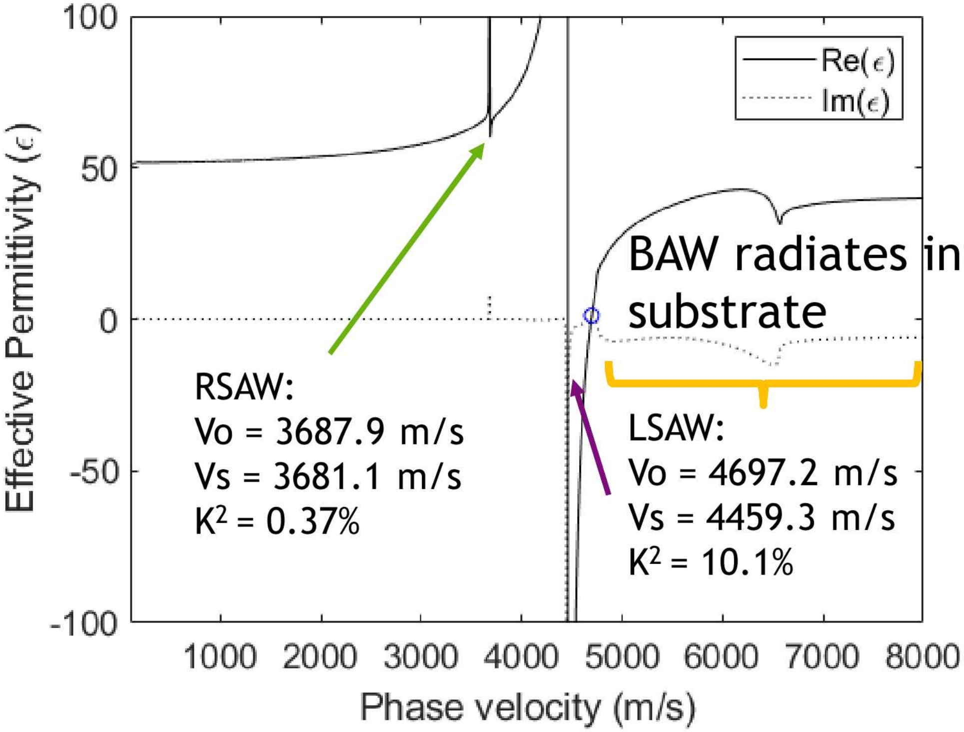

BAW radiates into substrate

RSAW:
Vo = 3687.9 m/s
Vs = 3681.1 m/s
$K^2$ = 0.37%

LSAW:
Vo = 4697.2 m/s
Vs = 4459.3 m/s
$K^2$ = 10.1%

# Ambiguity in Calculating Electromechanical Coupling

Formal Definition of Electromechanical Coupling:

$$K^2 = -2\varepsilon_o \operatorname{Res}\left(\bar{G}_{4,4}(k,0)\right) = -2\varepsilon_o G_{4,4}\Big|_{k=k_m} \quad \neq$$

R.F. Milsom et al. 1977, Y. Jin et al. 1991

Approximate Calculation of Electromechanical Coupling:

$$K^2 \approx 2\left(\frac{V_{open} - V_{short}}{V_{open}}\right)$$

$\frac{h}{\lambda} > 1$ For certain modes (e.g. Lamb), variation of the particle displacement is highly perturbed for the metallized case

---

Thickness modes (BAW):

$$k_t^2 = \frac{\frac{\pi f_r}{2 f_a}}{\tan\left(\frac{\pi f_r}{2 f_a}\right)}$$

Warner et al. 1966

$$k_t^2 = \frac{\pi}{2}\frac{f_r}{f_a}\tan\left(\frac{\pi}{2}\frac{f_a - f_r}{f_a}\right) \approx \frac{\pi^2}{4}\frac{(f_a - f_r)}{f_a}$$

D. Royer pg. 27 vol I

$$K^2 = \frac{\pi^2}{4}\frac{f_r(f_a - f_r)}{f_a^2}$$

N. F. Naumenko et al. e.g. Author intended $kt^2$ and not $K^2$

# Ambiguity in Calculating Electromechanical Coupling, cont'd

$$K^2 = \frac{e^2}{\varepsilon^S c^E}$$

B.A. Auld pg. 307 vol I
J. F. Rosenbaum pg. 146

$$k_t^2 = \frac{e^2}{\varepsilon^S\left(c^E + \frac{e^2}{\varepsilon^S}\right)} = \frac{\frac{e^2}{\varepsilon^S c^E}}{1+\frac{e^2}{\varepsilon^S c^E}} = \frac{K^2}{1+K^2}$$

$$k_t^2 = \frac{K^2}{1+K^2}$$

J.F Rosenbaum pg. 146

Thus, $k_t^2 < K^2$

$$k_t^2 = \frac{e^2}{\varepsilon^S c^D}$$

B.A. Auld pg. 322 vol I

Subscript "*t*" requires that the electric field is applied across the thickness of the crystal.

Note: In weak piezoelectric materials $k_t^2$ and $K^2$ are nearly identical, such as ZnO, $K^2 = 0.08$ implies $k_t^2 = 0.074$

If the device is not excited through the thickness the proper designation is to use big $K^2$.

Quick Proof: $K^2$ interpretation is the ratio of the **electrical** to **mechanical energy**:

$$\frac{u_E}{u_M} = \frac{\varepsilon^S E^2}{c^E S^2}, \because D = 0$$ inside piezoelectric, $$D = \varepsilon^S : E + e : S = 0 \rightarrow E = -\frac{eS}{\varepsilon^S} \rightarrow \frac{u_E}{u_M} = \frac{e^2}{c^E \varepsilon^S} = K^2$$

# Using the Green's function Method to Sweep an Euler Angle

X-cut LN as a thin plate with stress-free boundary conditions on top and bottom:

$\sigma$ **= 0** and $\phi$ **= 0** (short) **or** $\gamma$ **= 0** (open)

Advantages: Fast (10 min), no mode sorting

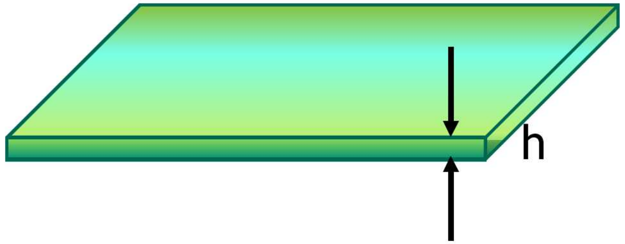

SH mode

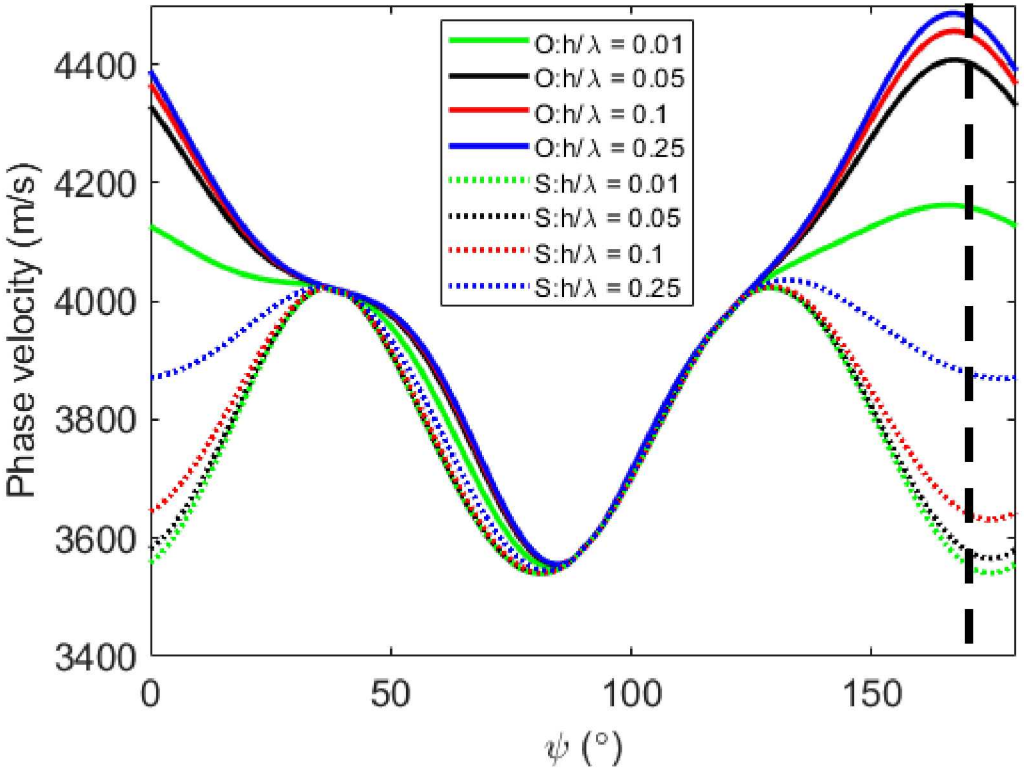

SH mode

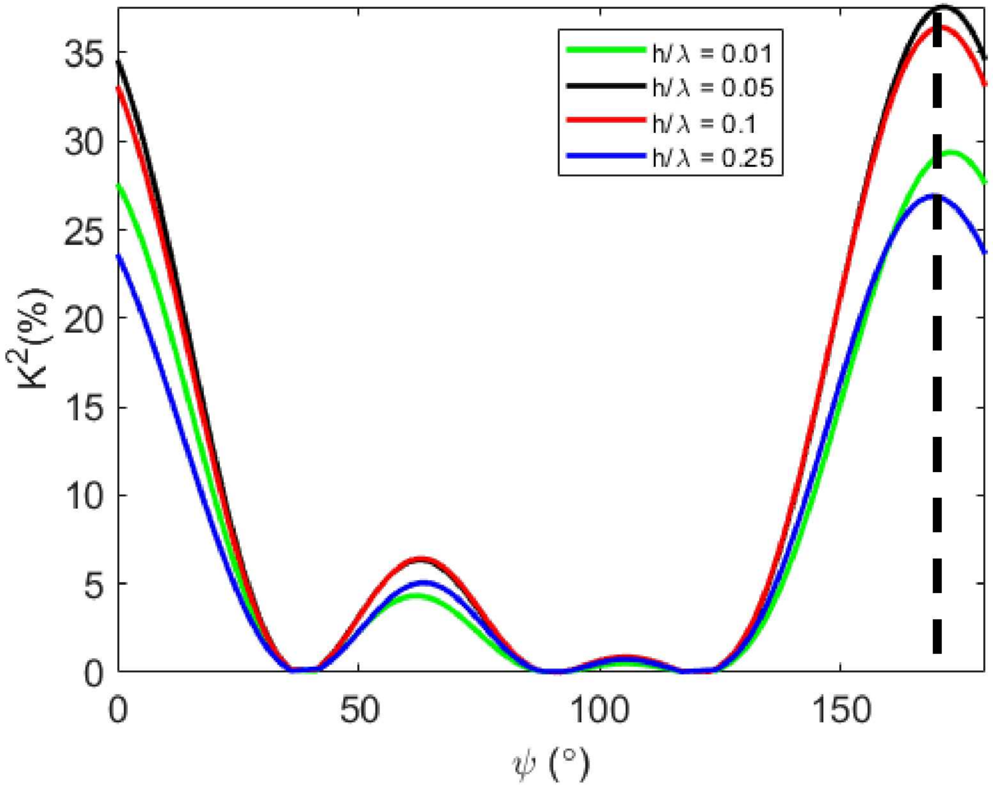

# Using the Green's function Method to Sweep an Euler Angle

Y-cut LN as a thin plate with stress-free boundary conditions on top and bottom:
$\sigma$ = **0** and $\phi$ = **0** (short) **or** $\gamma$ = **0** (open)
Advantages: Fast (10 min), no mode sorting

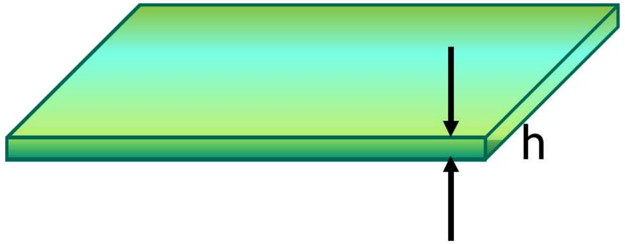

S0 mode

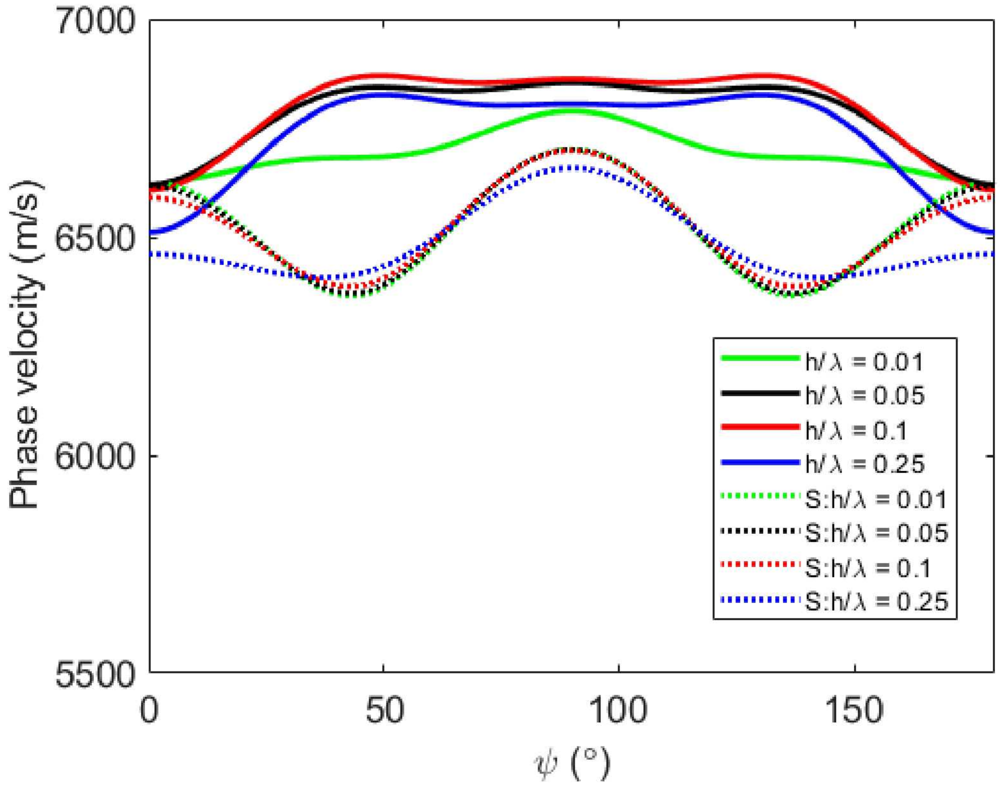

S0 mode

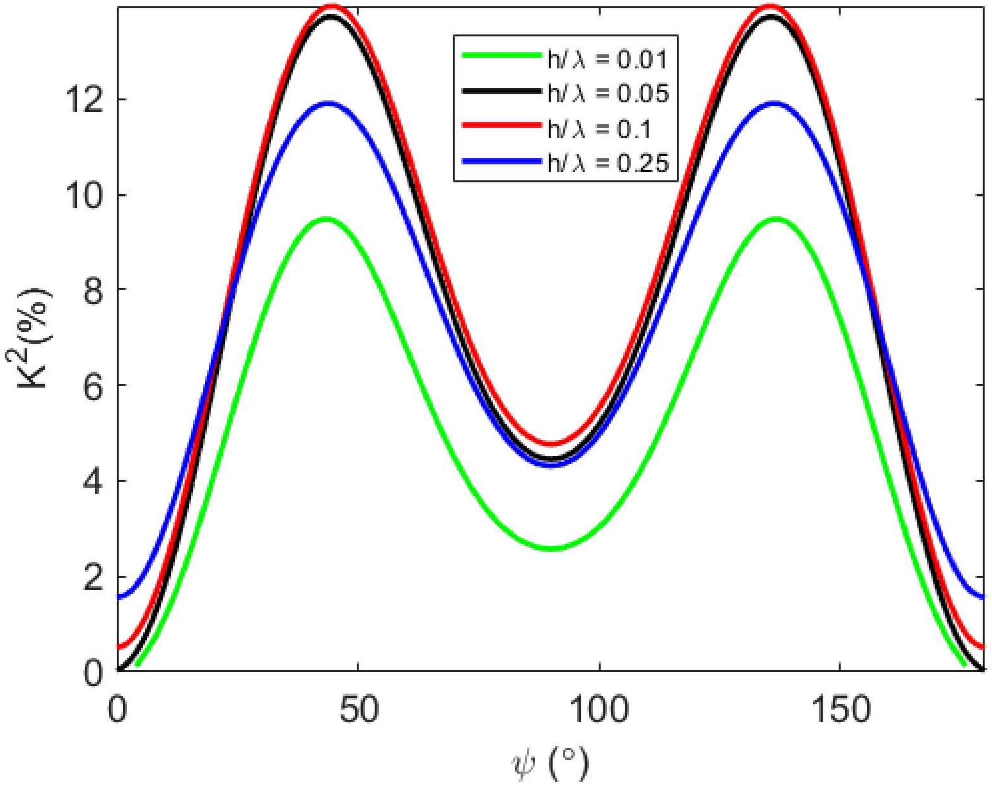

# X-cut LN Thin Plate: SH mode

Lithium niobate. free-bottom, no bottom electrode, h = 1.2 um, $h/\lambda = 0.1$

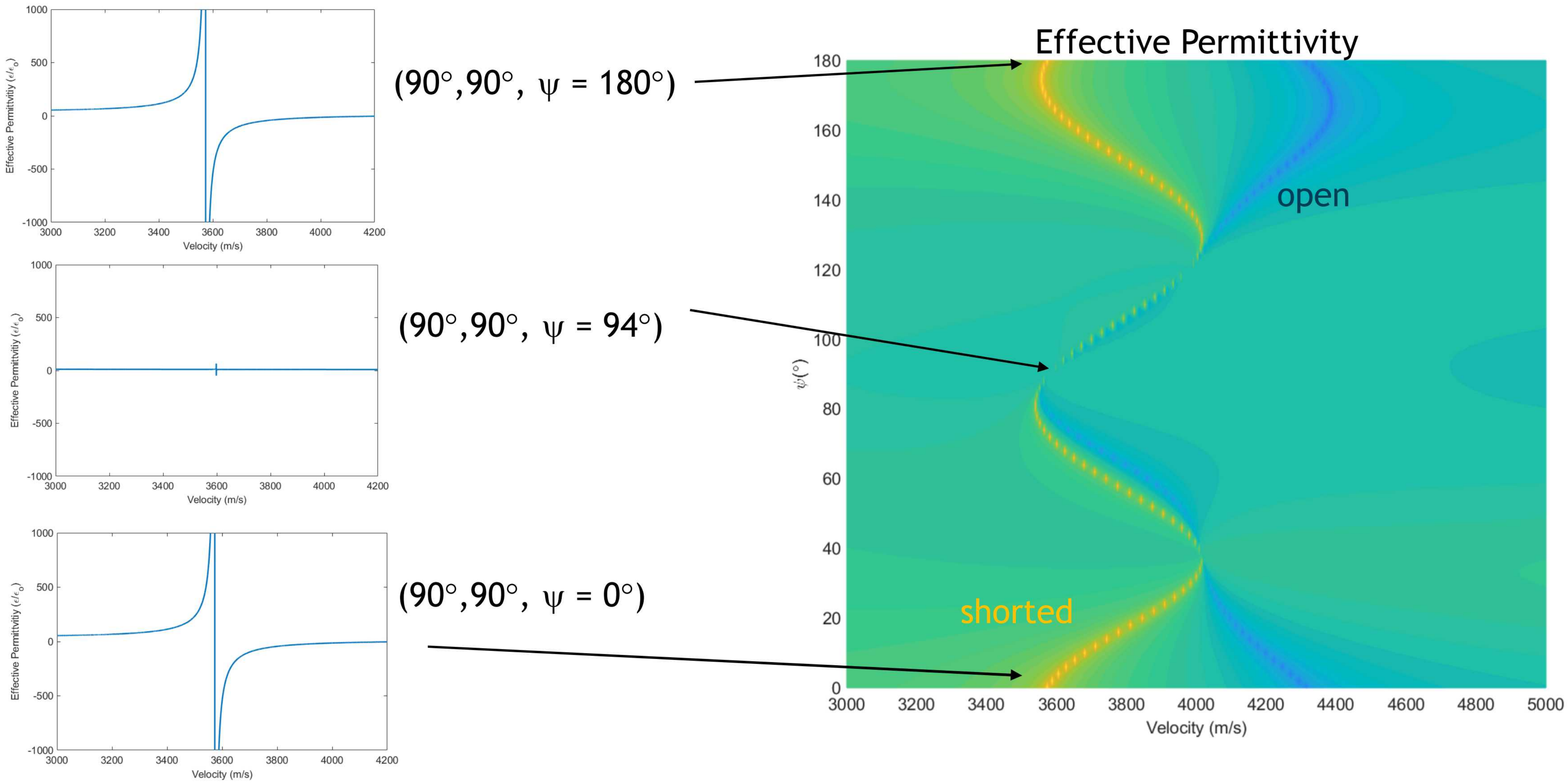

(90°,90°, $\psi$ = 180°)

(90°,90°, $\psi$ = 94°)

(90°,90°, $\psi$ = 0°)

# Piezoelectric/Piezomagnetic Layered Modeling

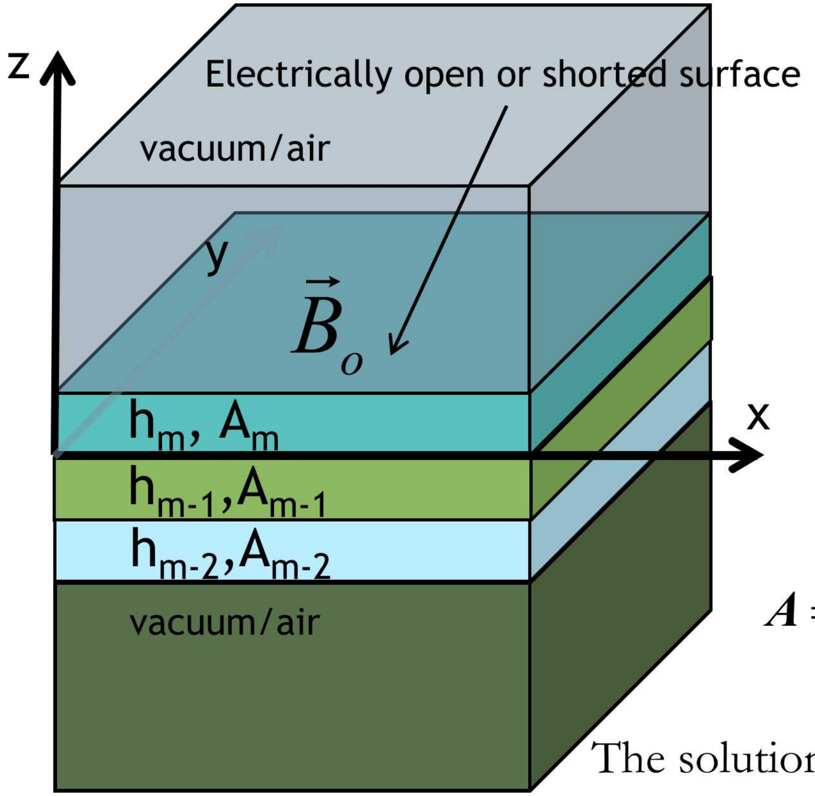

Approach:

$$\frac{d}{dz}\begin{bmatrix} \boldsymbol{U}(z) \\ \boldsymbol{T}(z) \end{bmatrix} = i\boldsymbol{A}\begin{bmatrix} \boldsymbol{U}(z) \\ \boldsymbol{T}(z) \end{bmatrix}$$ Eigenvalue Problem

$\boldsymbol{U} = [u, \phi, \psi]^T \qquad \boldsymbol{u} = [u_1, u_2, u_3]$ displacement

$\boldsymbol{T} = [\sigma, D_3, B_3]^T \qquad \boldsymbol{\sigma} = [\sigma_{13}, \sigma_{23}, \sigma_{33}]$ stress

The general anisotropic electro-elastic media acoustic Stroh tensor (A) describes all wave behavior in each layer, (8x8):

$$\boldsymbol{A} = \begin{bmatrix} k_x \boldsymbol{X}\Gamma_{31} & -i\boldsymbol{X} \\ -i\left(\Gamma_{11} - \Gamma_{13}\boldsymbol{X}\Gamma_{31}\right)k_x^2 + i\rho\omega^2 \boldsymbol{I}' & k_x \Gamma_{13}\boldsymbol{X} \end{bmatrix}$$

$$\Gamma_{ik} = \begin{bmatrix} c_{1i1k} & c_{1i2k} & c_{1i3k} & e_{k1i} & q_{k1i} \\ c_{2i1k} & c_{2i2k} & c_{2i3k} & e_{k2i} & q_{k2i} \\ c_{3i1k} & c_{3i2k} & c_{3i3k} & e_{k3i} & q_{k3i} \\ e_{i1k} & e_{i2k} & e_{i3k} & -\varepsilon_{ik} & -\alpha_{ik} \\ q_{i1k} & q_{i2k} & q_{i3k} & -\alpha_{ik} & -\mu_{ik} \end{bmatrix}$$

The solution can be expressed as a transfer matrix B:

$$\xi(z+h) = B\xi(z)$$

$$B = e^{iAh} \qquad B_J = B_j \prod_{i=1}^{J-1} B_i$$

# Piezoelectric/Piezomagnetic Layered Modeling

In the Quasi-Static approximation for magneto-electro-elastic solid:

$$T_{ij,j} = \rho \frac{\partial^2 u_i}{\partial t^2}, D_{i,j} = 0, B_{j,j} = 0$$

$$E_i = -\phi_i, H_i = -\psi_i$$ Electric and Magnetic Potentials

Then,

$$T_{ij,j} = c_{ijkl} u_{k,l} + e_{lij} \phi_l + q_{lij} \psi_l$$

$$D_i = e_{ikl} u_{k,l} - \varepsilon_{il} \phi_l - \alpha_{il} \psi_l$$

$$B_i = q_{ikl} u_{kl} - \alpha_{il} \phi_l - \mu_{il} \psi_l$$

Units:
c: N/m$^2$
e: C/m$^2$
ε: F/m

magnetoelectric, α: C/A·m
magnetic permeability, μ: N/A$^2$
piezomagnetic, q: N/A·m

Write solution as stiffness matrix:

$$K = \begin{bmatrix} B_{22}(B_{12})^{-1} & B_{21} - B_{22}(B_{12})^{-1} B_{11} \\ (B_{12})^{-1} & -(B_{12})^{-1} B_{11} \end{bmatrix}$$

Define a Piezoelectric/Magnetic Green's function:

$$\begin{bmatrix} u_1 \\ u_2 \\ u_3 \\ \phi \\ \psi \end{bmatrix} = \boldsymbol{S} \begin{bmatrix} T_{13} \\ T_{23} \\ T_{33} \\ D_3 \\ B_3 \end{bmatrix} = \begin{bmatrix} \boldsymbol{S}_S^f & \boldsymbol{S}_S^{fe} & S_S^{fm} \\ \boldsymbol{S}_S^{ef} & S_S^e & S_S^{em} \\ S_S^{mf} & S_S^{me} & S_S^m \end{bmatrix} \begin{bmatrix} \boldsymbol{T}_n \\ D_{3n} \\ B_3 \end{bmatrix} = \begin{bmatrix} \boldsymbol{S}_S^f & \boldsymbol{S}_S^{fe} & S_S^{fm} \\ \boldsymbol{S}_S^{ef} & S_S^e & S_S^{em} \\ S_S^{mf} & S_S^{me} & S_S^m \end{bmatrix} \begin{bmatrix} \boldsymbol{T}_n \\ \eta\phi_n - \gamma_n \\ B_3 - B_o \end{bmatrix}$$

$$\begin{bmatrix} u_1 \\ u_2 \\ u_3 \\ \phi \\ \psi \end{bmatrix} = \boldsymbol{G} \begin{bmatrix} T_{13} \\ T_{23} \\ T_{33} \\ \gamma_n \\ B_o \end{bmatrix}$$

Comsol Approach: couple Solid, Electrostatics, Magnetostatics:
e.g. top boundary conditions:

$$T_{13} = T_{23} = T_{33} = D_3 = B_3 = 0$$

$$T_{13} = T_{23} = T_{33} = \varphi_n = \psi_n = 0$$

# Comsol: Simulating Surface Acoustic Wave (SAW) on 128° Y – rotated X propagating Lithium Niobate

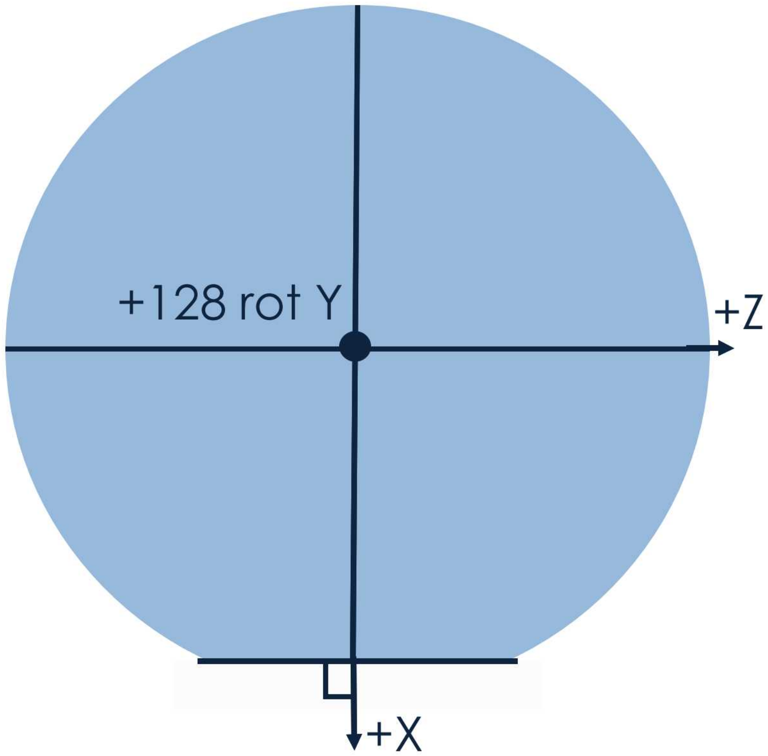

128° YX LN: <z,x,z>(0,38,0)

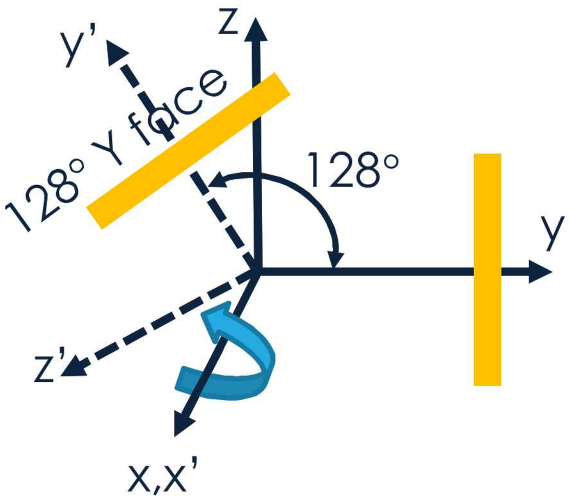

**Comsol rotates the coordinate system not the material tensors**

1. Draw a slab in Comsol then apply rotation using the rotated system: (0,38,0) for 128YX LN
2. Comsol rotates the coordinate axis from the drawn axis and which is viewed by plotting the coordinate system:

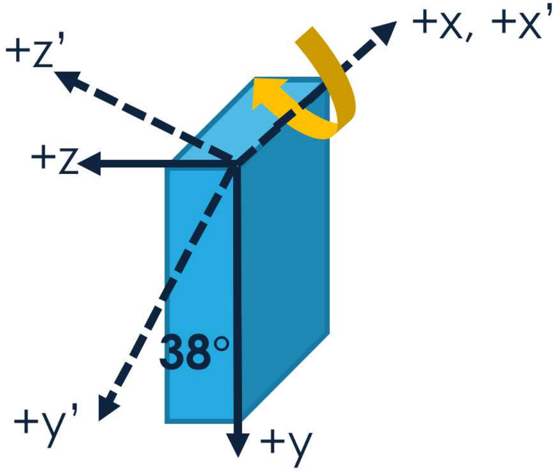

Comsol rotated axis: z'y' plane

# Comsol: Getting the Rotation Correct: YZ Lithium Niobate (0,90,90), <z,x,z>

Comsol drawn block:

Definition of Y-cut

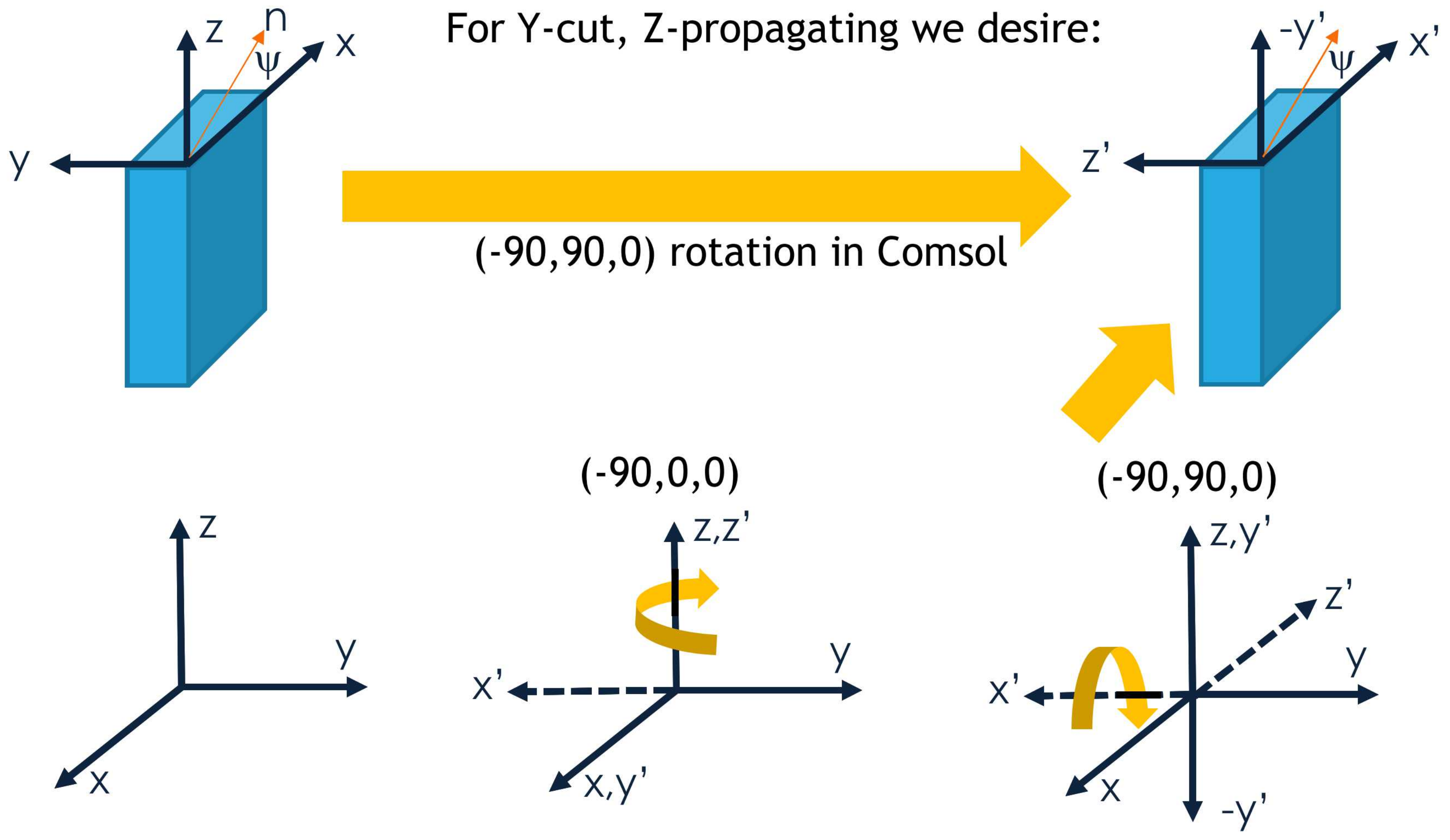
For Y-cut, Z-propagating we desire:

(-90,90,0) rotation in Comsol

(-90,0,0)

(-90,90,0)

Three Options:

1. Define the model in the unrotated axis then apply Euler rotation to obtain desired cut and orientation.
2. Draw the model in the rotated cut if possible then apply additional rotation if needed.
3. Draw the model in the unrotated axis and rotate the material tensors directly using Euler rotation matrix.

# Comsol: Getting the Rotation Correct, cont'd

**X-cut:**
**90,90,ψ**

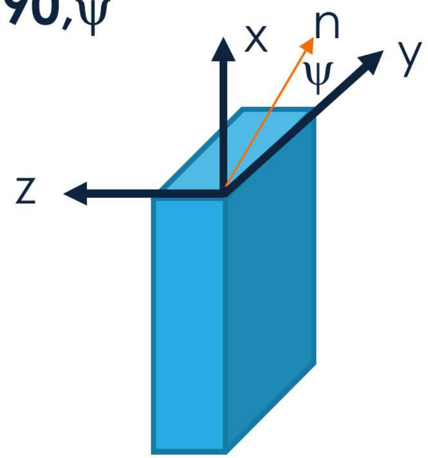

**Y-cut:**
**0,90,ψ**

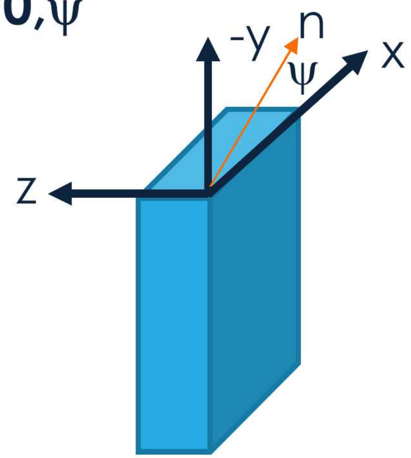

**Z-cut:**
**0,0,ψ**

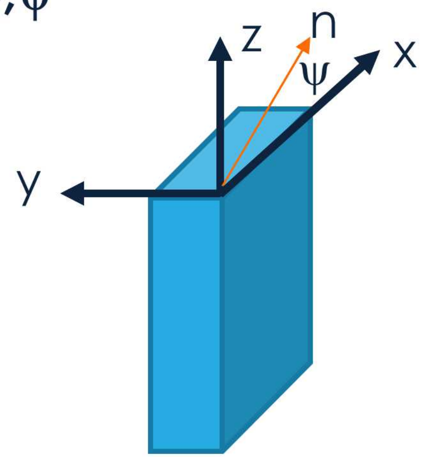

---

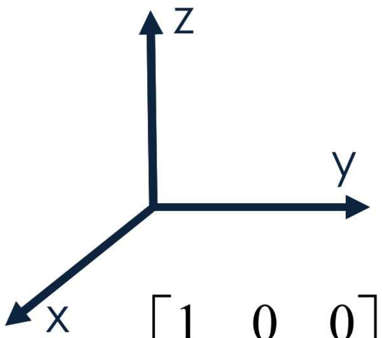

$$M = \begin{bmatrix} 1 & 0 & 0 \\ 0 & 1 & 0 \\ 0 & 0 & 1 \end{bmatrix}$$

Rotation Matrix (Auld vol I, 1990)

$$A = \overset{\textbf{z}}{\begin{bmatrix} \cos(\psi) & \sin(\psi) & 0 \\ -\sin(\psi) & \cos(\psi) & 0 \\ 0 & 0 & 1 \end{bmatrix}} \overset{\textbf{x}}{\begin{bmatrix} \cos(\phi) & \sin(\phi) & 0 \\ -\sin(\phi) & \cos(\phi) & 0 \\ 0 & 0 & 1 \end{bmatrix}} \overset{\textbf{z}}{\begin{bmatrix} 1 & 0 & 0 \\ 0 & \cos(\theta) & \sin(\theta) \\ 0 & -\sin(\theta) & \cos(\theta) \end{bmatrix}}$$

# Comsol: Getting the Rotation Correct, cont'd

Using X-cut rotation (90,90,170) for large SH mode where $K^2$ = 35% @ $h/\lambda$ =0.1

$$A = \begin{bmatrix} 0 & -0.9848 & 0.1736 \\ 0 & -0.1736 & -0.984 \\ 1 & 0 & 0 \end{bmatrix}$$

Base vector rotation is: $$M / A = \begin{bmatrix} 0 & 0 & 1 \\ -0.9848 & -0.1736 & 0 \\ 0.1736 & -0.9848 & 0 \end{bmatrix}$$

Enter into Comsol's "base vector system"

**At least Four Options to perform rotations:**

1. Define the model in the unrotated axis then apply Euler rotations to obtain desired orientation.

2. Draw the model in the rotated cut if possible then apply additional rotation if needed.

3. Draw the model in the unrotated axis and rotate the material tensors directly using Euler rotation matrix using MATLAB. Downside of this method is can't perform rotations using the sweep option.

4. Draw the model in the unrotated axis and use base vector system to define the rotation. Need to perform rotations in another tool to obtain the "base vector system."

# X-cut SH mode on thin LN plate at 170°deg rotation from y-axis

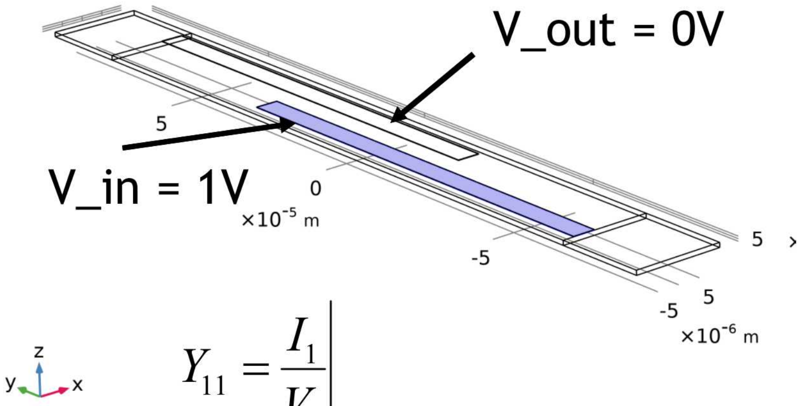
V_out = 0V

V_in = 1V

$$Y_{11} = \left.\frac{I_1}{V_1}\right|_{V_2=0}$$

$$Y_{12} = \left.\frac{I_1}{V_2}\right|_{V_1=0}$$

$$Y_{21} = \left.\frac{I_2}{V_1}\right|_{V_2=0}$$

$$Y_{22} = \left.\frac{I_2}{V_2}\right|_{V_1=0}$$

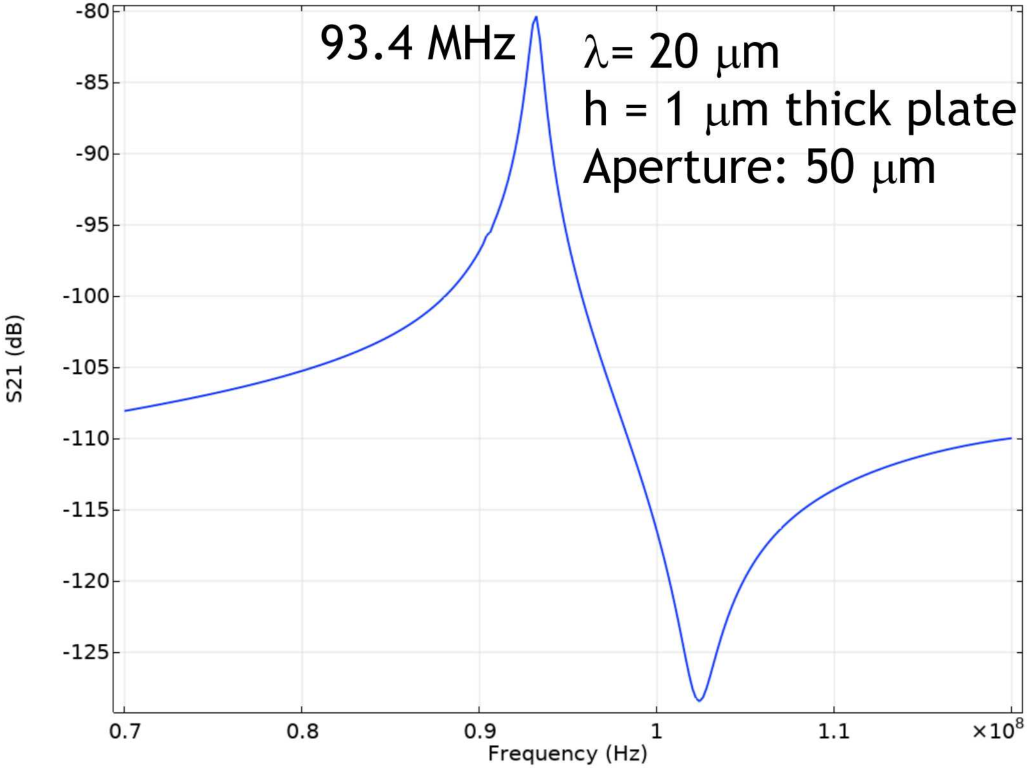
93.4 MHz

$\lambda$= 20 $\mu$m

h = 1 $\mu$m thick plate

Aperture: 50 $\mu$m

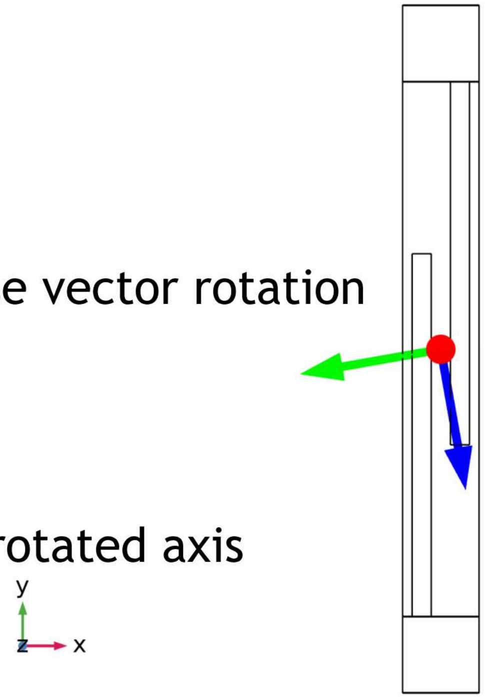
Base vector rotation

Unrotated axis

SH displacement at resonance

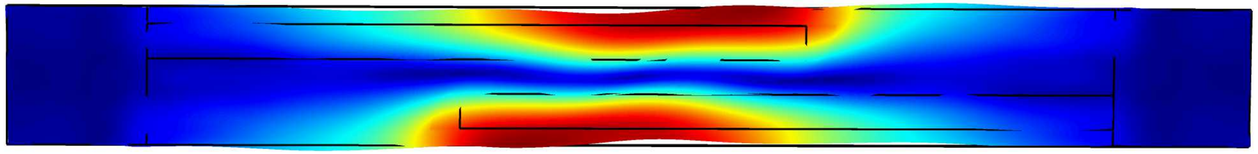

# X-cut SH mode on thin LN plate at 170°deg rotation from y-axis

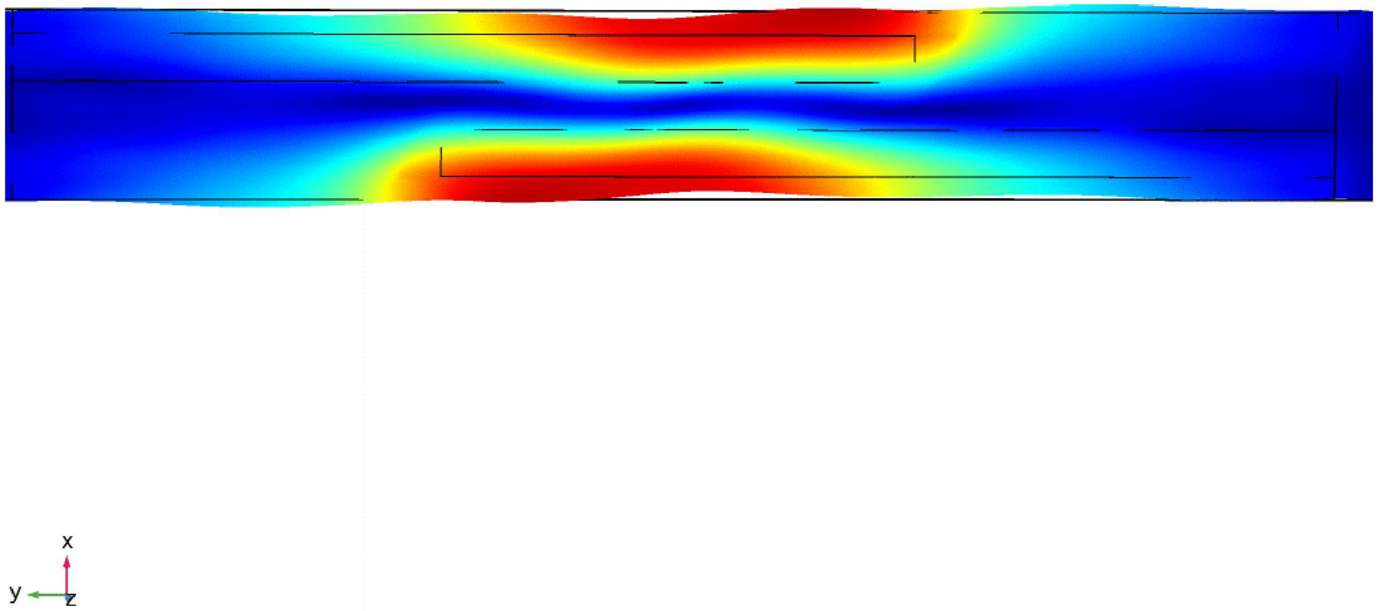

# Comsol: Simulating Surface Acoustic Wave (SAW) on 128° Y – rotated X propagating Lithium Niobate: **Dispersion Plot**

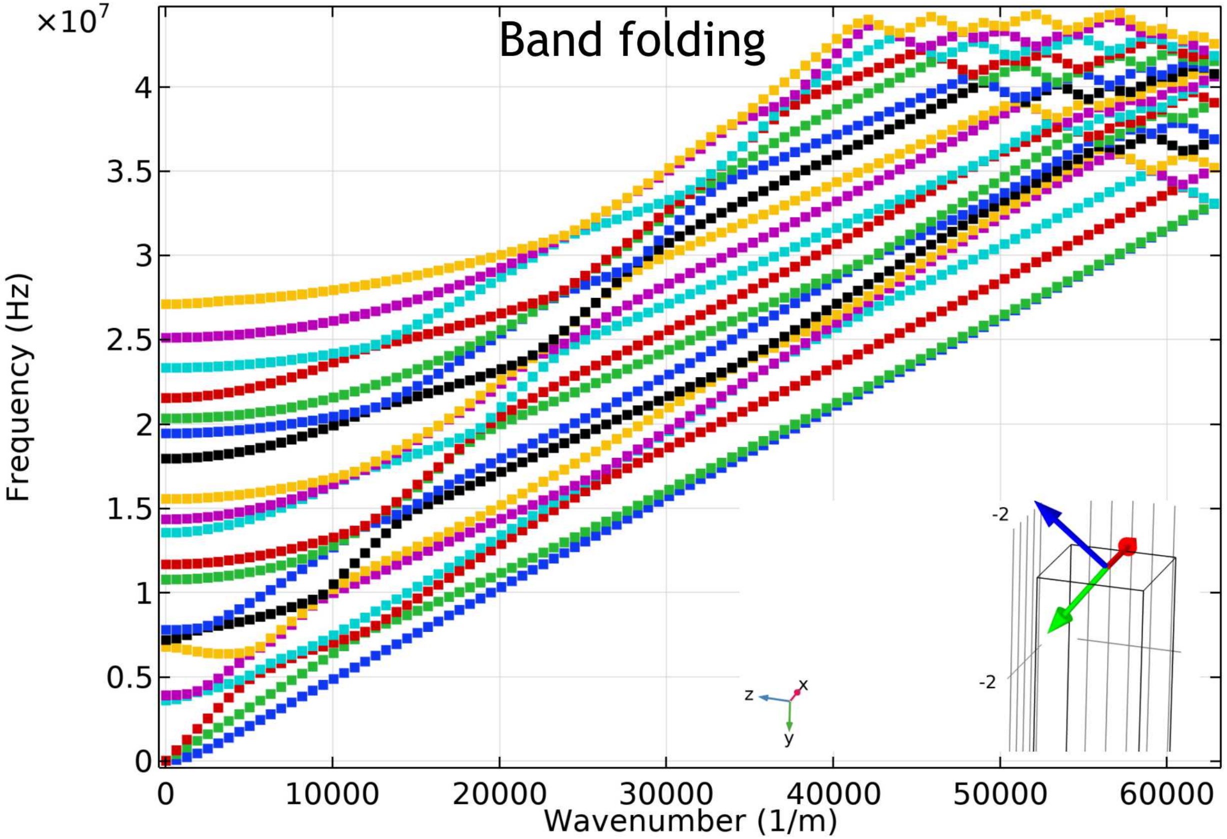

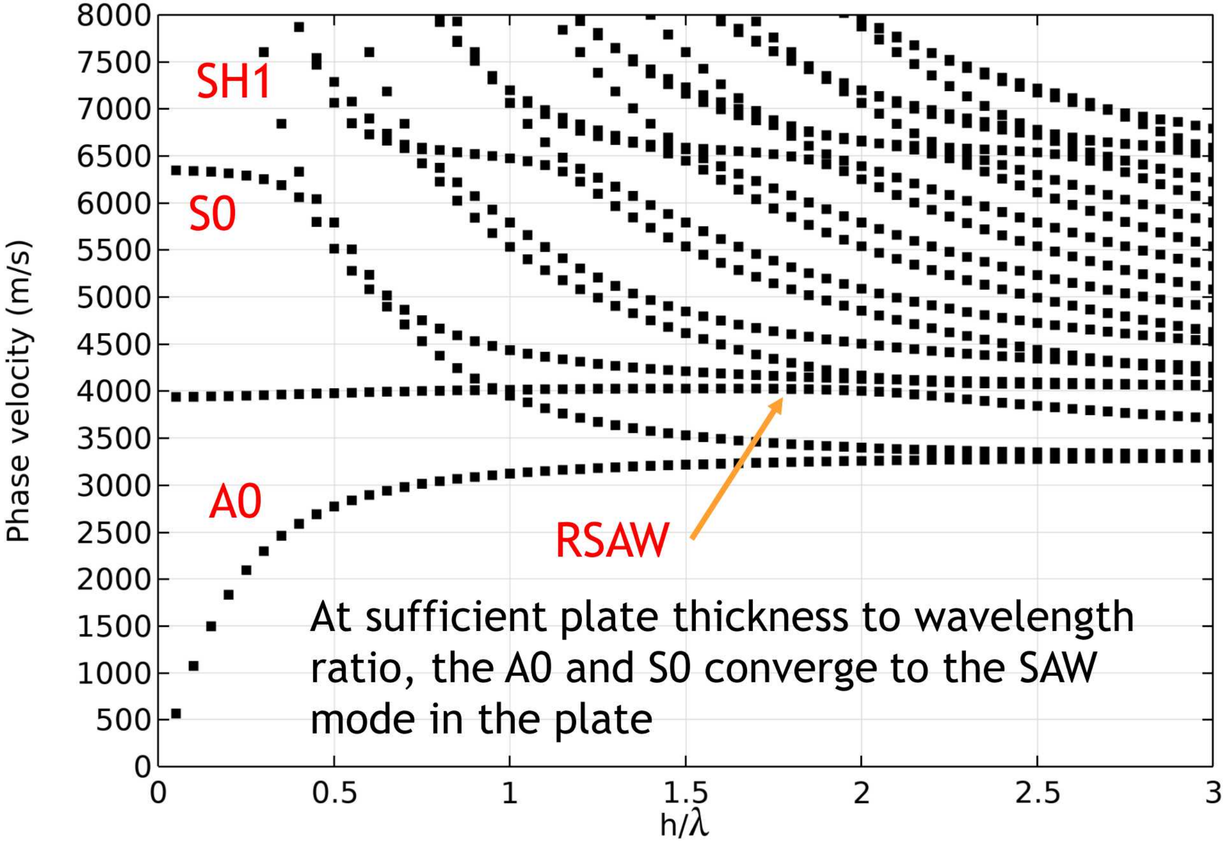

At sufficient plate thickness to wavelength ratio, the A0 and S0 converge to the SAW mode in the plate

$$\frac{hk}{2\pi} = \frac{h}{\lambda}$$

# Comsol: Simulating Surface Acoustic Wave (SAW) on 128° Y – rotated X propagating Lithium Niobate: **Modes**

fr = 485 MHz

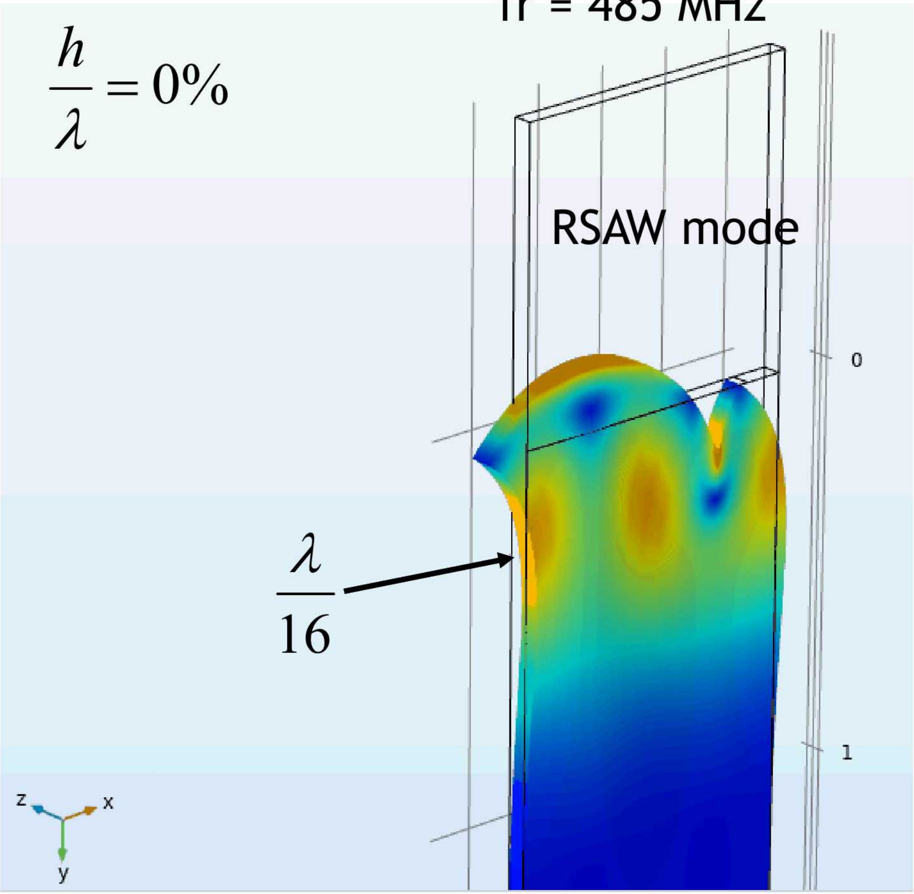

$\frac{h}{\lambda} = 0\%$

RSAW mode

$\frac{\lambda}{16}$

fa = 495.0 MHz

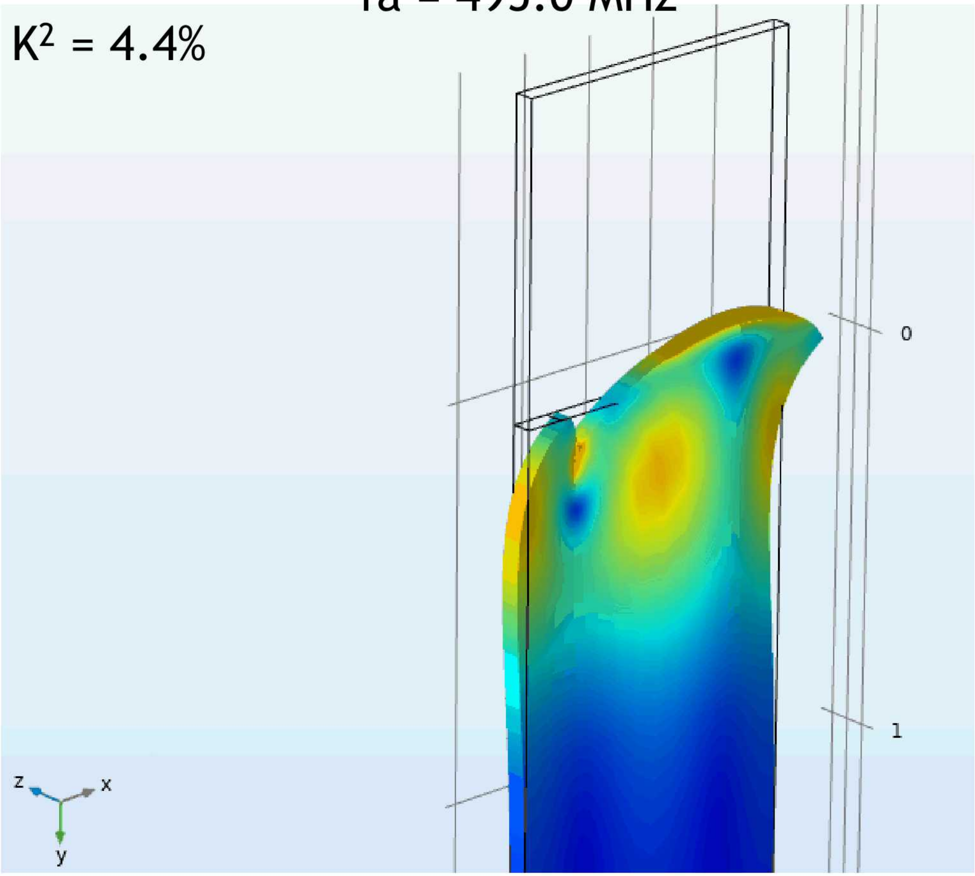

K$^2$ = 4.4%

# Comsol: Simulating Surface Acoustic Wave (SAW) on 128° Y – rotated X propagating Lithium Niobate: **Admittance**

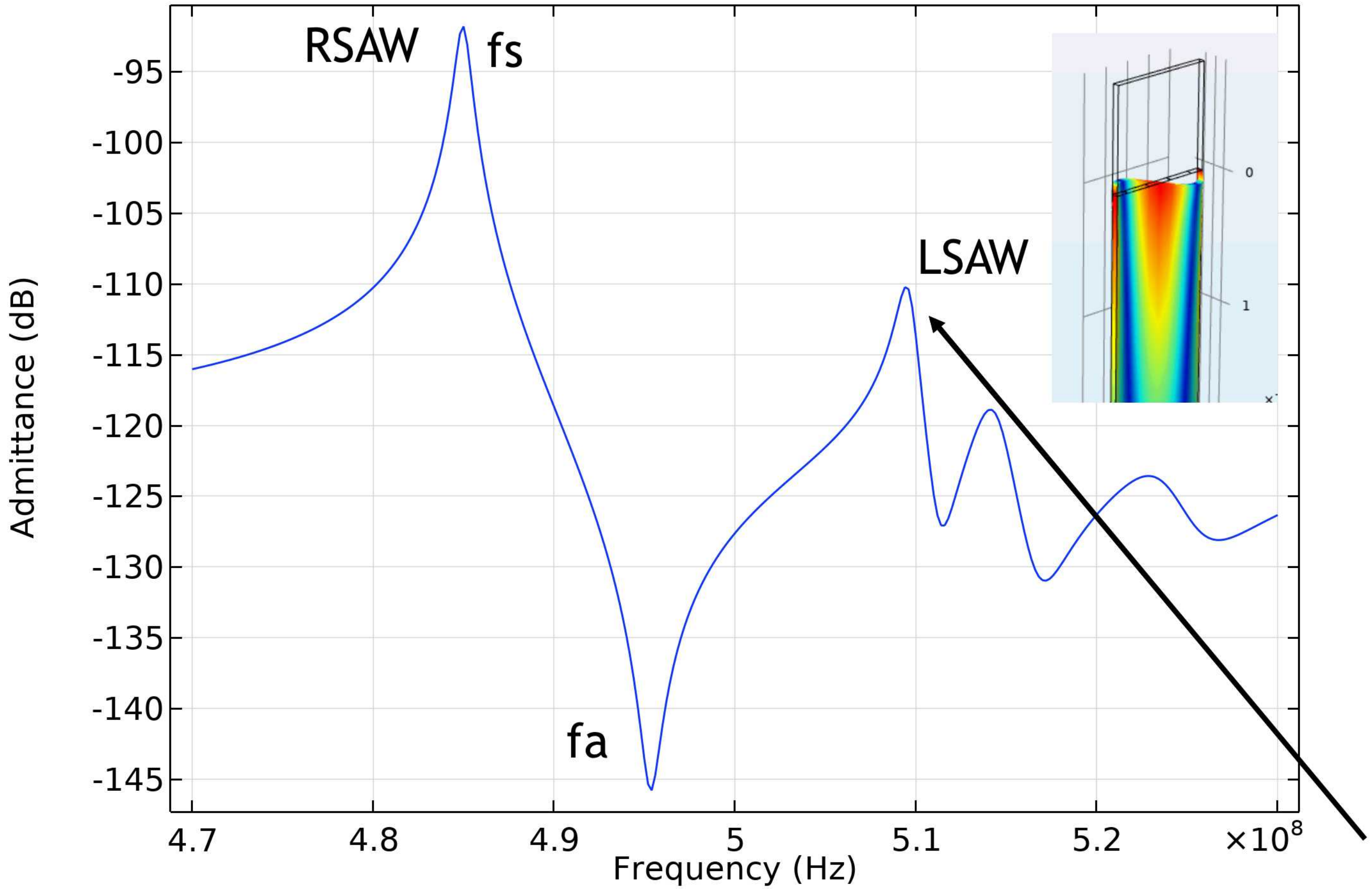

Rotated Coordinate System

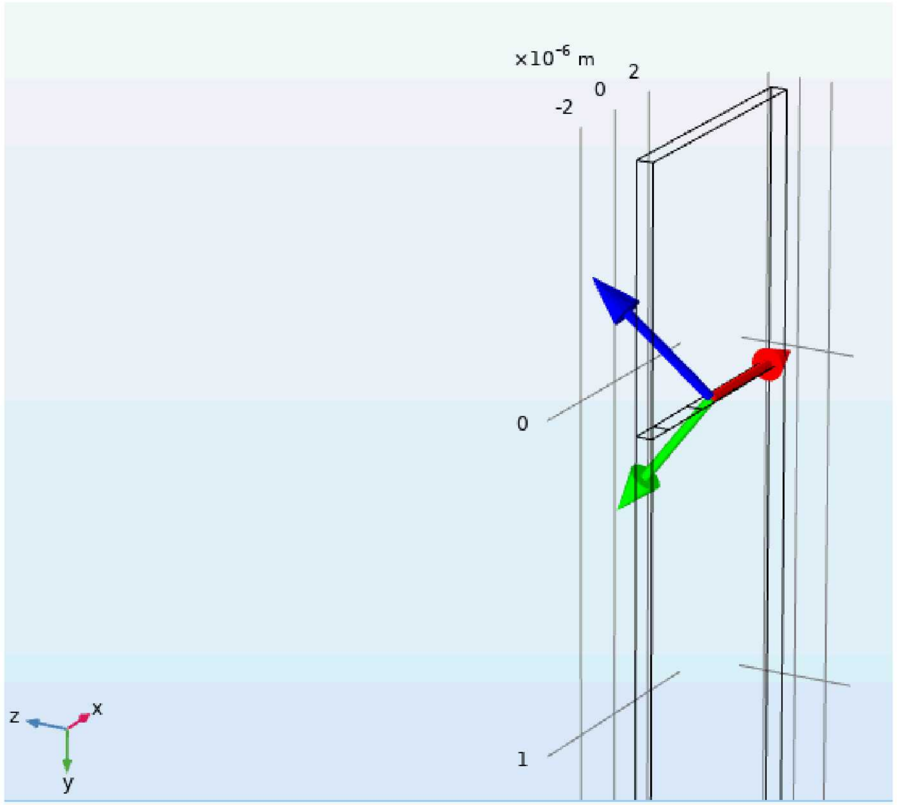

Leaky Surface Acoustic Wave (LSAW).
A true surface wave is confined within one-wavelength from the top surface

# Comsol: Simulating Surface Acoustic Wave (SAW) on 128° Y – rotated X propagating Lithium Niobate: **Admittance Part #2**

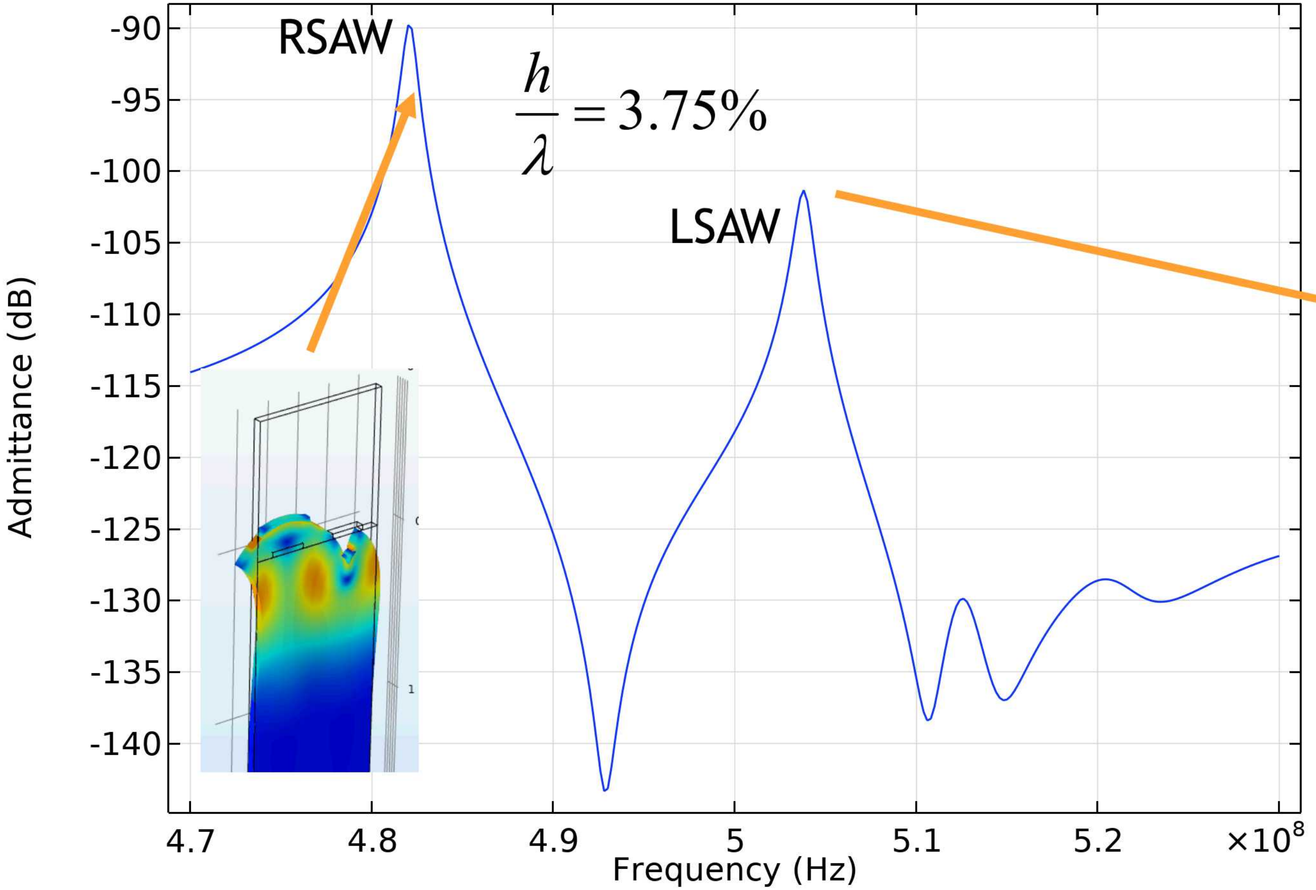

$$\frac{h}{\lambda} = 3.75\%$$

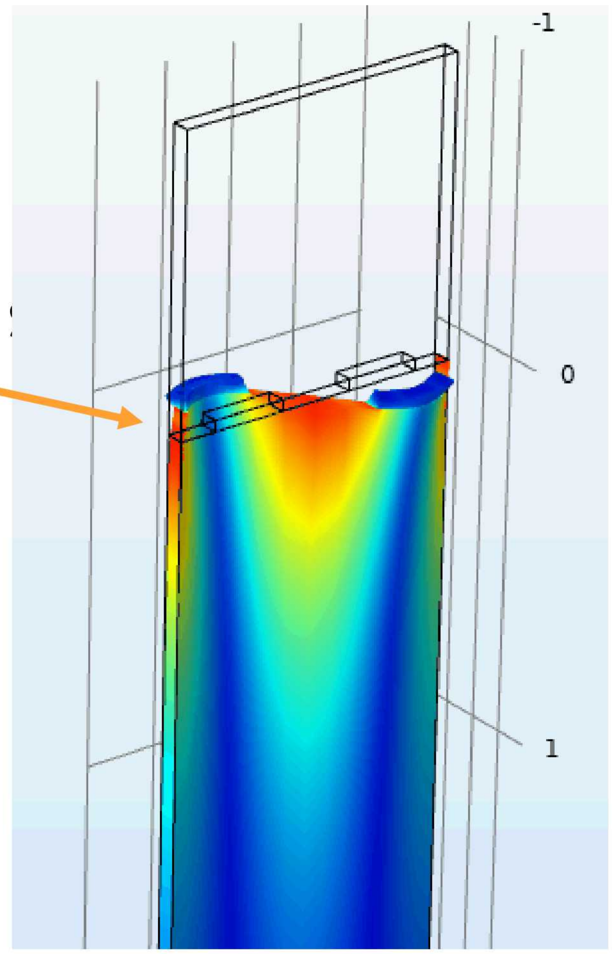

# Simulating Surface Acoustic Wave (SAW) on 64° Y –rotated X propagating Lithium Niobate

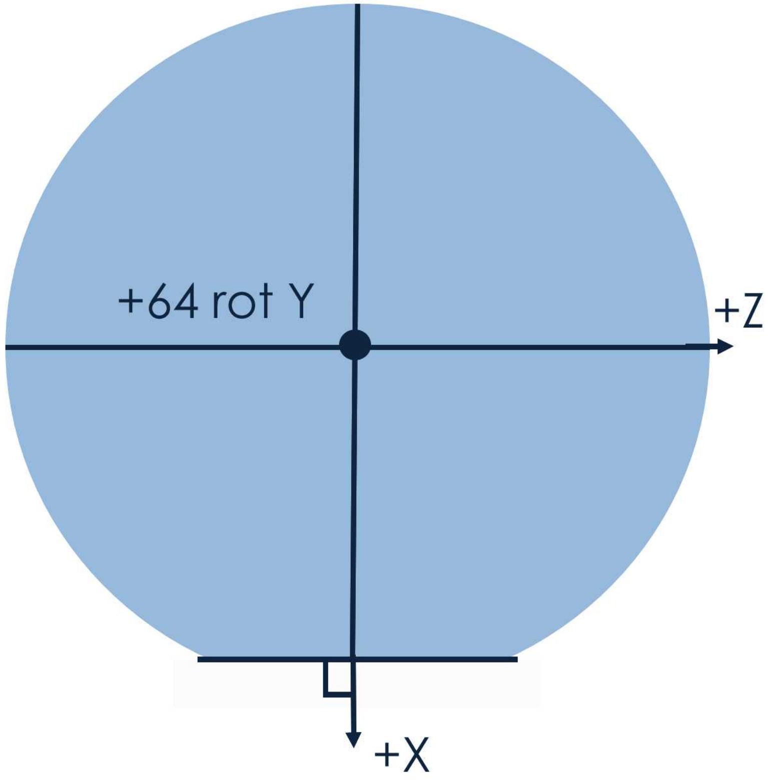

64° YX LN: <z,x,z>(0,-26,0)

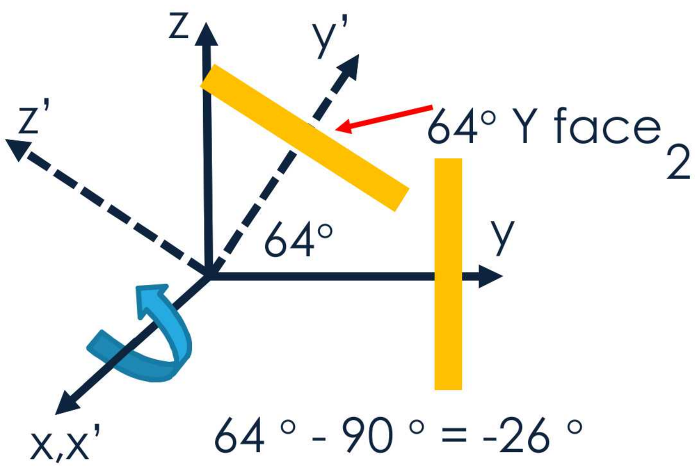

**Comsol rotates the coordinate system not the material tensors**

1. Draw slab in Comsol then apply rotation using the rotated system: (0,-26,0) for 64YX LN
2. Comsol rotates the coordinate axis from the drawn axis and which is viewed by plotting the coordinate system:

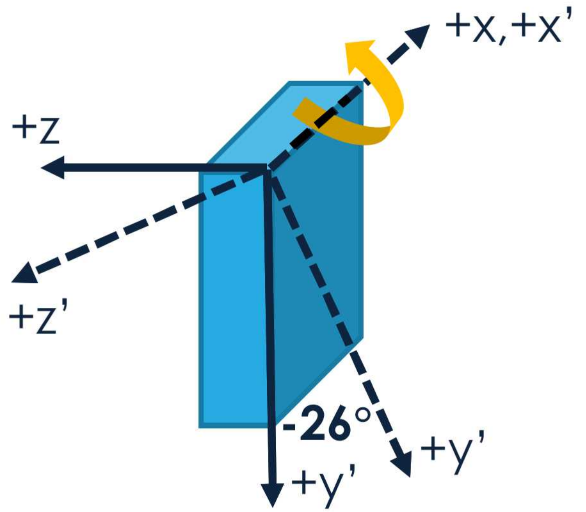

# Simulating Surface Acoustic Wave (SAW) on 64° Y –rotated X propagating Lithium Niobate: Results

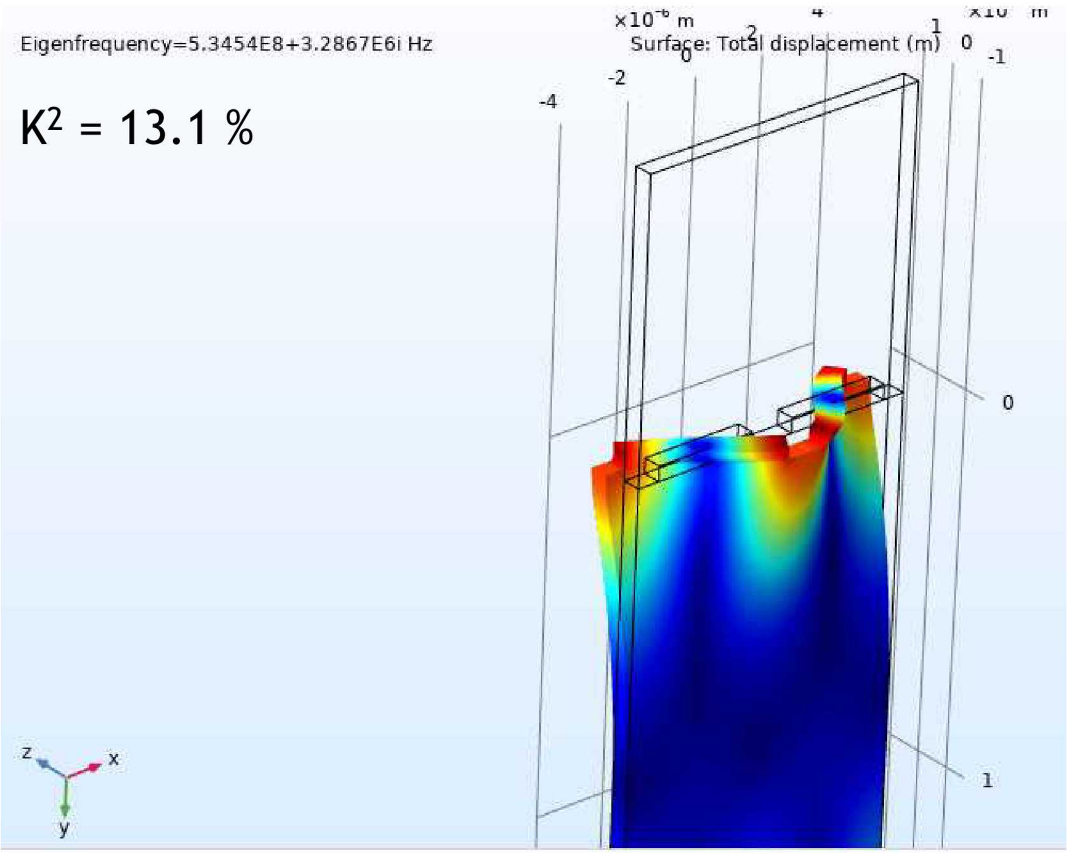

K$^2$ = 13.1 %

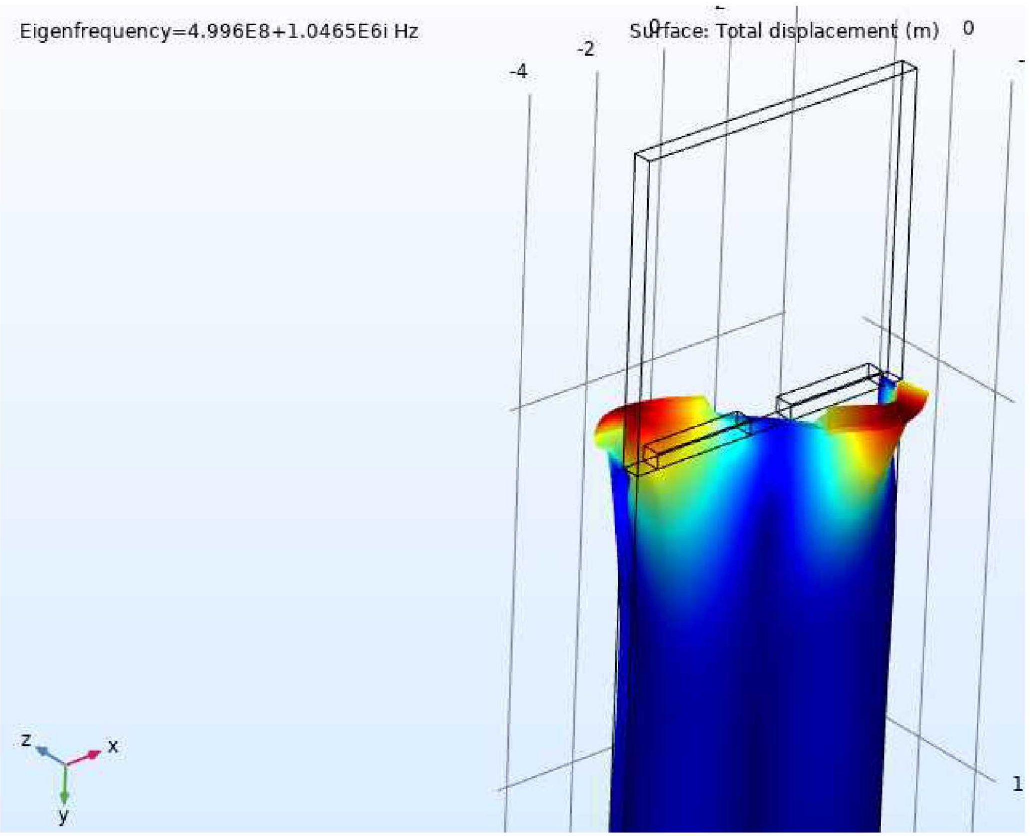

# Y-cut Lithium Niobate on Si

Y-cut X-prop (0,90,θ)

Y-cut definition

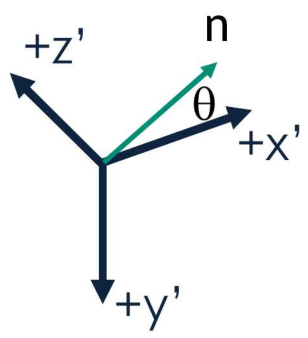

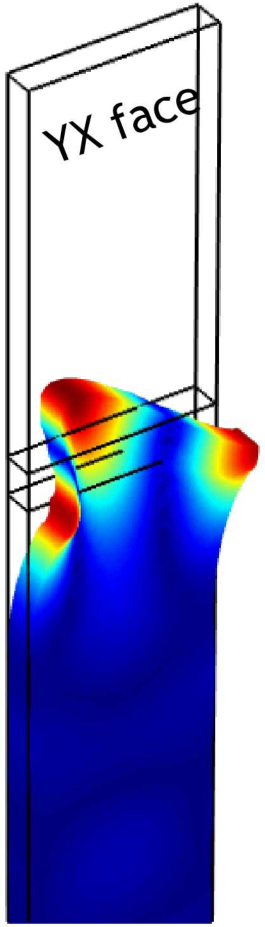

Phase velocities

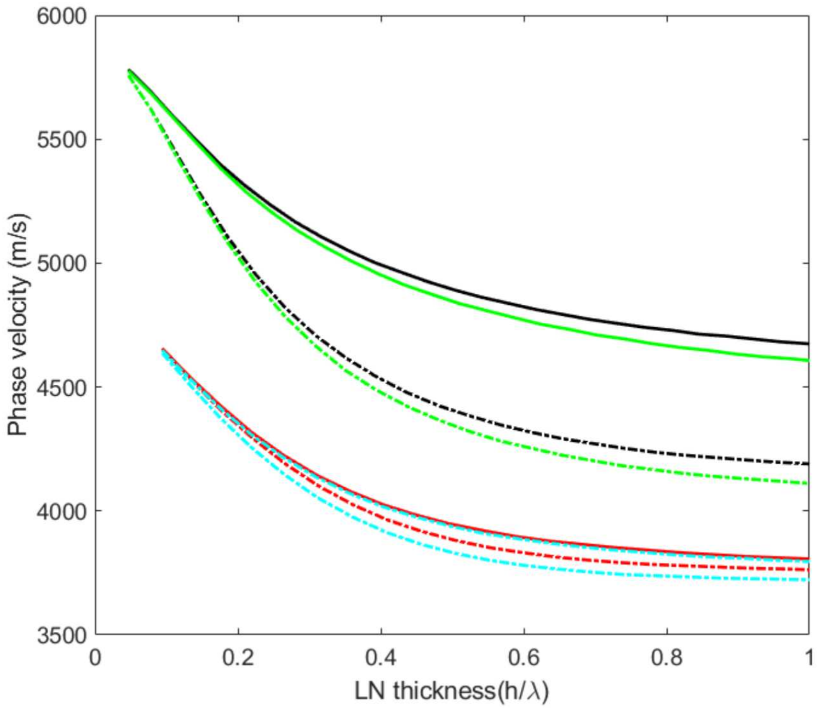

Electromechanical Coupling

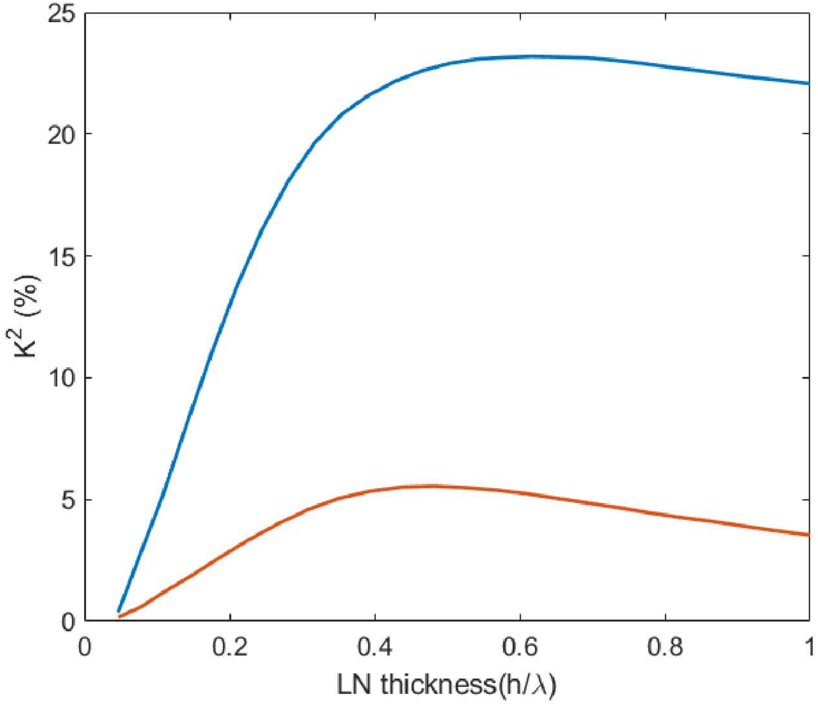

# Comsol: Modeling Newtonian Fluid Loading on Acoustic Devices

$$u_i = \beta_i e^{j\omega t} e^{-j\omega x_1/V} e^{\alpha\omega x_3/V}, v = j\omega u$$

Hydrostatic pressure of fluid

$$T_{11} = -K\left(\frac{\partial u_1}{\partial x_1} + \frac{\partial u_2}{\partial x_2} + \frac{\partial u_3}{\partial x_3}\right) - \frac{2}{3}\eta\left(\frac{\partial v_1}{\partial x_1} + \frac{\partial v_2}{\partial x_2} + \frac{\partial v_3}{\partial x_3}\right) + 2\eta\frac{\partial v_1}{\partial x_1}$$

$$T_{12} = \eta\left(\frac{\partial v_1}{\partial x_2} + \frac{\partial v_2}{\partial x_1}\right)$$

$$T_{22} = -K\left(\frac{\partial u_1}{\partial x_1} + \frac{\partial u_2}{\partial x_2} + \frac{\partial u_3}{\partial x_3}\right) - \frac{2}{3}\eta\left(\frac{\partial v_1}{\partial x_1} + \frac{\partial v_2}{\partial x_2} + \frac{\partial v_3}{\partial x_3}\right) + 2\eta\frac{\partial v_2}{\partial x_2}$$

$$T_{13} = \eta\left(\frac{\partial v_1}{\partial x_3} + \frac{\partial v_3}{\partial x_1}\right)$$

$$T_{33} = -K\left(\frac{\partial u_1}{\partial x_1} + \frac{\partial u_2}{\partial x_2} + \frac{\partial u_3}{\partial x_3}\right)_s - \frac{2}{3}\eta\left(\frac{\partial v_1}{\partial x_1} + \frac{\partial v_2}{\partial x_2} + \frac{\partial v_3}{\partial x_3}\right) + 2\eta\frac{\partial v_3}{\partial x_3}$$

$$T_{23} = \eta\left(\frac{\partial v_2}{\partial x_3} + \frac{\partial v_3}{\partial x_2}\right)$$

$$\boldsymbol{T} = \begin{bmatrix} K - \frac{2j\omega\eta}{3} + 2j\omega\eta & K - \frac{2j\omega\eta}{3} & 0 & 0 & 0 & 0 \\ K - \frac{2j\omega\eta}{3} & K - \frac{2j\omega\eta}{3} + 2j\omega\eta & 0 & 0 & 0 & 0 \\ K - \frac{2j\omega\eta}{3} & K - \frac{2j\omega\eta}{3} & K - \frac{2j\omega\eta}{3} + 2j\omega\eta & 0 & 0 & 0 \\ 0 & 0 & 0 & j\omega\eta & 0 & 0 \\ 0 & 0 & 0 & 0 & j\omega\eta & 0 \\ 0 & 0 & 0 & 0 & 0 & j\omega\eta \end{bmatrix} \boldsymbol{S}$$

Longitudinal and Shear velocity in the Fluid:

$$V_L = \sqrt{\frac{K + \frac{4j\omega\eta}{3}}{\rho_f}}, V_S = \sqrt{\frac{j\omega\eta}{\rho_f}}$$

# Fluid Loading on a SH-SAW Sensor (36° Y Lithium Tantalate)

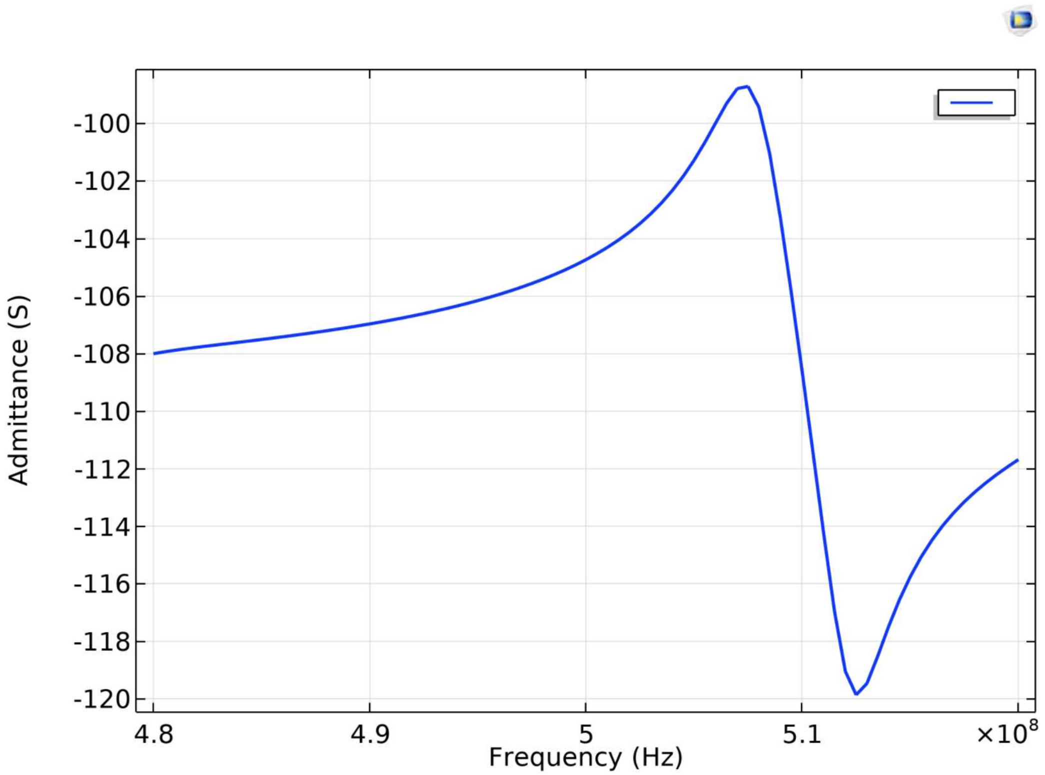

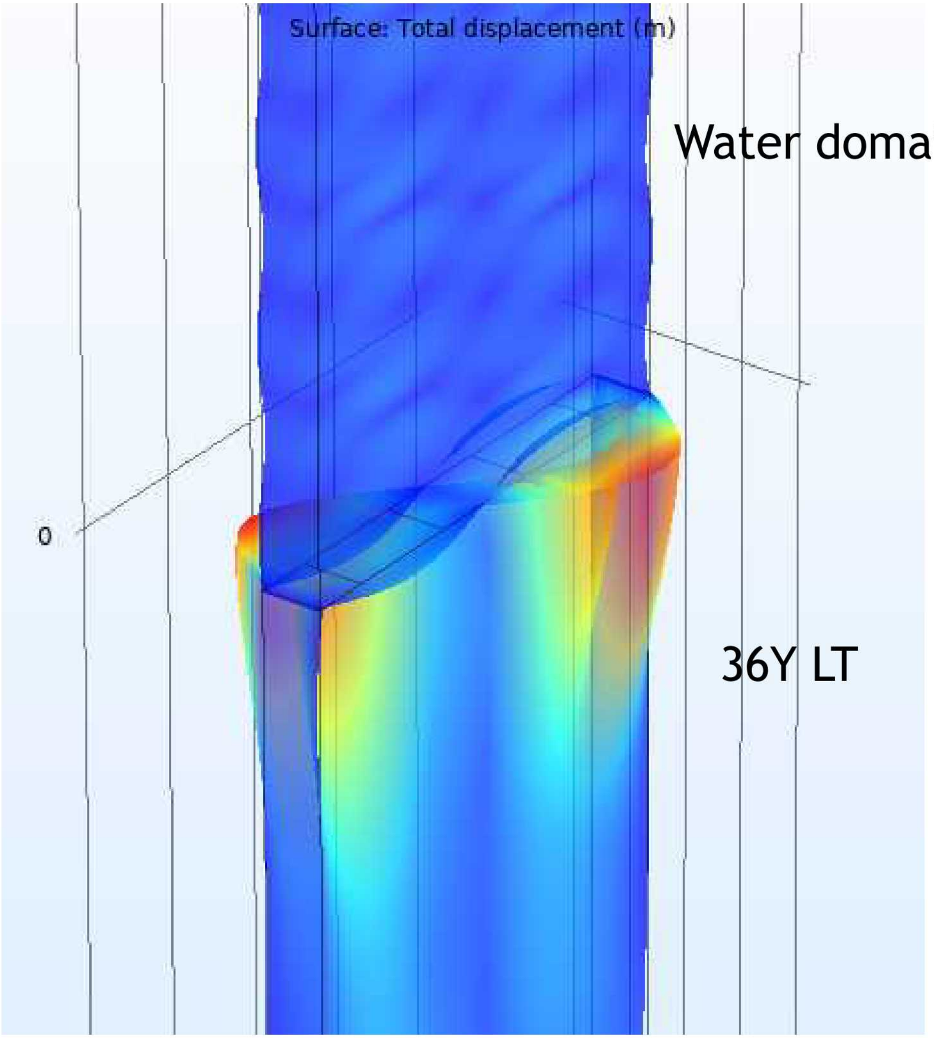

Water domain

36Y LT

PML

# Fluid Loading on a SH-SAW Sensor (36° Y Lithium Tantalate)

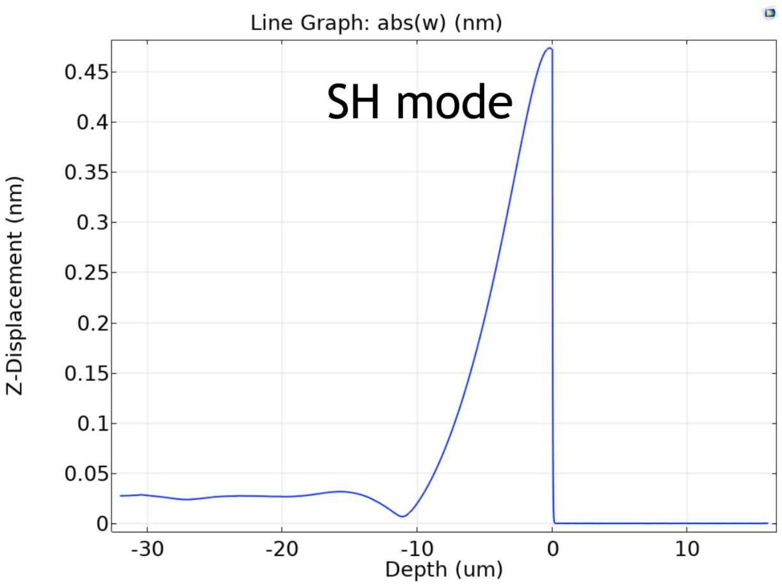

SH mode

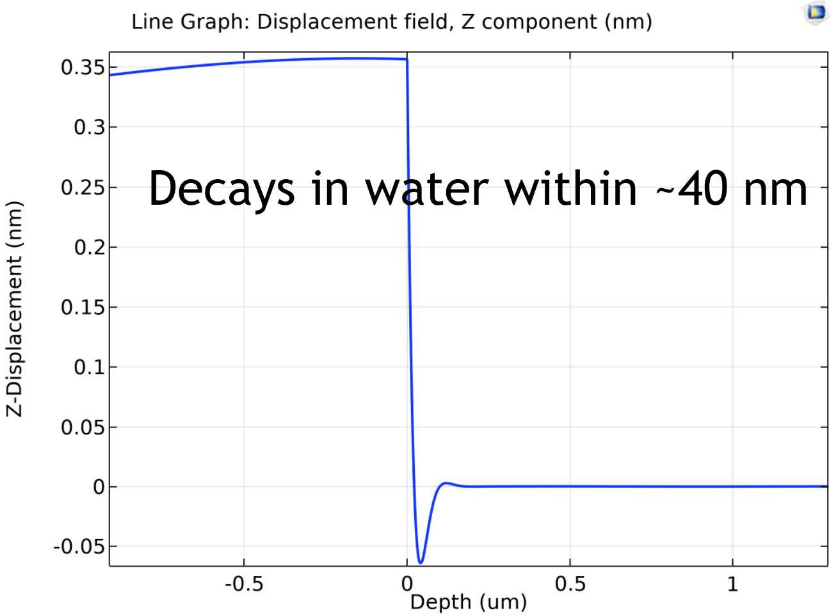

Decays in water within ~40 nm

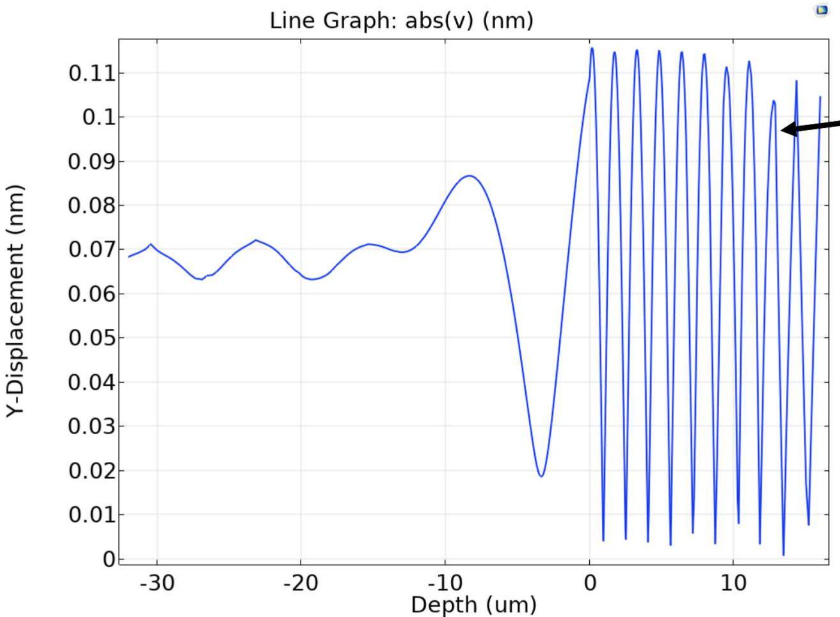

Standing wave near interface with gradual decay into fluid

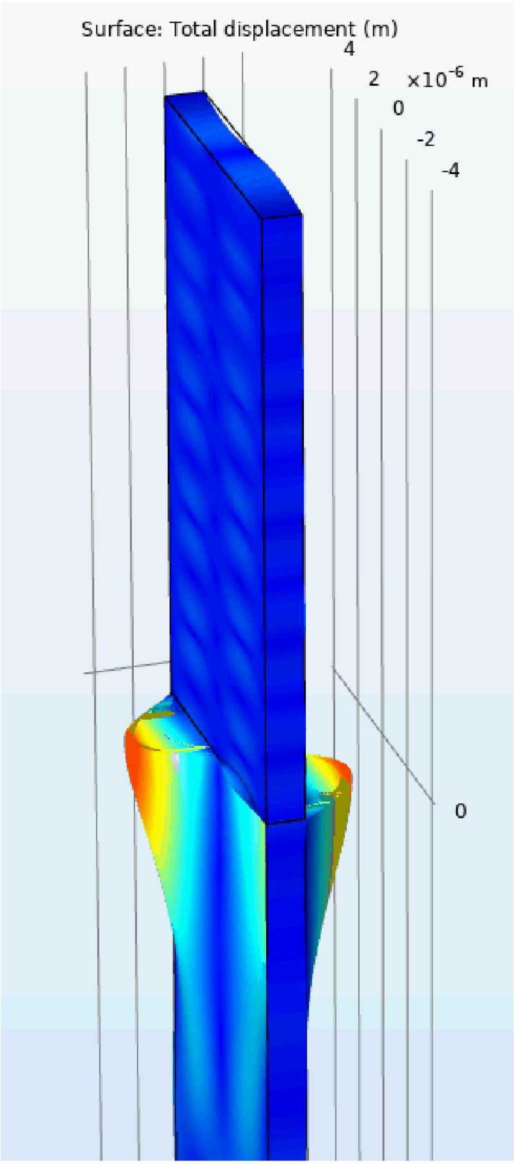

# Fluid Loading on a SH-SAW Sensor (36° Y Lithium Tantalate), cont’d

Water motion at resonance

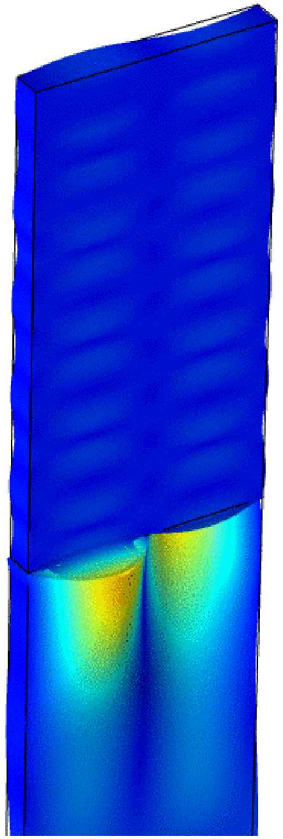

# Comsol: Leaky SAW on 36° Y (0,-54°,0) Lithium Tantalate: Transient Model

Geometry with Rotated Coordinate System set at -54° from positive y-axis

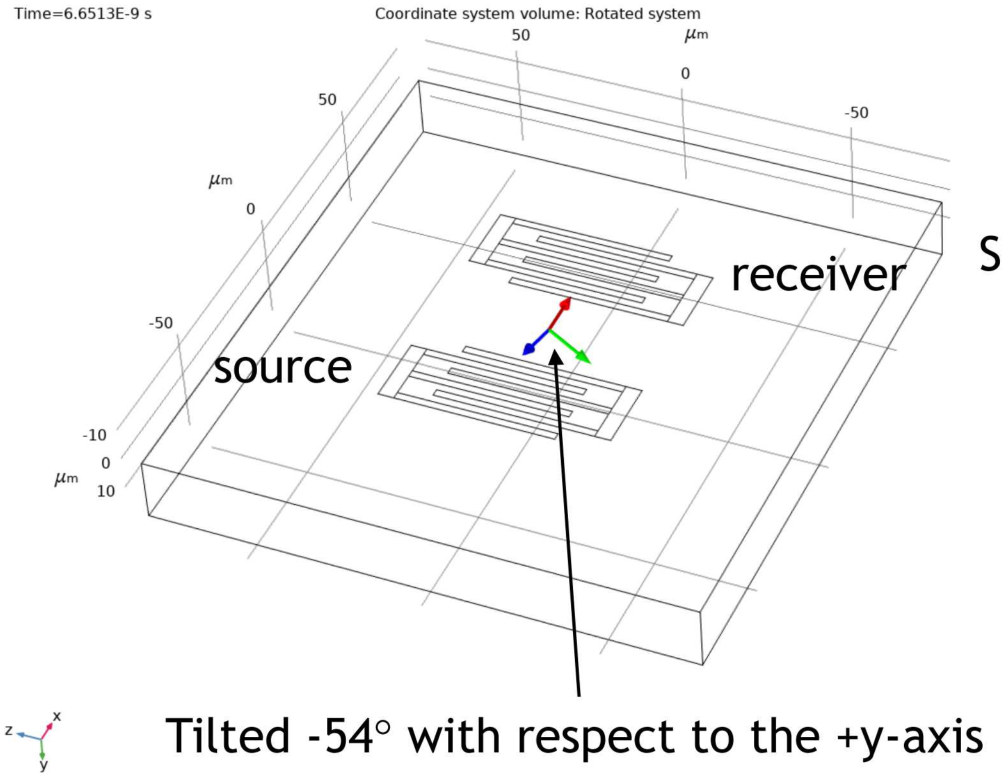

receiver

source

Tilted -54° with respect to the +y-axis

grounds

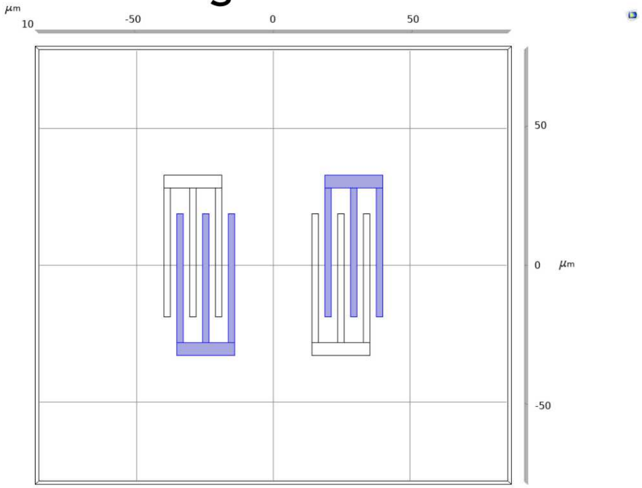

Synchronous drive:

$$V = V_o \sin\left(2\pi f t\right)$$

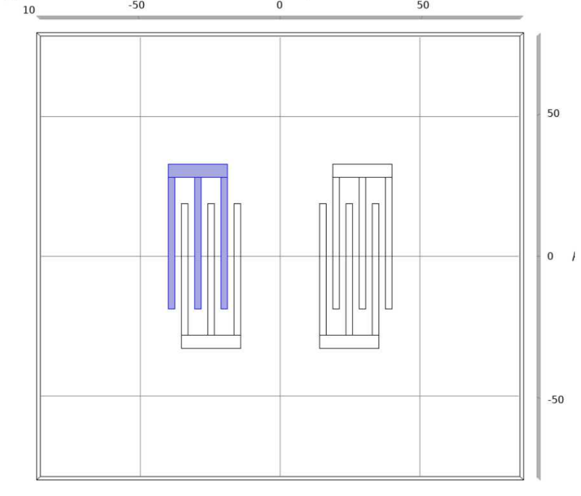

$$\int n \cdot dS = Q_o$$

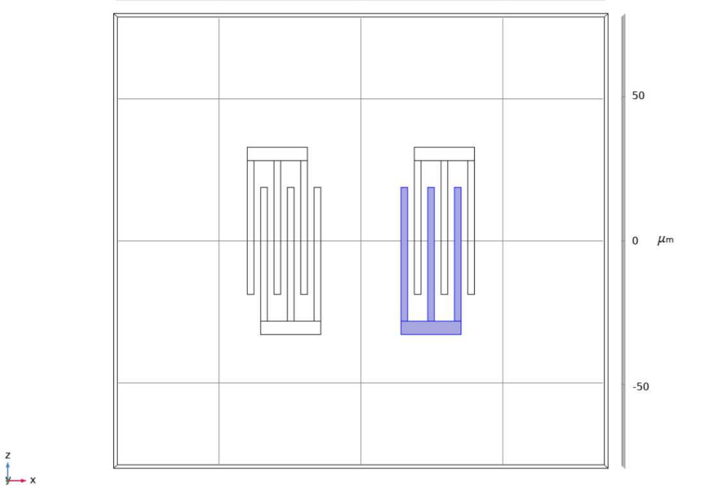

# Leaky SAW on 36 Y Lithium Tantalate, cont'd

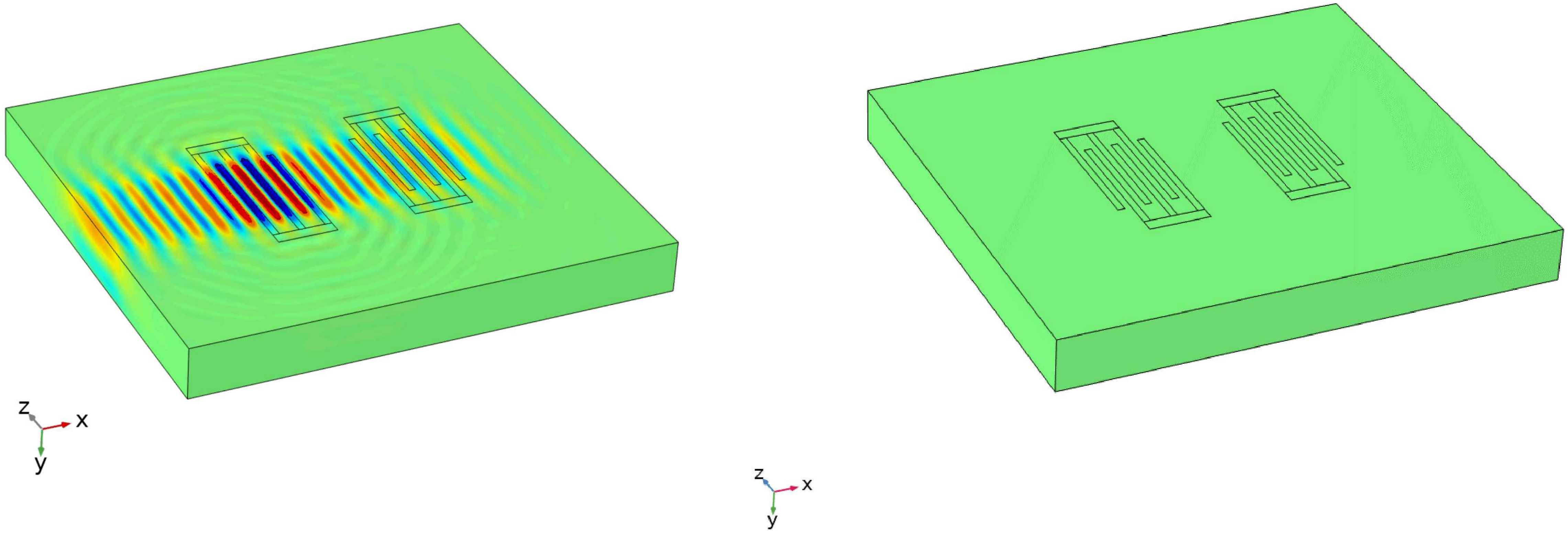

# Leaky SH-SAW on 36° Y Lithium Tantalate, cont'd

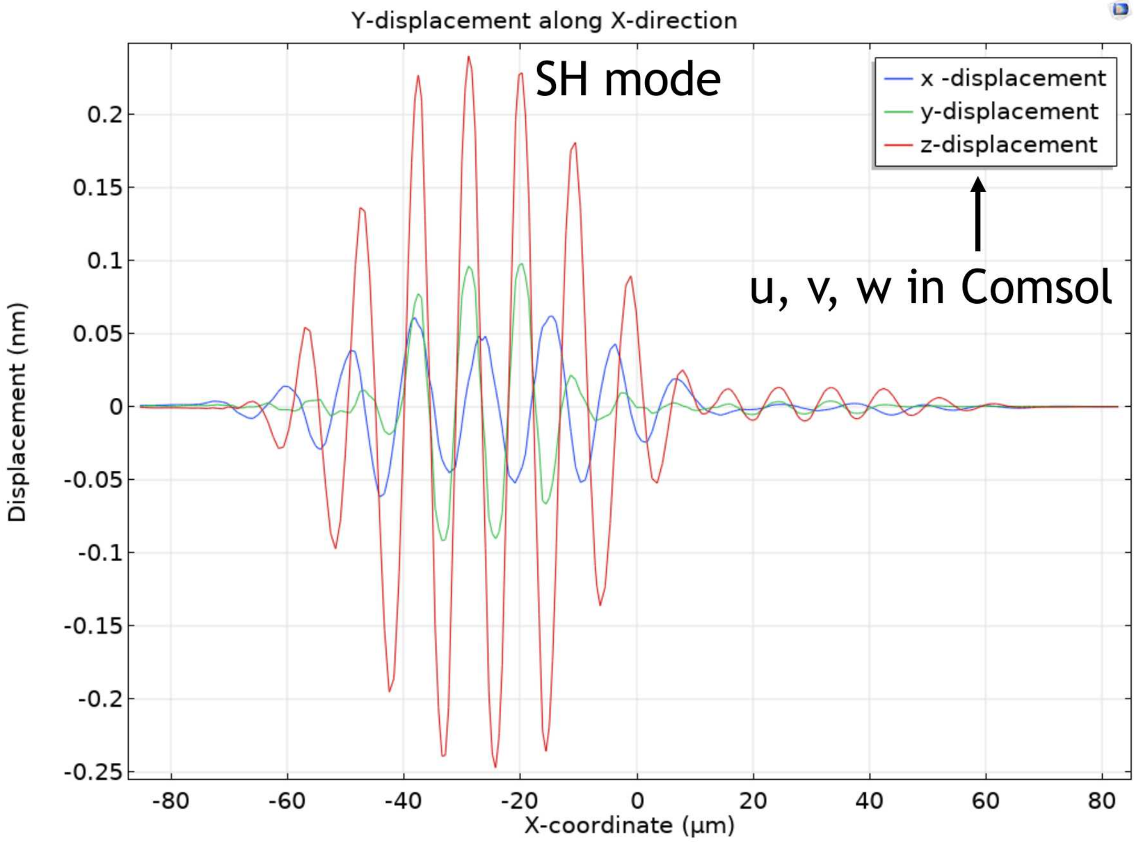

SH mode

u, v, w in Comsol

Propagation direction

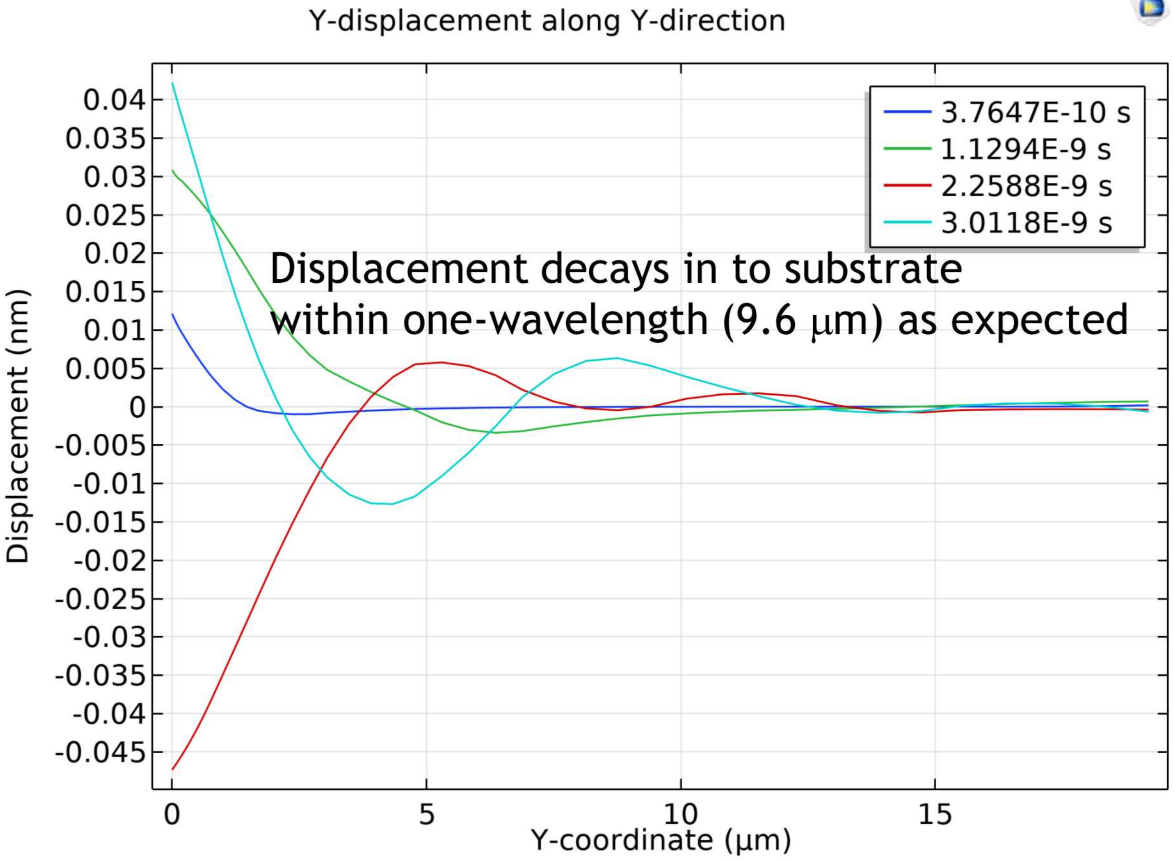

Displacement decays in to substrate within one-wavelength (9.6 μm) as expected

Depth into substrate

Why is y-displacement larger than expected compared to z-displacement?

A: Infinitesimal thin metal electrodes doesn't excite the shear mode adequately.

Solution: Use thicker metal electrodes

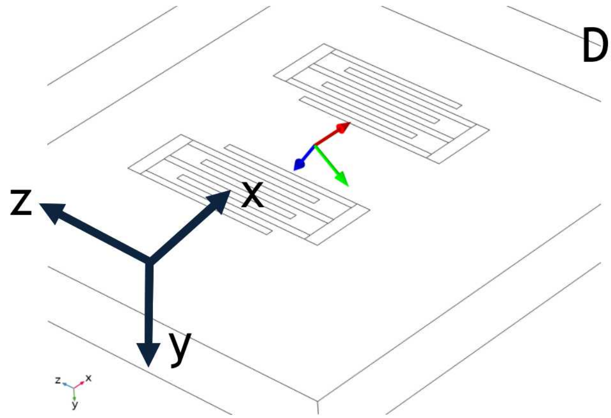

# 2D Coupling of Modes using Comsol: Customized Interface

In some cases, you have to develop an interface to couple specific types of physics or solve coupled PDEs not currently defined in Comsol. Consider a contour mode microresonator using the S0 mode:

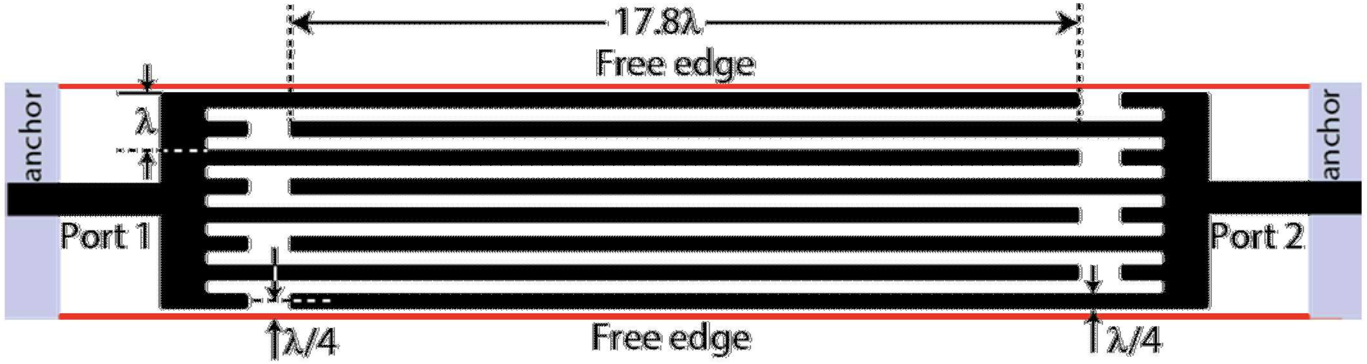

What's the admittance?

A full 3D FEA simulation takes about 20 hrs. Can we speed this up without going to a very large machine (e.g. 1000 cores)? Note: FEA solve time scales more strongly with CPU clock speed than number of cores.

PDE interface in Comsol:

$$e\frac{\partial^2 u}{\partial t^2}+d_a\frac{\partial u}{\partial t}+\nabla\cdot\left(-c\nabla u-\alpha u+\gamma\right)+\beta\cdot\nabla u+au=f$$

$$\boldsymbol{n}\cdot\left(-c\nabla u+\alpha u-\gamma\right)=g-qu+h^T\mu$$

$$0=R$$

$$u=r$$

# 2D Coupling of Modes using Comsol: Customized Interface, cont'd

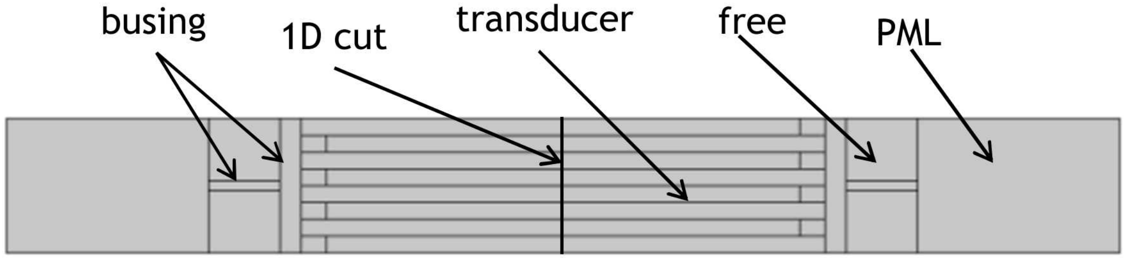

2D COM Equations:

$$\nabla\cdot j\begin{bmatrix}\begin{bmatrix}0&0\\0&\frac{\gamma_a}{2k_o}\end{bmatrix} & [0]\\ [0] & \begin{bmatrix}0&0\\0&-\frac{\gamma_a}{2k_o}\end{bmatrix}\end{bmatrix}\begin{bmatrix}0\\\frac{\partial A^+}{\partial y}\\0\\\frac{\partial A^-}{\partial y}\end{bmatrix} + \nabla\cdot\begin{bmatrix}1&0\\0&0\\0&1\\0&0\end{bmatrix}\begin{bmatrix}A^+\\A^-\end{bmatrix} + j\begin{bmatrix}\delta & \kappa_{12}\\-\kappa_{12}^* & -\delta\end{bmatrix}\begin{bmatrix}A^+\\A^-\end{bmatrix} = \begin{bmatrix}\alpha\\\alpha^*\end{bmatrix}\begin{bmatrix}V\\-V\end{bmatrix}$$

Detuning parameter: $\delta = k - k_o - j\gamma$

Once the fields are known, then the current can be computed

Currents:

$$I_i(\omega) = \iint\left(2\alpha^* A^+ + 2\alpha A^- + j\omega C(x,y)V_i\right)dx\,dy$$

$$I_o(\omega) = \iint\left(2\alpha^* A^+ + 2\alpha A^-\right)dx\,dy$$

PML: $k(r) \rightarrow k_f\left(1 - j\eta(r)\right) = k_f\left(1 - j\eta_o\frac{|r - r_i|}{d}\right)$

# 2D Coupling of Modes using Comsol: Customized Interface, cont'd

Next, we use Comsol to determine the COM parameters ($\kappa$, $\alpha$, and $C_s$) for each domain and store them:

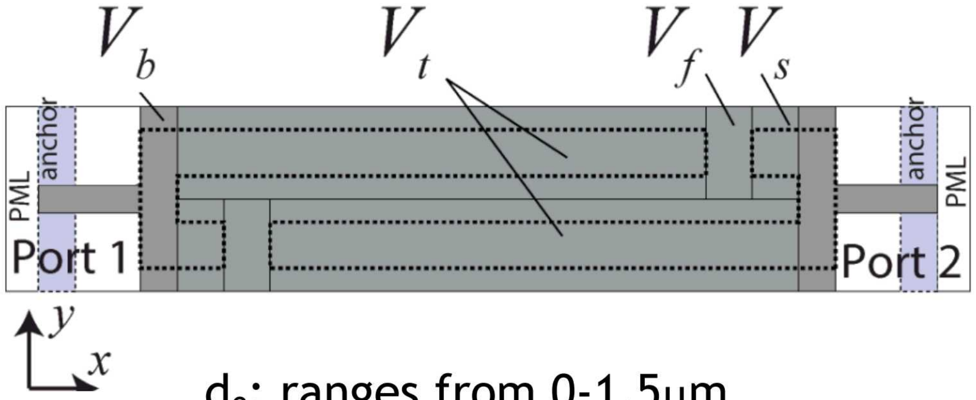

$d_0$: ranges from 0-1.5$\mu$m

Free Domain (1): $V_f$:

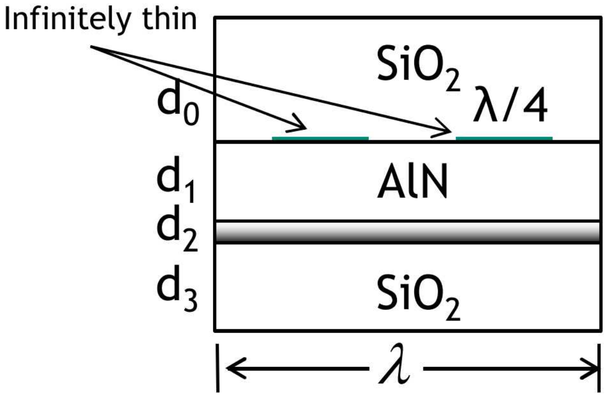

Transducer Domains: $V_t$, $V_s$:

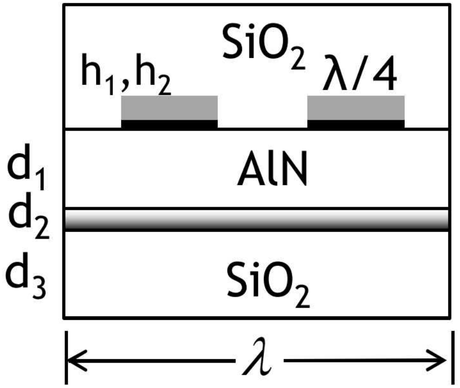

Buss Domains: $V_b$:

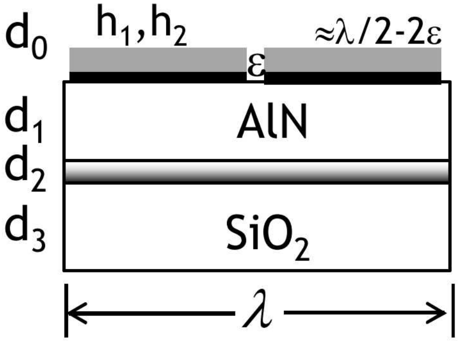

# 2D Coupling of Modes using Comsol: Customized Interface, cont'd

| COM Parameters | | | | | |
|---|---|---|---|---|---|
| **Domain** | **δ** | **v (m/s)** | **$\kappa_{12}p$ (%)** | **$\lvert\zeta p\rvert^2/\omega C_s$ ($m^2\Omega^{-1/2}$)** | **$C_o$ (pF/p/m)** |
| Transducer | $k_t - k_o - j\gamma$ | 7873 | -0.08 | 0.004 | 512.3 |
| Buss | $k_m - k_o - j\gamma$ | 7828 | 0 | 0 | 512.3 |
| Free Space | $k_f - k_o - j\gamma$ | 7910 | 0 | 0 | 0 |
| Stub | $k_s - k_o - j\gamma$ | 7873 | -0.08 | 0.004 | 512.3 |

## Layout

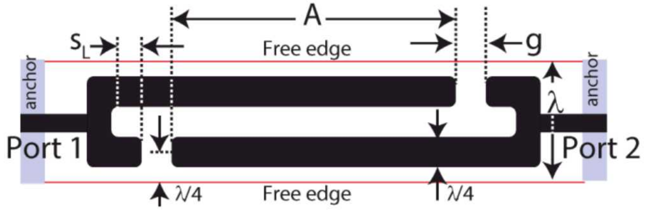

## Equivalent Field Model Layout

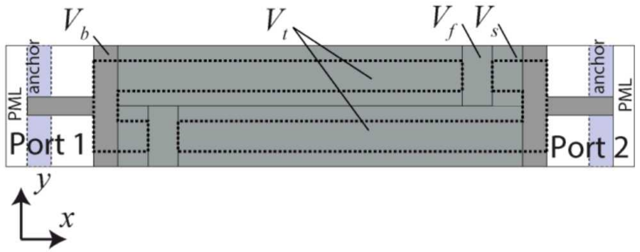

## Cross-Section

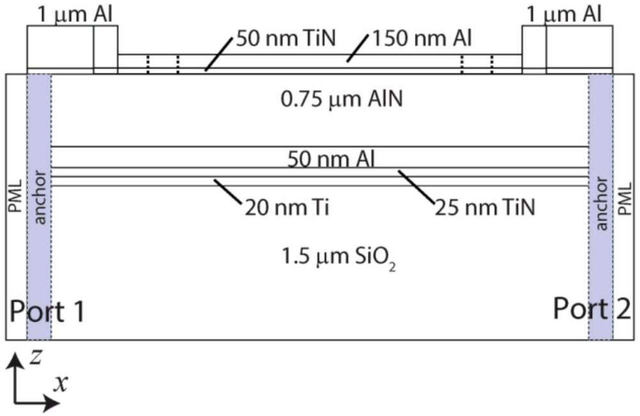

# 2D Coupling of Modes using Comsol: Customized Interface, cont’d

The 2D COM simulation predicted two distinct spurious modes at 487.8 MHz and a second at 491.3 MHz and tracked the measurement

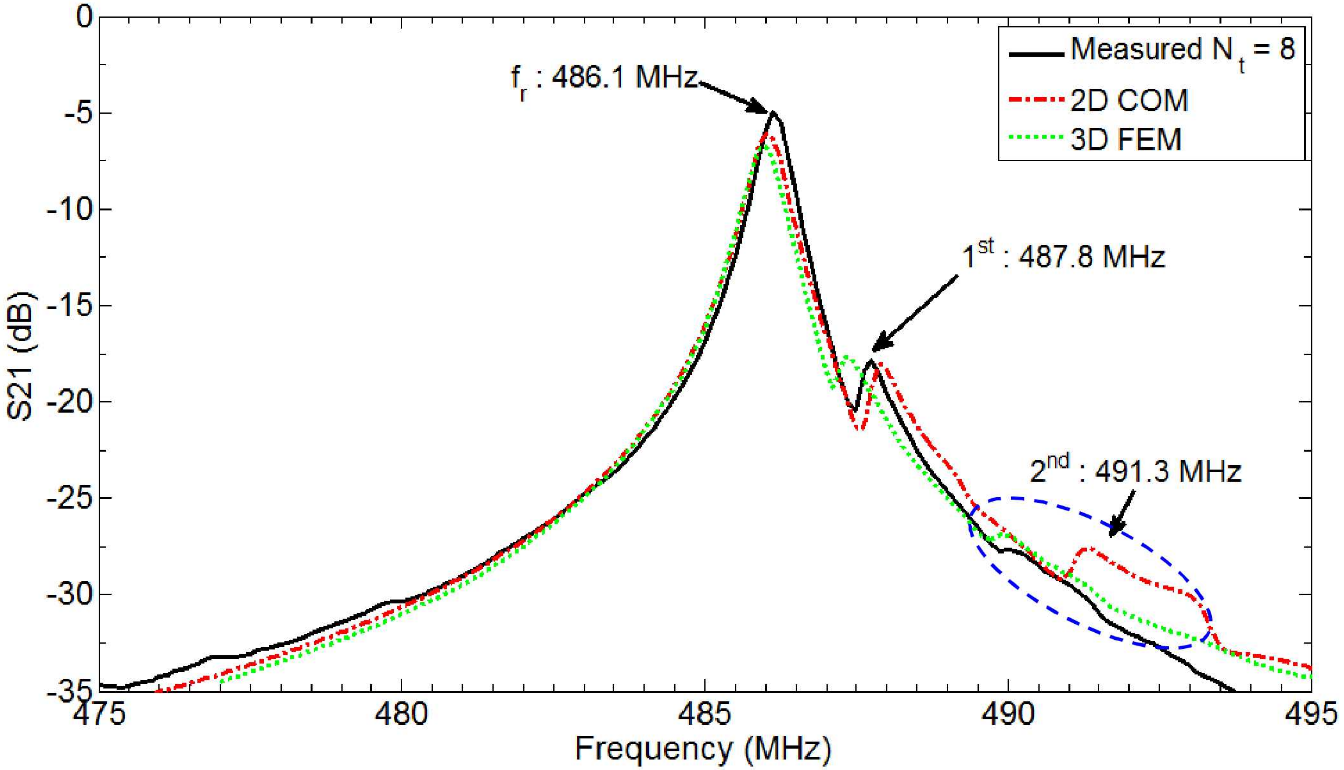

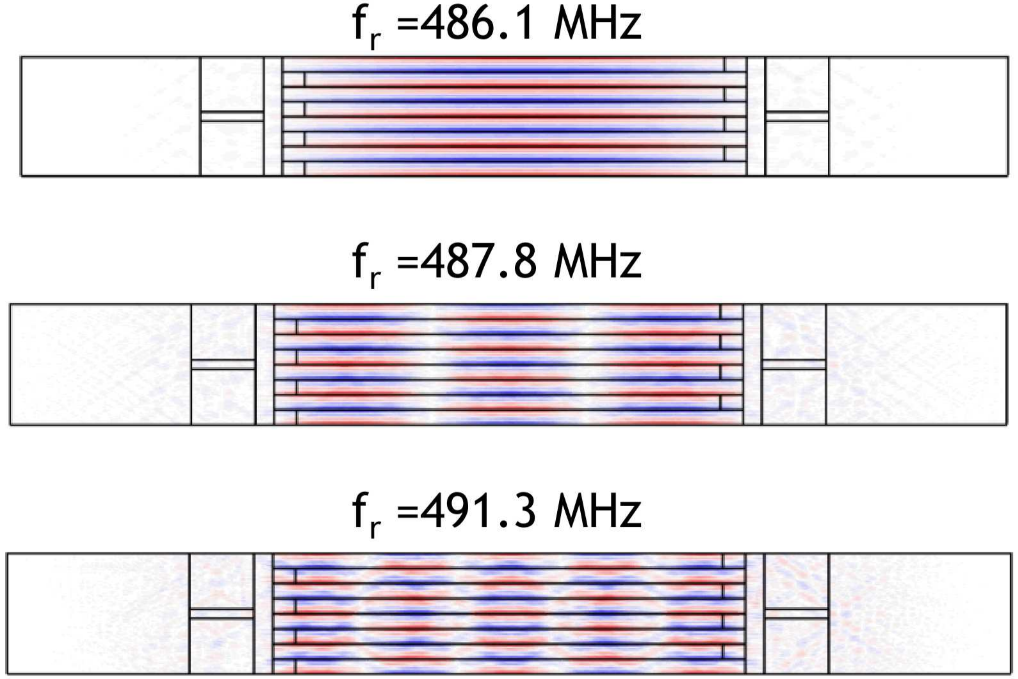
$f_r$ =486.1 MHz

$f_r$ =487.8 MHz

$f_r$ =491.3 MHz

D. Branch, IEEE-UFFC Intern. Sym., Chicago, 2014, **DOI:** 10.1109/ULTSYM.2014.0141

# Useful Method for Spurious Mode Control

Blue Region:
Oxide film: 0.75μm

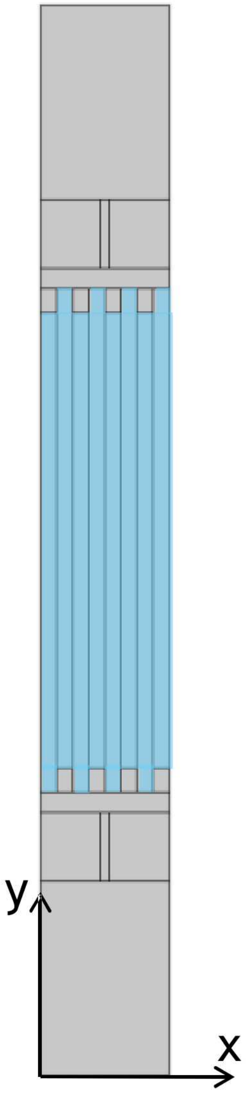

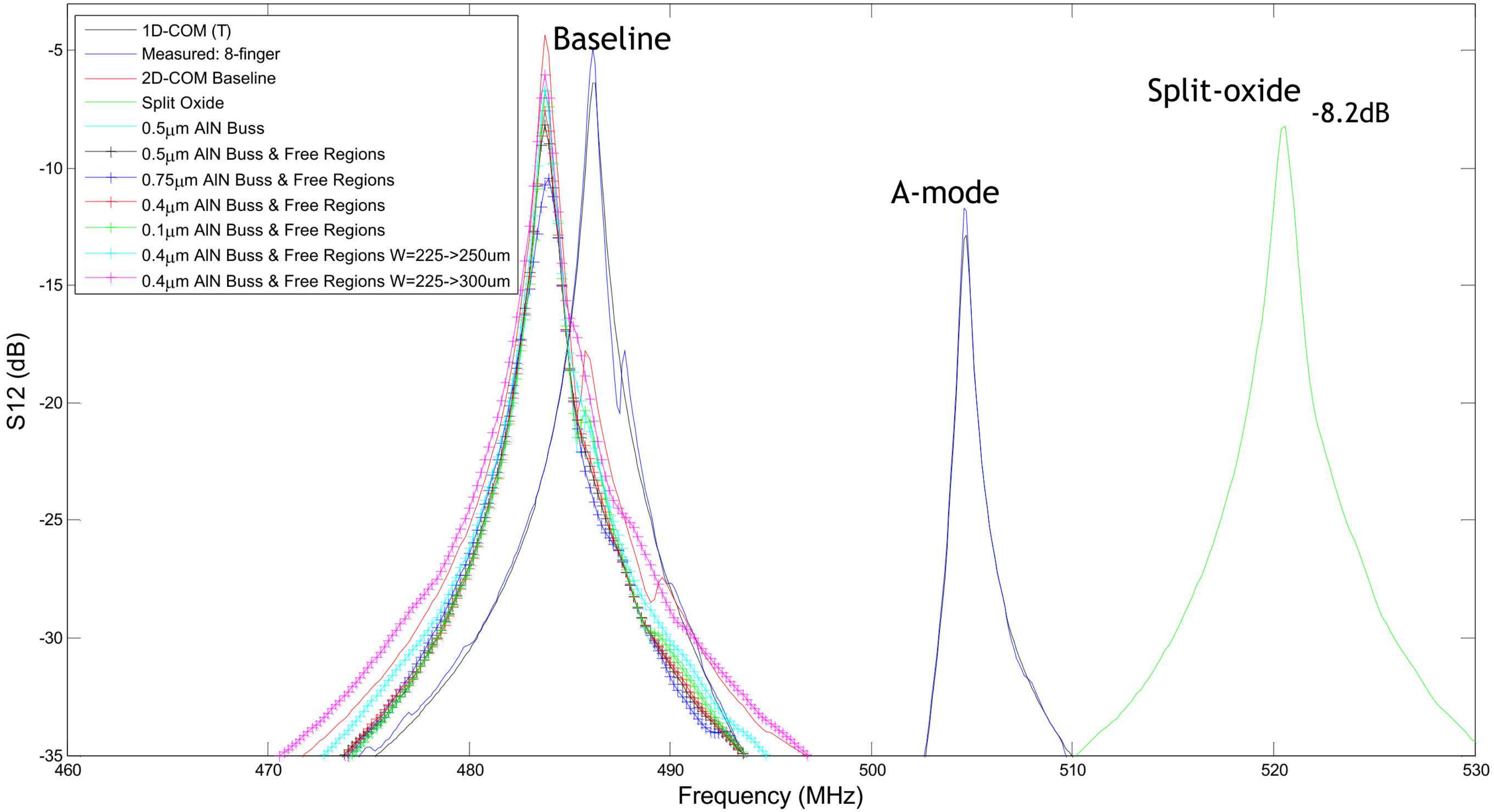

# Coupled Resonant Filter in Comsol (2D COM): 2-Port, Bragg, λ=4μm

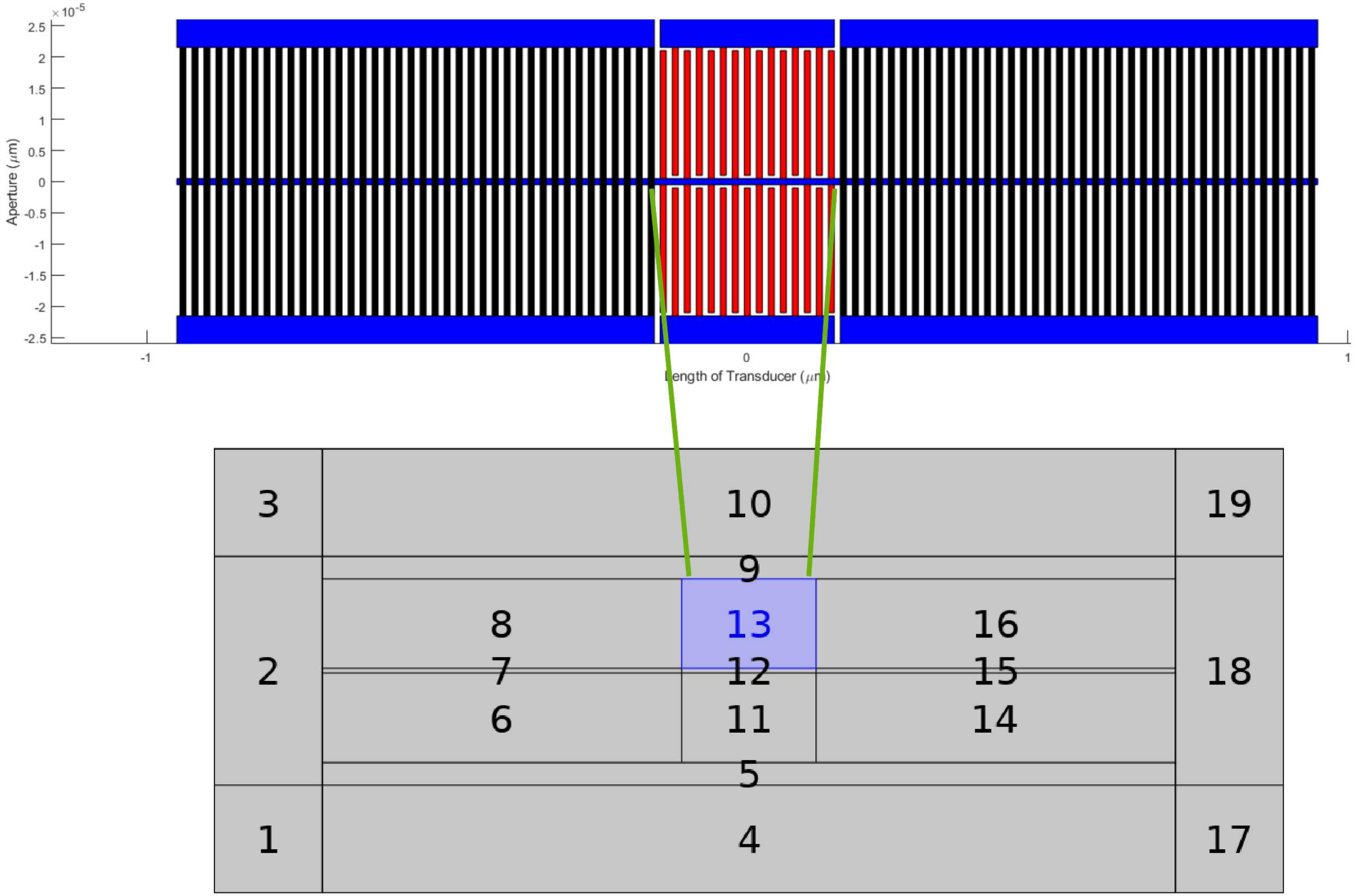

# Coupled Resonant Filter in Comsol (2D COM): 2-Port, Bragg, λ=4μm

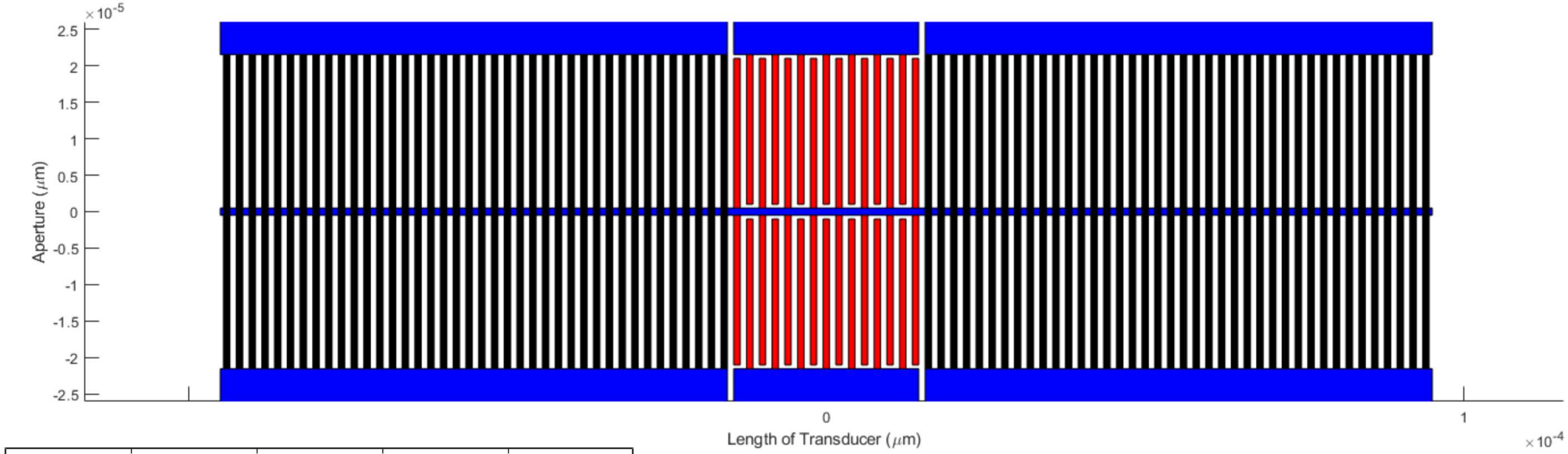

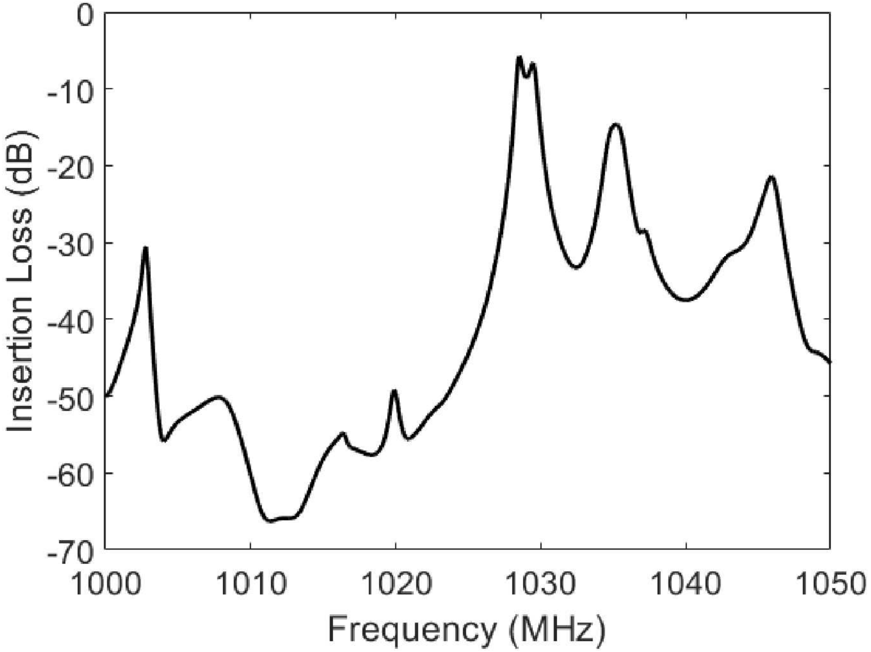

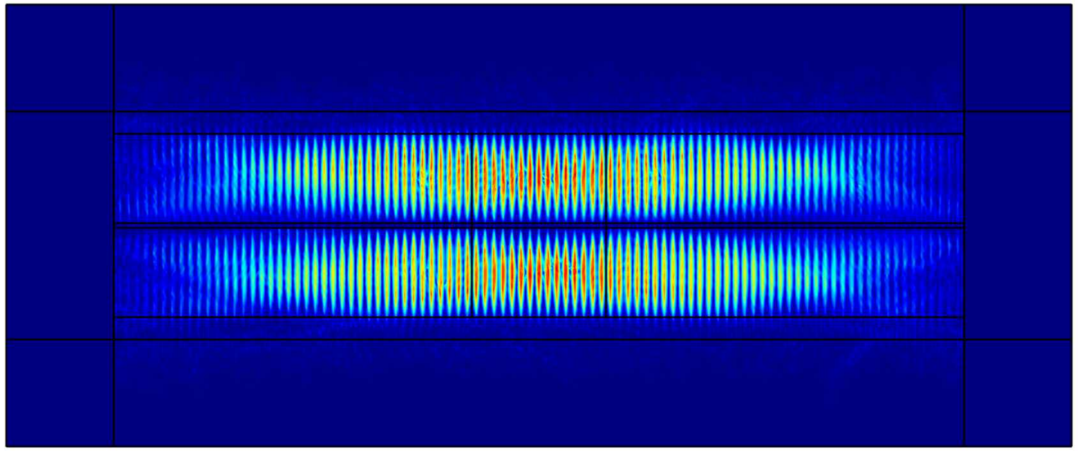

# BAW Dispersion

Model:

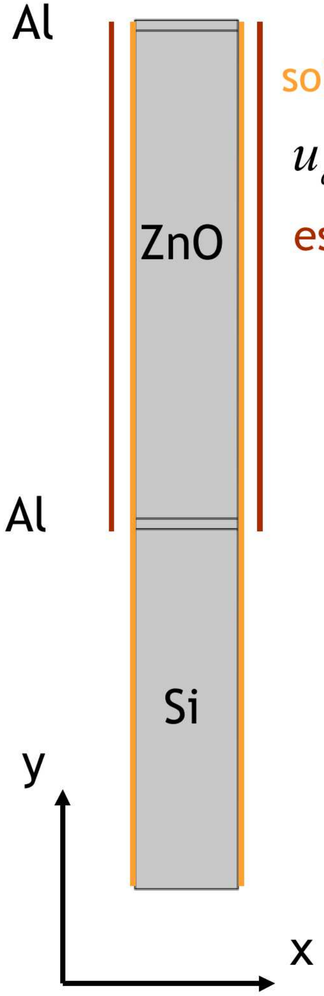

solid: Floquet conditions

$$u_{dst} = u_{src} e^{-ik\left(r_{dst} - r_{src}\right)}$$

es: Floquet conditions

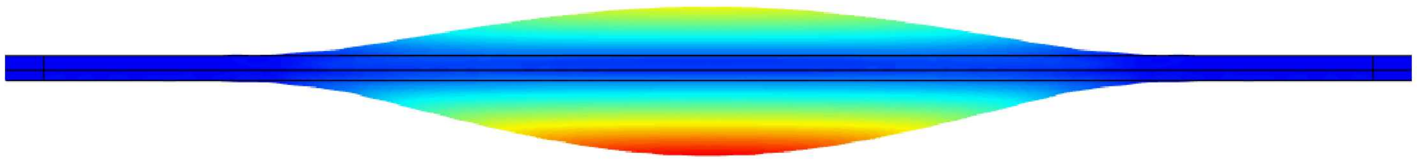

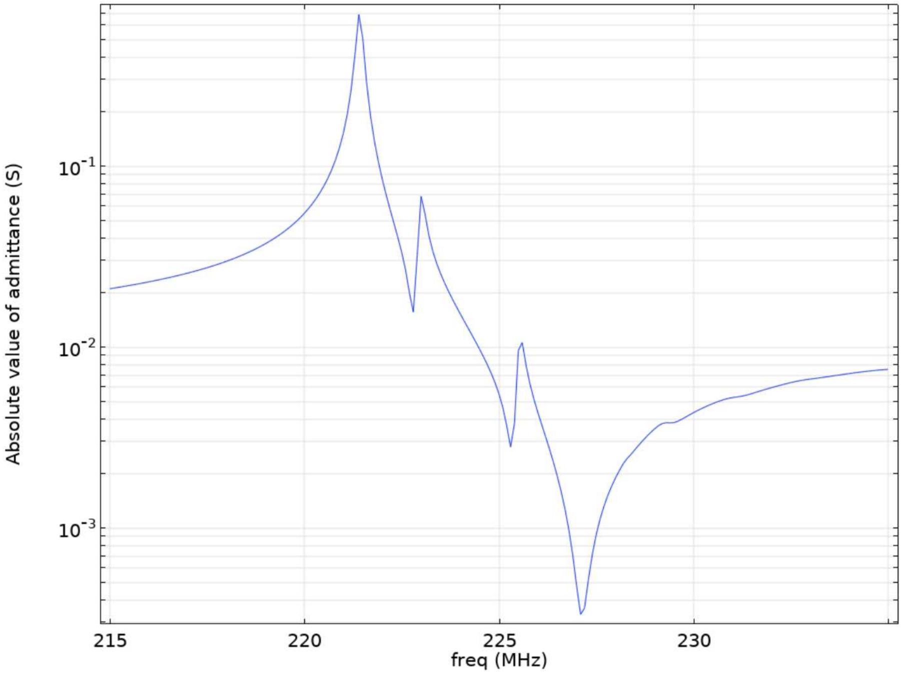

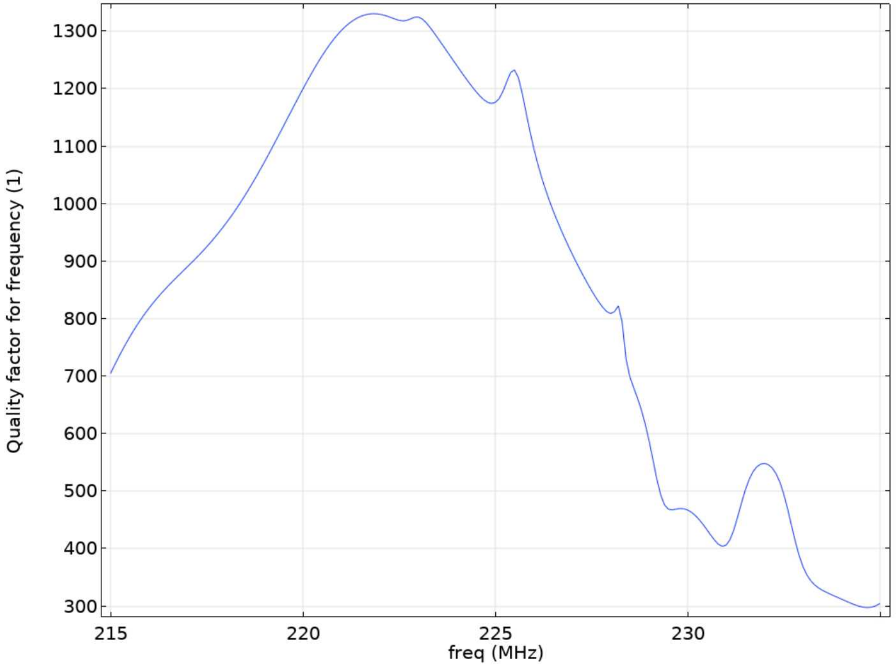

# BAW Dispersion, cont'd

Imag part of k

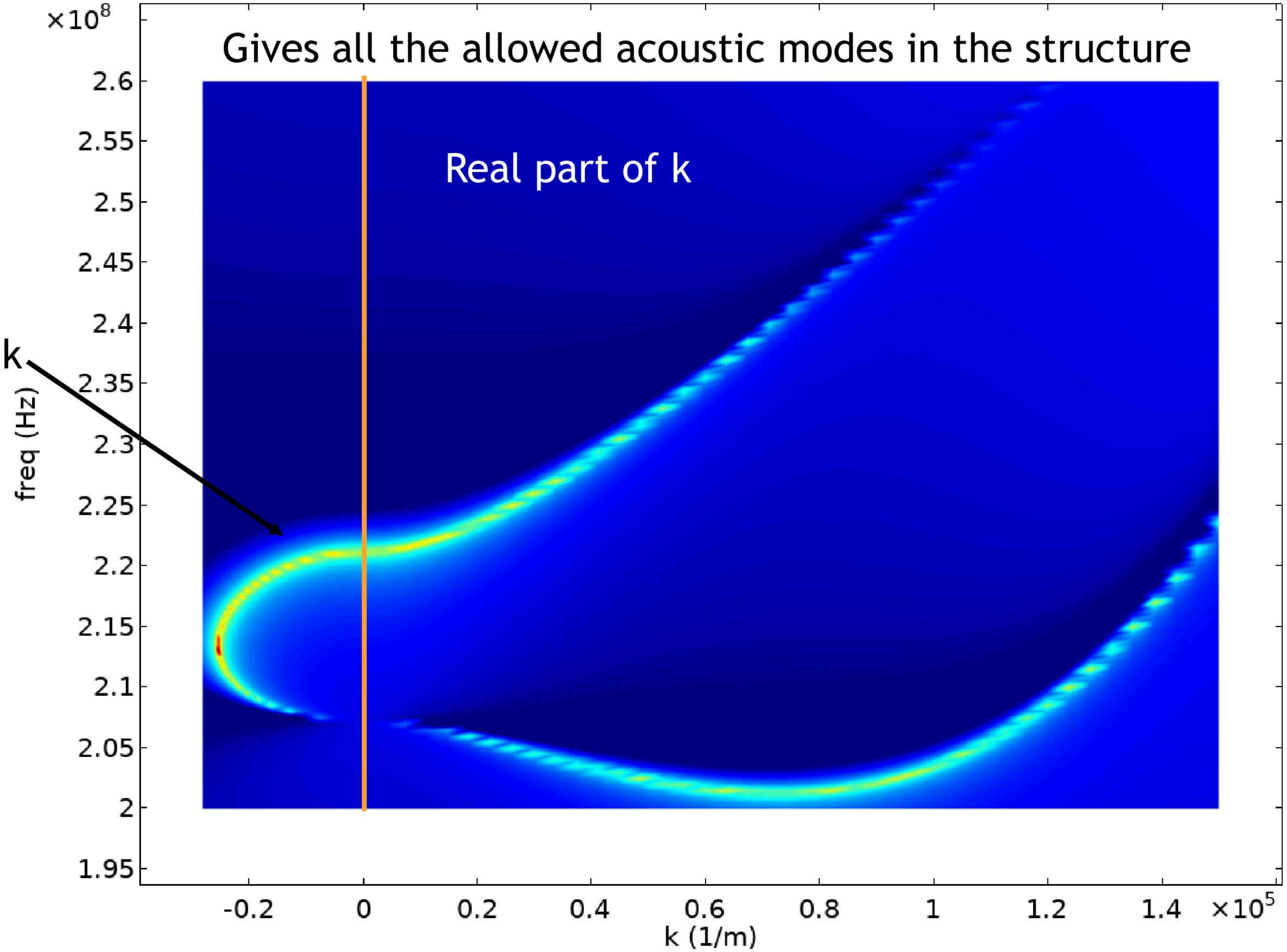

Gives all the allowed acoustic modes in the structure

Real part of k

# ZnO Shear BAW in Air, 28° c-axis tilt

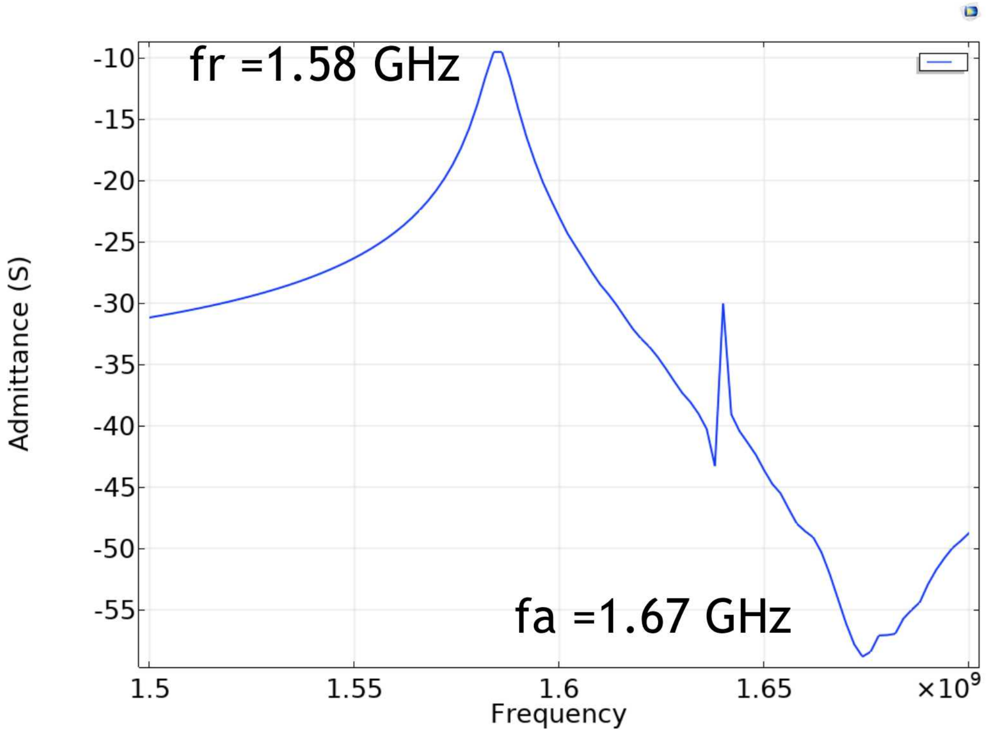

fr =1.58 GHz

fa =1.67 GHz

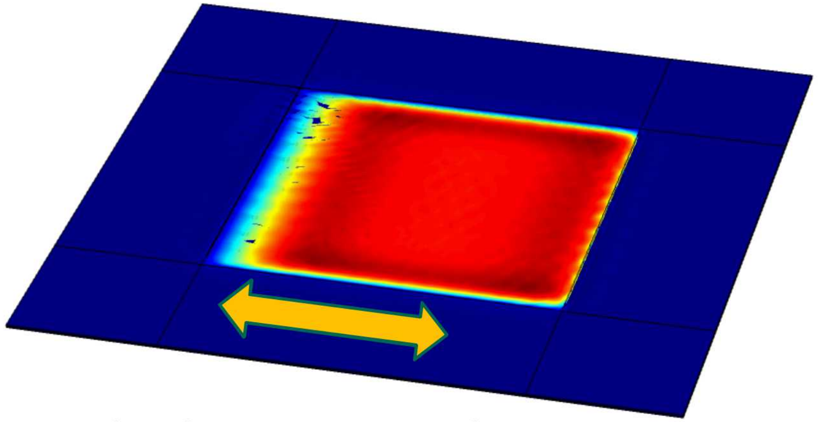

Shear displacement is along y-axis

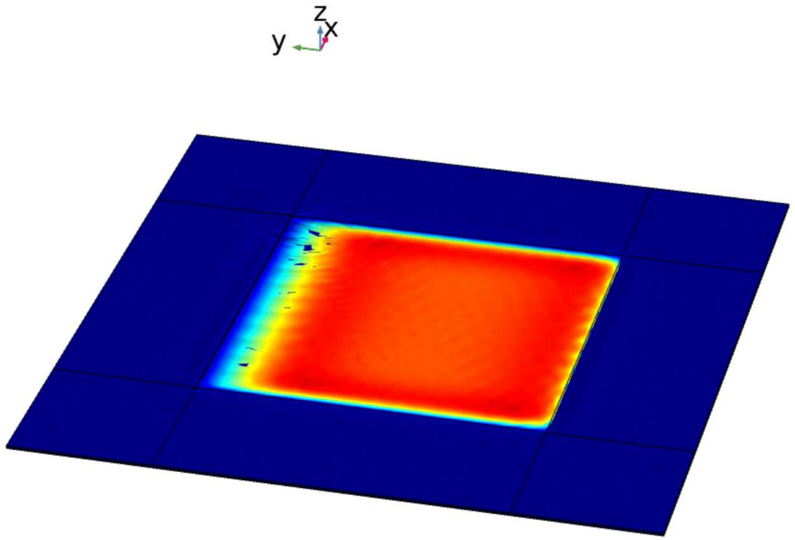

# ZnO Shear BAW with Fluid Loading, 28° c-axis tilt

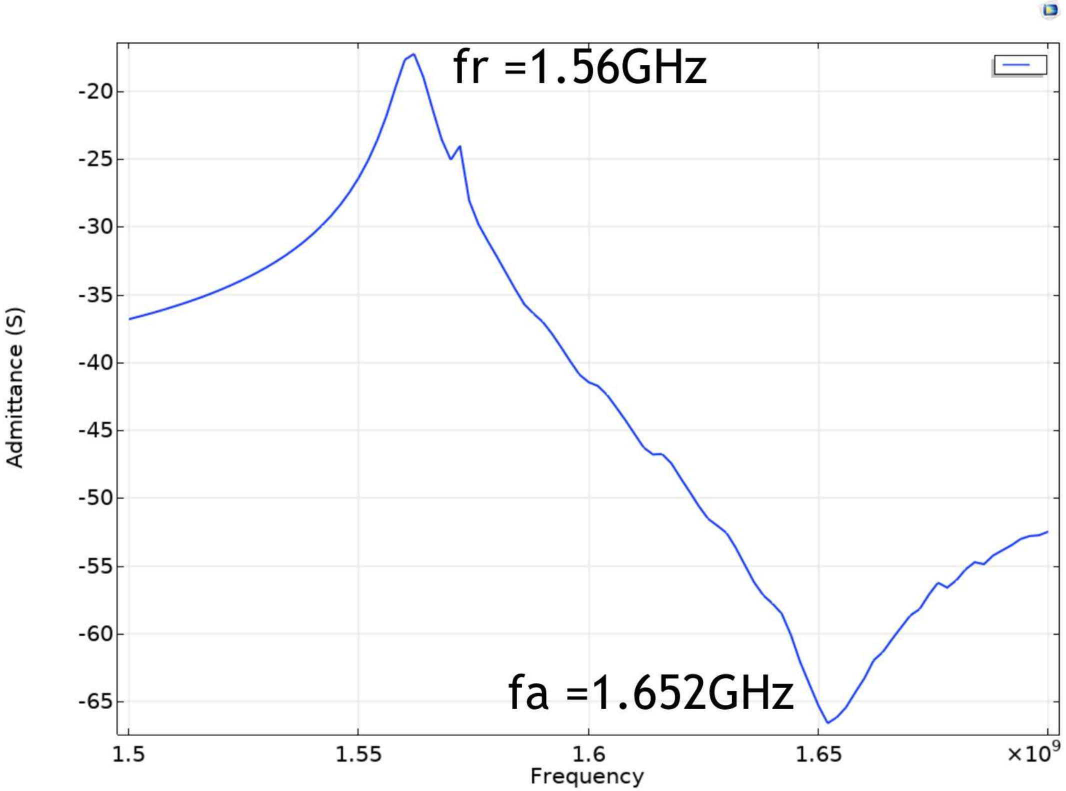

fr =1.56GHz

fa =1.652GHz

Cross-section through the thickness

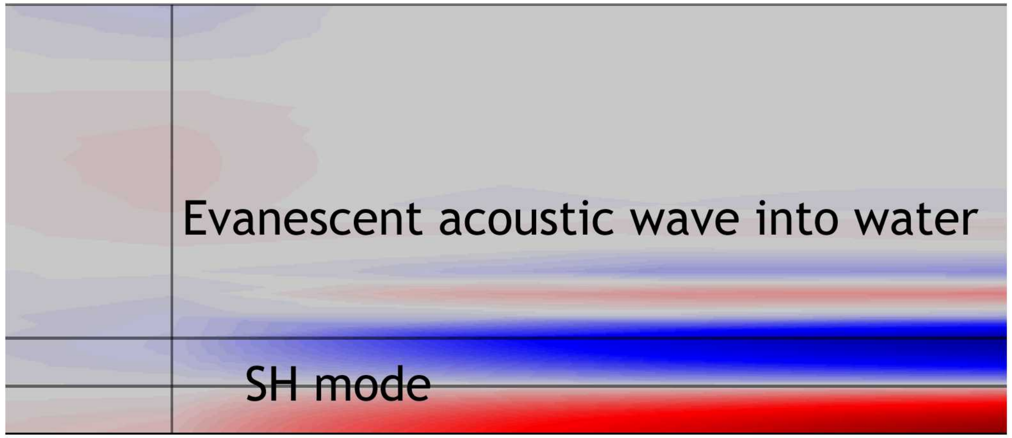

Evanescent acoustic wave into water

SH mode

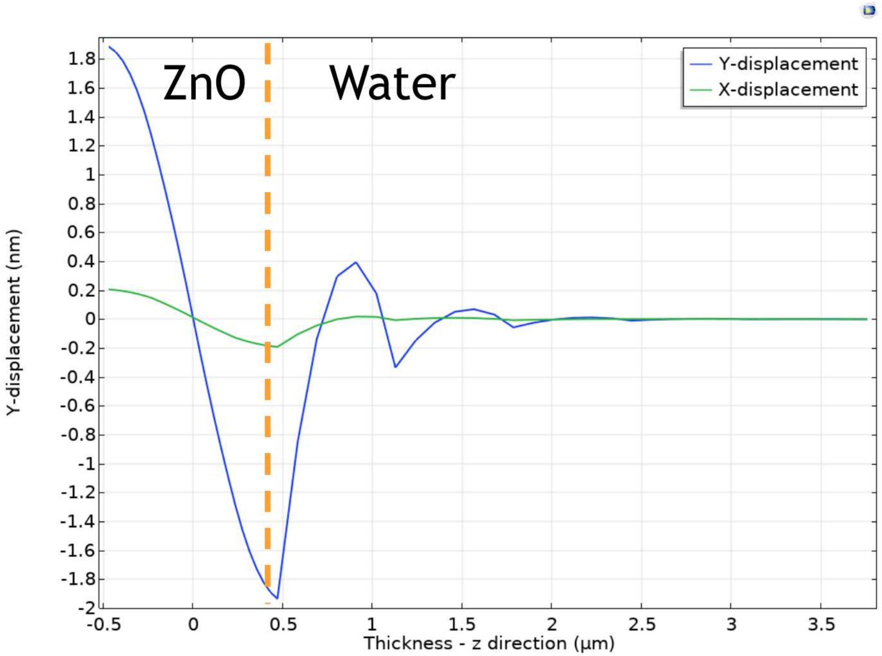

ZnO

Water

# ZnO Shear BAW with Fluid Loading

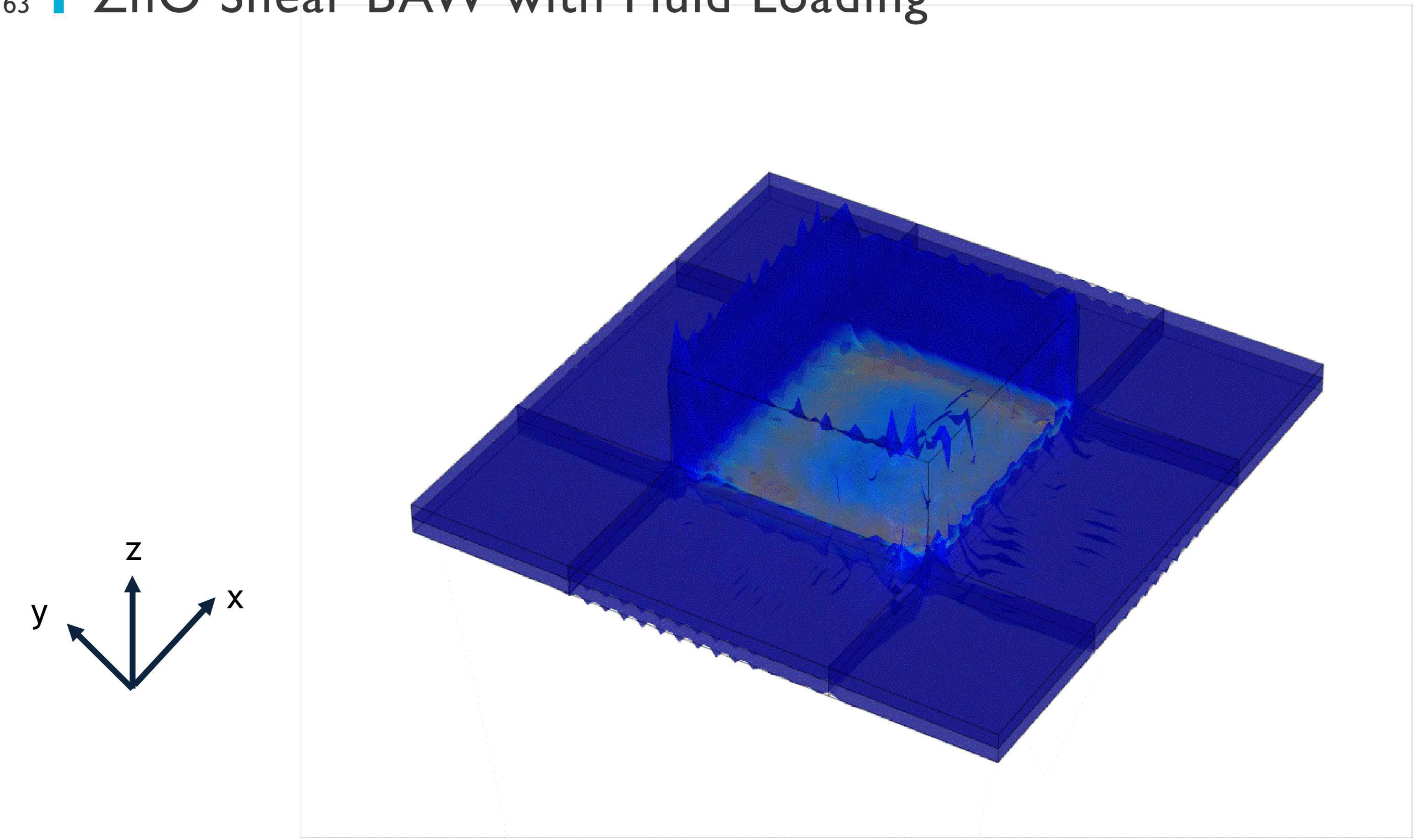

# Specialized Monitoring Circuits for One-Port Resonators

Impact of shunt capacitance $C_o$ on the resonator. Red: Non-zero $C_o$ = 4pF and Blue: $C_o$ = 0.

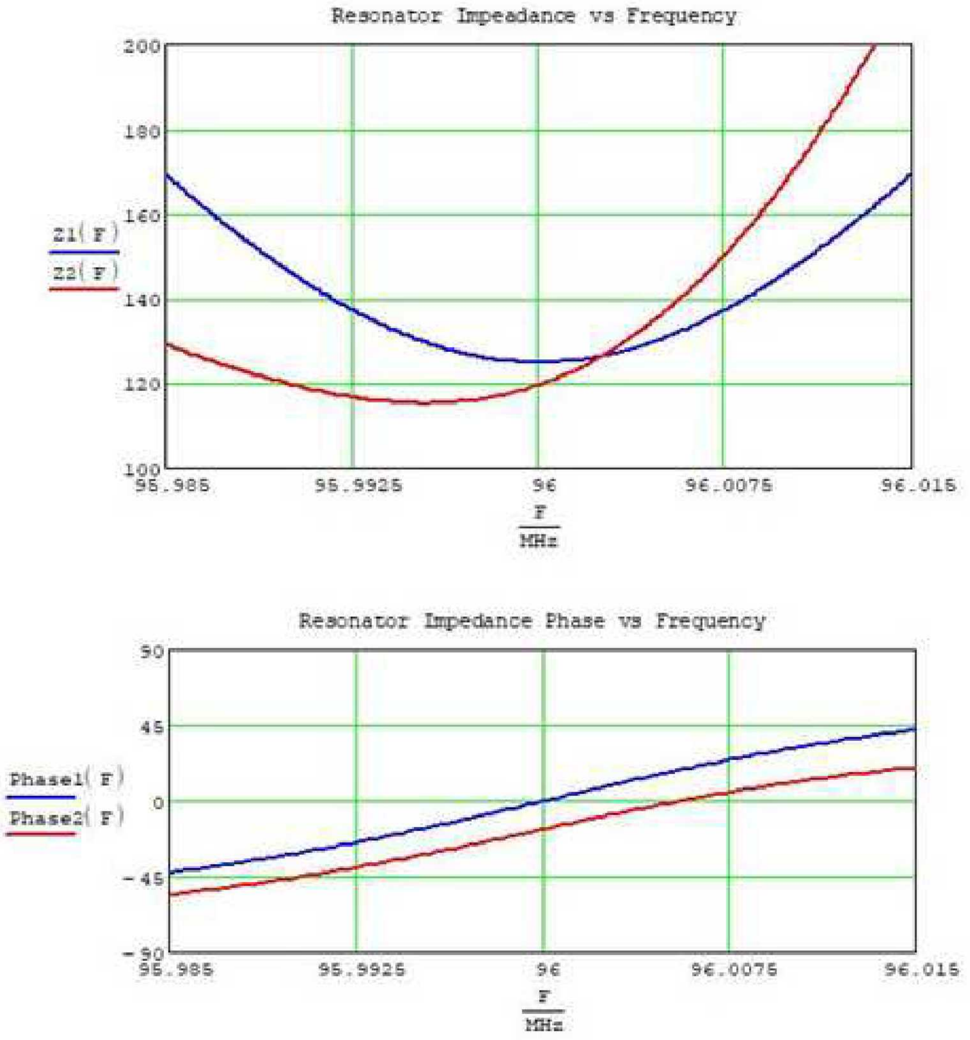

**Key Points:**

- Non-zero shunt capacitance alters the impedance by shifting the location of the minimum and the zero phase crossing while causing significant distortion.
- The distortion for non-zero shunt capacitance becomes increasingly worse as the resonator loss increases (i.e. low Q).
- To obtain the true $F_s$ and resonator loss it is highly desirable remove the shunt capacitance.
- When $C_o$ = 0, the series resonance occurs exactly where the phase crosses zero at the minimum impedance or series resonance.

# Specialized Monitoring Circuits for One-Port Resonators, cont'd

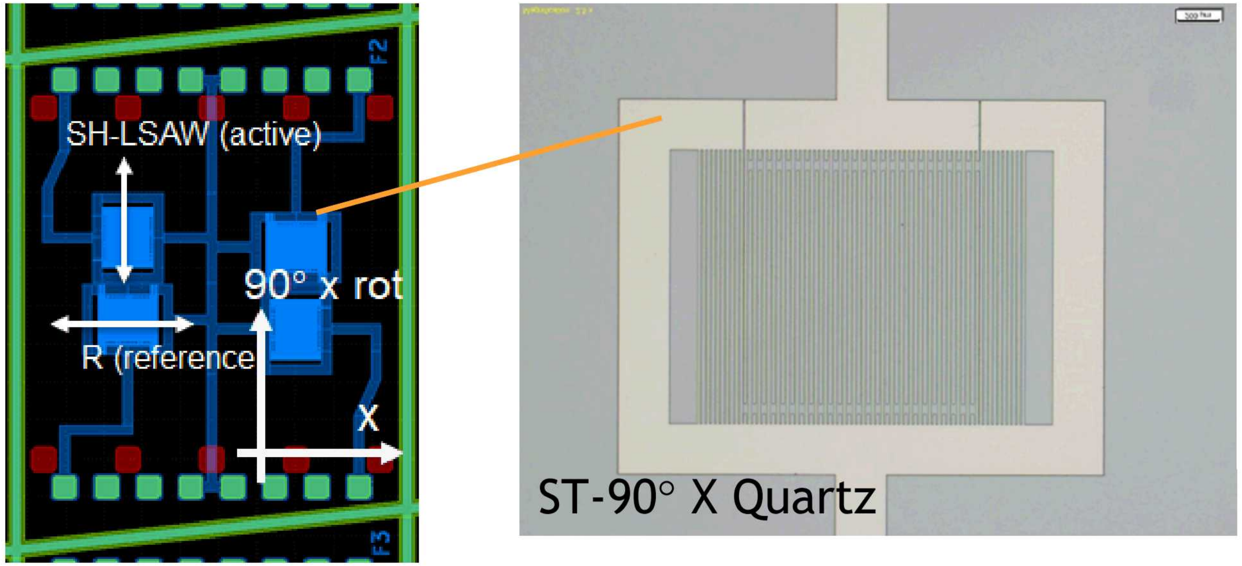

- Device has one active resonator and a dummy or reference that has approximately the same shunt capacitance
- The resonators can be SAW, BAW, or MEMs devices

$$Q_s = \frac{F_s}{2}\frac{d\angle Z_{11}}{df} = \frac{2\pi F_s L_m}{R_m}$$

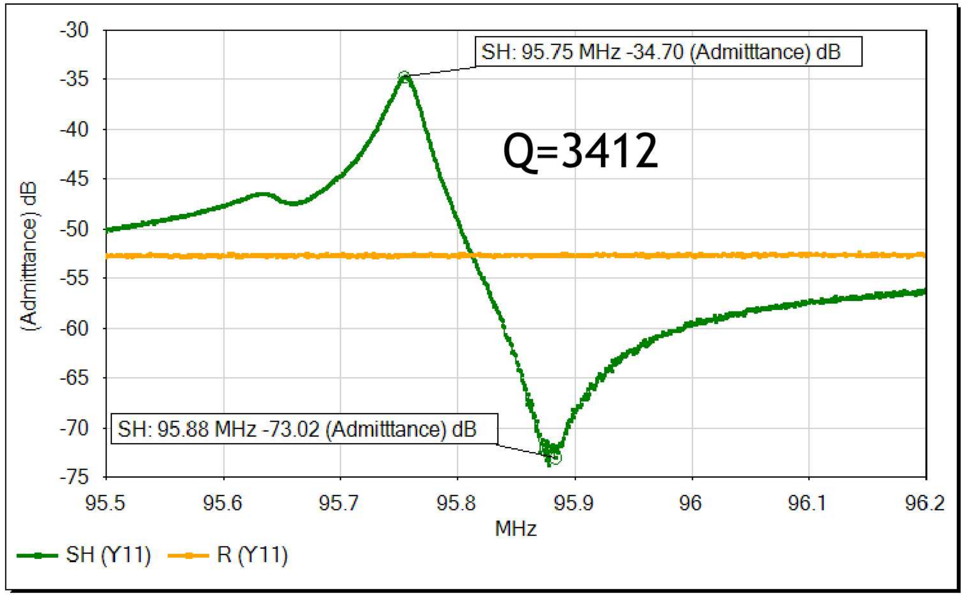

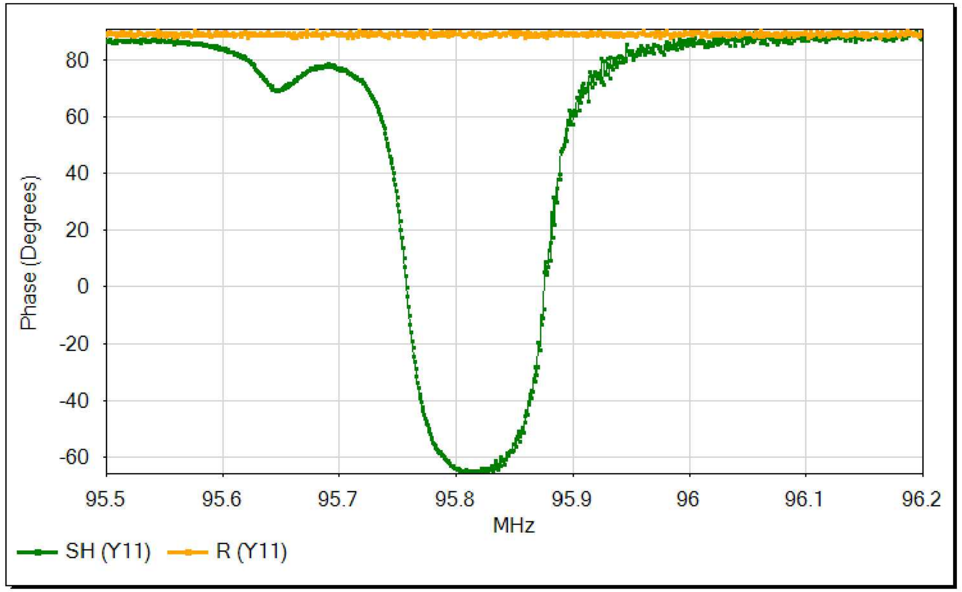

# Specialized Monitoring Circuits for One-Port Resonators, cont’d

- The oscillator effectively removes shunt capacitance across the motional arm of the resonator therefore oscillating very close to the series resonance frequency ($F_s$).
- The circuit outputs a dc voltage proportional to the amplitude of oscillation, which is also proportional to resonator loss, $R_m$.
- The circuit uses a limiter amplifier U1 and emitter followers, $Q_1$ and $Q_2$ as active ports to convert impedances of the resonator and shunt capacitances $C_o + C_1$ (emitter of $Q_1$) and a dummy capacitance, $C_2$ (emitter of $Q_2$) into currents. The currents are summed via current mirrors M1 and M2 and converted to a voltage at $R_1$. This equivalent circuit functions as an oscillator where the frequency only depends on the motional arm of the resonator circuit. The circuit will oscillate when the loop gain is greater than one and the oscillation frequency occurs where the loop function is real, or $2\pi$ radians. This condition only occurs when $XC_m + XL_m = 0$ or when: $F_{osc}=1/(2\pi\surd(L_mC_m)$.

Concept:

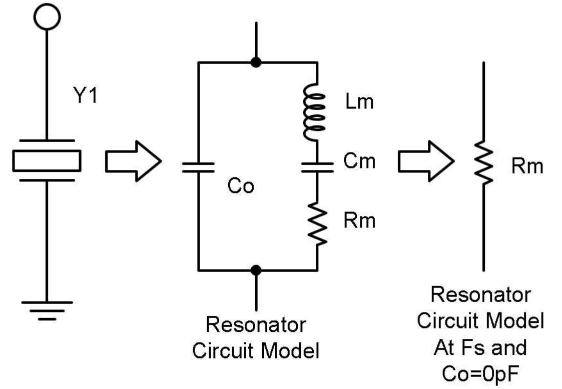

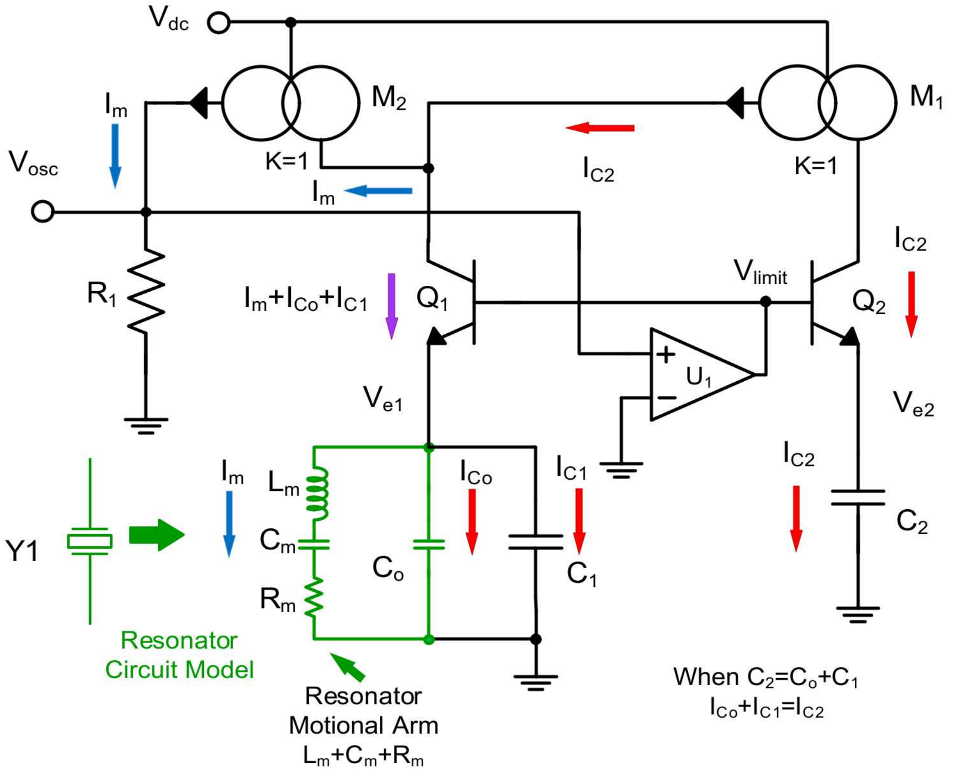

# Specialized Monitoring Circuits for One-Port Resonators, cont’d

Demonstration at 96 MHz

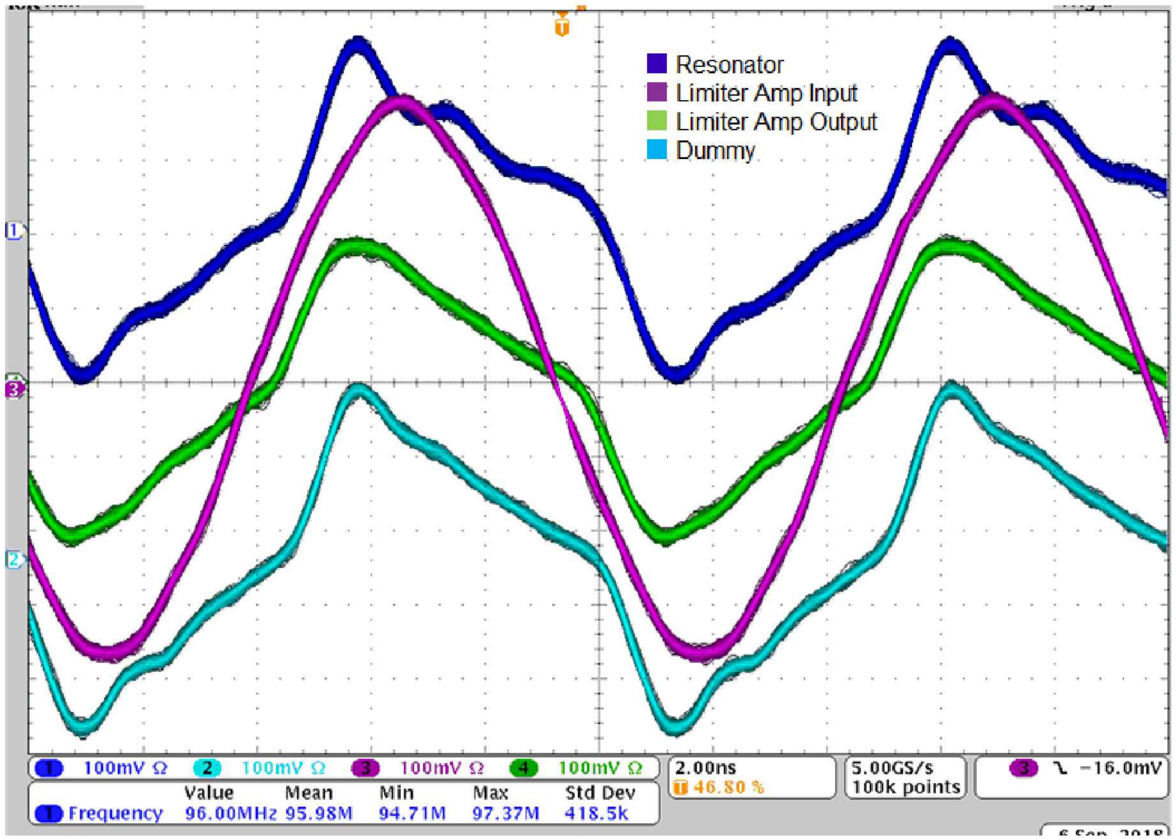

| | Value | Mean | Min | Max | Std Dev |
|---|---|---|---|---|---|
| 1 Frequency | 96.00MHz | 95.98M | 94.71M | 97.37M | 418.5k |

- The oscillator used ST-90° rotated X-cut Quartz resonators, where the active port had $F_s$ = 96 MHz and the dummy is a Rayleigh SAW that is out of band compared to the SH mode due to the orthogonal propagation direction.

- To confirm the circuit is removing the shunt capacitance and tracking the true series resonance, capacitance was added to the active and dummy oscillator ports in sequence. Adding a 2.5 pF capacitor to the active or dummy resonator port caused an equal but opposite frequency shift +30 ppm.

- The oscillator output was 96 MHz, where it can operate with a **series resistance from 10 Ω to 2kΩ without impedance matching.**

# Thank you!